ADA064831

ON THE PERFORMANCE OF AN IMPERFECTLY-IMPLEMENTED SYMMETRICAL DIFFERENTIAL DETECTOR

Ohio State University ElectroScience Laboratory

Jack H. Winters

D D C
RECEIVED
FEB 23 1979
D

79 02 21 022

This report has been reviewed by the RADC Information Office (OI) and is releasable to the National Technical Information Service (NTIS). At NTIS it will be releasable to the general public, including foreign nations.

RADC-TR-78-253 has been reviewed and is approved for publication.

APPROVED:

STUART H. TALBOT.
Project Engineer

APPROVED:

FRED I. DIAMOND
Technical Director
Communication & Control Division

FOR THE COMMANDER:

JOHN P. HUSS
Acting Chief, Plans Office

If your address has changed or if you wish to be removed from the RADC mailing list, or if the addressee is no longer employed by your organization, please notify RADC (DCCR) Griffiss AFB NY 13441. This will assist us in maintaining a current mailing list.

Do not return this copy. Retain or destroy.

REPORT DOCUMENTATION PAGE

READ INSTRUCTIONS
BEFORE COMPLETING FORM

1. REPORT NUMBER	2. GOVT ACCESSION NO.	3. RECIPIENT'S CATALOG NUMBER
RADC-TR-78-253		

4. TITLE *(and Subtitle)*

ON THE PERFORMANCE OF AN IMPERFECTLY-IMPLEMENTED
SYMMETRICAL DIFFERENTIAL DETECTOR.

5. TYPE OF REPORT & PERIOD COVERED

Interim Report,

6. PERFORMING ORG. REPORT NUMBER

ESL-710300-3

7. AUTHOR(s)

Jack H. Winters

8. CONTRACT OR GRANT NUMBER(s)

F30602-75-C-0061

9. PERFORMING ORGANIZATION NAME AND ADDRESS

The Ohio State University ElectroScience Lab
Department of Electrical Engineering
Columbus OH 43212

10. PROGRAM ELEMENT, PROJECT, TASK
AREA & WORK UNIT NUMBERS

62702F
65230907

11. CONTROLLING OFFICE NAME AND ADDRESS

Rome Air Development Center (DCCR)
Griffiss AFB NY 13441

12. REPORT DATE

December 1978

13. NUMBER OF PAGES

98

14. MONITORING AGENCY NAME & ADDRESS *(if different from Controlling Office)*

Same

15. SECURITY CLASS. *(of this report)*

UNCLASSIFIED

15a. DECLASSIFICATION/DOWNGRADING
SCHEDULE

N/A

16. DISTRIBUTION STATEMENT *(of this Report)*

Approved for public release; distribution unlimited

17. DISTRIBUTION STATEMENT *(of the abstract entered in Block 20, if different from Report)*

Same

18. SUPPLEMENTARY NOTES

RADC Project Engineer: Stuart H. Talbot (DCCR)
The material contained in this report is also used as a Thesis submitted to
the Department of Electrical Engineering, The Ohio State University as partial
fulfillment for the degree Master of Science.

19. KEY WORDS *(Continue on reverse side if necessary and identify by block number)*

Symmetrical differential phase shift keying
Differential phase shift keying
Symmetrical differential detection
Differential detection
Bit synchronization error

Frequency uncertainty
Bandlimiting
Hardlimiting
Bit synchronization

20. ABSTRACT *(Continue on reverse side if necessary and identify by block number)*

An investigation into the performance of a differential detector (DD) used
to demodulate a carrier which is modulated differentially with plus and minus
ninety degree phase shifts by a bit stream is presented. The plus-minus ninety
degree (symmetrical) DD is analyzed both analytically and experimentally in
terms of the effects of bit synchronization error, carrier frequency uncer-
tainty, and signal bandlimiting and hardlimiting. In all cases the performance
of the symmetrical DD is compared to that for the conventional (zero-one
hundred eighty degree) DD. An expression for the performance of (Cont'd)

DD FORM 1 JAN 73 **1473** EDITION OF 1 NOV 65 IS OBSOLETE

(Item 20 Cont'd)

cont.

both DD's when the noise at the receiver input is white and Gaussian dis-
tributed, the bit synchronization error is Gaussian distributed, and the
carrier frequency estimate is constant as a function of time is derived.
The effects of bandlimiting and hardlimiting on the signal in both the
frequency and time domain is considered. The circuitry for generating the
symmetrical differential phase shift keyed (DPSK) signal is presented and
an analysis of the circuitry required for bit synchronization is performed.
The results presented provide both the motive and the means for implementing
symmetrical DPSK and DD in present and future communication systems where
severe bandlimiting and hardlimiting effects and/or changing system geo-
metries must be considered.

PREFACE

This report, OSURF Report Number 710300-3, was prepared by the ElectroScience Laboratory, Department of Electrical Engineering, The Ohio State University at Columbus, Ohio. Research was conducted under Contract F30602-75-C-0061. Mr. Stuart Talbot was the RADC Program Monitor for this research.

The author wishes to acknowledge the role of Dr. Ronald J. Huff in contributing many of the initial ideas for this report and to express appreciation for his guidance throughout its writing. A special thanks is also in order to Messrs. R. C. Taylor and R. W. Evans for their assistance in the experimentation associated with this report.

The material contained in this report is also used as a Thesis submitted to the Department of Electrical Engineering, The Ohio State University as partial fulfillment for the degree Master of Science.

iii

TABLE OF CONTENTS

CHAPTER I
INTRODUCTION

In digital communication systems, such as time division multiple access (TDMA), where burst type or short duration signals make an accurate phase reference at the receiver impractical, differential phase shift keying (DPSK) with differential detection provides a vast improvement over coherent modulation schemes. Numerous studies (e.g., [1,2]) have analyzed DPSK with differential detection in terms of the various degradations in ideal performance that exist in a practical system. Some of the effects of these degradations, as noted in [1], include the unequal bit error probabilities (BEP) for transmission of the bits "0" and "1" in the receiver with timing jitter and/or band-limiting present. Also of interest [5] is the spectrum spreading which results when the bandlimited signal with 180 degree phase transitions is hardlimited in a repeater. Modulation techniques which attempt to reduce this spreading include offset keyed quadrature phase shift keying (OK-QPSK) [5], whereby 180 degree phase shifts are avoided.

Correct demodulation of the signal requires accurate bit synchronization at the receiver, which is usually derived either from the data signal itself or a coded clock signal. In such cases, with DPSK, timing information is obtained from the random 180 degree phase shifts of the signal. These transitions occur between only half the bits, however, resulting in half the energy of the signal not being utilized for bit synchronization, and also resulting in the accuracy of the timing being dependent on the received bit stream.

One modulation scheme which employs phase transitions at each bit interval is the differential employment of plus and minus 90 degree phase shifts on the carrier. Such a technique is antipodal and can, therefore, be shown to have the same BEP in the differential detector in the presence of white Gaussian noise as conventional DPSK (CDPSK). This modulation and detection scheme will, thus, be referred to as symmetrical differential phase shift keying (SDPSK) and, correspondingly, symmetrical differential detection (SDD), throughout this report. Due to the equal magnitude of the phase transitions in the carrier the BEP will be approximately the same for both transmission of a "0" or a "1" in the system. Also of importance is the absence of zero crossings in the signal envelope for reasons mentioned previously.

The subject of this report is an investigation into the performance and improvement possible with the introduction of SDPSK into

1

systems now employing CDPSK. The report is divided in six chapters. Chapter II deals with the BEP performance of SDPSK and CDPSK in the differential detector when timing jitter and frequency offset are present. Chapter III is concerned with the differential detector performance with timing jitter when the data is mixed with a pseudorandom code bit stream of equal or greater symbol rate (spread spectrum). Bandlimiting and hardlimiting of the signal waveform are examined in Chapter IV. In Chapter V hardware implementation of SDPSK modulation and the performance of a method of SDPSK bit synchronization is investigated. A summary of results is presented in Chapter VI.

2

CHAPTER II
IMPERFECTLY-TIMED DIFFERENTIAL DETECTION
WITH FREQUENCY UNCERTAINTY

A.   Introduction

In this section the bit error probability (BEP) performance of a
differential detector (DD) in the presence of white Gaussian noise
when the demodulator is imperfectly timed and frequency uncertainty
exists at the receiver is analyzed. Previous studies [1,2], have
analyzed the independent effect of imperfectly timed demodulation and
frequency uncertainty in DPSK systems employing 0° and 180° phase
shifts (i.e., conventional differential detection (CDD)). This
chapter extends the analysis to the joint effect of these imperfec-
tions. Furthermore, a symmetrical differential detector (SDD) is
studied in terms of the imperfections mentioned above.

The configuration of the DD to be analyzed is shown in Fig. 1.
The only difference between the CDD and SDD is the processing and de-
cision devices as described in Section II.B. It has been assumed that
at the receiver the bit timing synchronization is in error by ϵ sec-
onds and that the carrier frequency of the received signal differs
from the receiver local oscillator radian frequency, ω_d, by $\Delta\omega$ radians.
It has been shown [1] that ϵ as a function of time has a Gaussian dis-
tribution. In the following analysis it has been assumed that ϵ, as a
random sample from the distribution, varies slowly with time, and,
hence, is constant over the interval in which the BEP is to be calcu-
lated. The BEP is determined for an ensemble of received signals
(random ϵ) and local oscillator signals (random γ), where the duration
of each sample in the ensemble is four bit durations. Although $\Delta\omega$ may
also vary slowly with time, its probability density function has not
been determined. Thus, in the BEP equations to be derived, the BEP is
calculated for a given timing error mean and variance, and a single
value of frequency offset. From a computer evaluation of these equa-
tions a comparison of the CDD and SDD was performed.

In addition to the inaccuracies mentioned above, imperfect inte-
gration and the filtering of the signal also cause a degradation in
receiver performance. The effect of imperfect integration has been
assumed to be negligible compared to other errors (i.e., $\delta=0$). The
effect of bandlimiting is considered in Chapter IV.

3
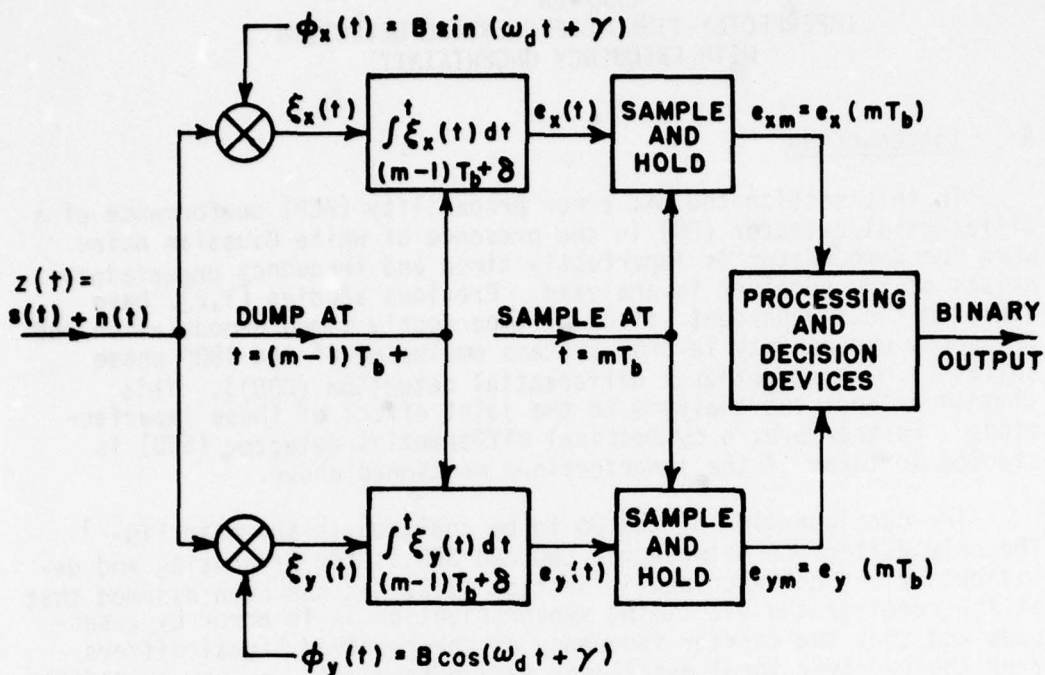
Figure 1. The differential detector.

B. Preliminary Signal Analysis

The method of generation and detection of both conventional DPSK (CDPSK) and symmetrical DPSK (SDPSK) signals will now be investigated. At the transmitter the message-carrying signal, $S_0(t_t)$, is expressible as

$$S_0(t_t) = A_0(t_t) \sin[\omega_0 t_t + \alpha(t_t) + \alpha_t] \quad , \tag{1}$$

where $A_0(t_t)$ is the peak signal amplitude, $\alpha(t_t)$ is the message carry-ing parameter, and α_t is the phase of the signal at time t_t equal to zero. For the mth bit interval of duration T_b seconds (i.e., $T_b < t_t < mT_b$), the message carrying parameter is given by

$$\alpha(t_t) = \alpha_m = \alpha_{m-1} + \frac{\pi}{2} \delta_m \quad , \tag{2}$$

where for CDPSK

4

$$\delta_m \triangleq \begin{cases} 0, \text{ when the mth data bit is a "0"} \\ 2, \text{ when the mth data bit is a "1"} \end{cases} , \qquad (3)$$

and for SDPSK

$$\delta_m \triangleq \begin{cases} -1, \text{ when the mth data bit is a "0"} \\ 1, \text{ when the mth data bit is a "1"} \end{cases} . \qquad (4)$$

Thus, for CDPSK the modulation scheme employed is the transmission of a "0" by a 0° phase shift and a "1" by a 180° phase shift, with respect to the preceding bit interval. For SDPSK transmission of a "0" is achieved by a -90° phase shift and a "1" by a 90° phase shift with respect to the preceding bit interval.

At the receiver, the message-carrying signal has a relative timing error and frequency offset and may be expressed as

$$s(t) = A(t-\varepsilon) \sin[(\omega_0 + \Delta\omega_0)t + \alpha(t-\varepsilon) + \alpha_r] . \qquad (5)$$

Furthermore noise, $n(t)$, is present at the receiver, and, thus, the receiver input signal, $z(t)$, is given by

$$z(t) = s(t) + n(t) . \qquad (6)$$

The noise under consideration is Gaussian distributed and white with single sided power spectral density N_0.

As seen in Fig. 1, $z(t)$ is split into orthogonal components and integrated over each bit interval. The mth bit signal vector is, therefore, given by

$$\bar{z}_m = e_{x_m} \bar{a}_x + e_y \bar{a}_{y_m} , \qquad (7)$$

where $\bar{a}_x$ and $\bar{a}_y$ are unit vectors defining a rectangular coordinate frame. As stated previously, the CDD and the SDD differ only in their processing and decision circuitry. For the CDD, in the decision circuitry the magnitude of the angle between $\bar{z}_{m-1}$ and $\bar{z}_m$ defined in the interval $[0,\pi]$ is compared with the decision angle to determine the received bit. For the ideal CDD with equiprobable "0"'s and "1"'s in the presence of white Gaussian noise this decision angle is $\pi/2$, and the decision device employs the sign of the dot product of the two vectors. Thus, the receiver rule is

5

$$\bar{z}_{m-1} \cdot \bar{z}_m = e_{x_{(m-1)}} e_{x_m} + e_{y_{(m-1)}} e_{y_m} > 0 \quad , \quad \text{"1" transmitted,} \quad (8)$$

and

$$\bar{z}_{m-1} \cdot \bar{z}_m \leq 0 \quad , \quad \text{"0" transmitted} \quad . \quad (9)$$

For the SDD, in the decision circuitry the angle between $\bar{z}_{m-1}$ and $\bar{z}_m$ defined in the interval $[-\pi, \pi]$ is compared with the decision angle to determine the received bit. For the ideal SDD with equiprobable "0"'s and "1"'s in the presence of white Gaussian noise this decision angle is $0°$, and the decision device utilizes the sign of the coefficient of the vector cross product of the two vectors. Thus, the receiver rule is

$$e_{x_{(m-1)}} \cdot e_{y_m} - e_{y_{(m-1)}} \cdot e_{x_m} > 0 \quad , \quad \text{"1" transmitted,} \quad (10)$$

and

$$e_{x_{(m-1)}} \cdot e_{y_m} - e_{y_{(m-1)}} \cdot e_{x_m} \leq 0 \quad , \quad \text{"0" transmitted} \quad . \quad (11)$$

In Eqs. (8) through (11) the orthogonal signal components at the receiver are given by

$$e_{x_m} = \int_{(m-1)T_b}^{mT_b} z(t)\phi_x(t)dt = s_{x_m} + n_{x_m} \quad , \quad (12)$$

and

$$e_{y_m} = \int_{(m-1)T_b}^{mT_b} z(t)\phi_y(t)dt = s_{y_m} + n_{y_m} \quad , \quad (13)$$

where

$$s_{x_m} = \int_{(m-1)T_b}^{mT_b} s(t)\phi_x(t)dt \quad , \quad (14)$$

$$s_{y_m} = \int_{(m-1)T_b}^{mT_b} s(t)\phi_y(t)dt \quad , \quad (15)$$

6

$$n_{x_m} = \int_{(m-1)T_b}^{mT_b} n(t)\phi_x(t)dt \quad , \tag{16}$$

and

$$n_{y_m} = \int_{(m-1)T_b}^{mT_b} n(t)\phi_y(t)dt \quad . \tag{17}$$

In the remainder of Section II.B, Eqs. (14) and (15) will be analyzed in detail.

Given $s(t)$ as defined in Eq. (2), and $\phi_x(t)$ as shown in Fig. 1, let

$$A = \sqrt{2P_r} \quad , \tag{18}$$

and

$$B \triangleq \sqrt{2/T_b} \quad , \tag{19}$$

where P_r is the average power in the signal. Thus,

$$s_{x_m} = \int_{(m-1)T_b}^{mT_b} \sqrt{2P_r} \sin([\omega_0+\Delta\omega_0]t+\alpha(t-\epsilon)+\alpha_r) \tag{20}$$
$$\sqrt{2/T_b} \sin(\omega_d t+\gamma)dt$$

and

$$s_{y_m} = \int_{(m-1)T_b}^{mT_b} \sqrt{2P_r} \sin([\omega_0+\Delta\omega_0]t+\alpha(t-\epsilon)+\alpha_r) \sqrt{2/T_b} \sin(\omega_d t+\gamma)dt \quad . \tag{21}$$

Let E_b be defined as the energy per bit in the received signal, and the received signal vector of the mth bit employed in the decision circuitry be defined as

$$\overline{s}_m \triangleq s_{x_m} \overline{a}_x + s_{y_m} \overline{a}_y \quad . \tag{22}$$

Therefore, for m=1, with $T_b > \epsilon > 0$,

7

$$S_1 = \frac{2\sqrt{E_b}}{T_b} \left\{ \left[\int_0^\epsilon \sin([\omega_0+\Delta\omega_0]t+\alpha_1-\frac{\pi}{2}\delta_1+\alpha_r)\sin(\omega_d t+\gamma)dt \right. \right.$$

$$\left. + \int_\epsilon^{T_b} \sin([\omega_0+\Delta\omega_0]t+\alpha_1+\alpha_r)\sin(\omega_d t+\gamma)dt \right] \bar{a}_x$$

$$+ \left[\int_0^\epsilon \sin([\omega_0+\Delta\omega_0]t+\alpha_1-\frac{\pi}{2}\delta_1+\alpha_r)\cos(\omega_d t+\gamma)dt \right.$$

$$\left. \left. + \int_\epsilon^{T_b} \sin([\omega_0+\Delta\omega_0]t+\alpha_1+\alpha_r)\cos(\omega_d t+\gamma)dt \right] \bar{a}_y \right\} \quad . \tag{23}$$

Let

$$\omega_d \gg 2\pi/T_b \quad , \tag{24}$$

$$\Delta\omega \overset{\Delta}{=} \omega_0+\Delta\omega_0-\omega_d \quad , \tag{25}$$

$$\Delta\omega T_b < \pi/2 \quad , \tag{26}$$

and

$$\beta \overset{\Delta}{=} \alpha_r-\gamma \quad . \tag{27}$$

Thus,

$$S_1 = \frac{\sqrt{E_b}}{T_b} \left\{ \left[\int_0^\epsilon \cos(\Delta\omega t+\beta+\alpha_1-\frac{\pi}{2}\delta_1)dt \right. \right.$$

$$\left. + \int_\epsilon^{T_b} \cos(\Delta\omega t+\beta+\alpha_1)dt \right] \bar{a}_x$$

$$+ \left[\int_0^\epsilon \sin(\Delta\omega t+\beta+\alpha_1-\frac{\pi}{2}\delta_1)dt \right.$$

$$\left. \left. + \int_\epsilon^{T_b} \sin(\Delta\omega t+\beta+\alpha_1)dt \right] \bar{a}_y \right\} \quad . \tag{28}$$

8

If it is assumed that β changes only a few degrees in each bit interval, then

$$\bar{S}_1 = \frac{\sqrt{E_b}}{\Delta\omega T_b} \left\{ \left[\sin(\Delta\omega\epsilon+\beta+\alpha_1-\frac{\pi}{2}\delta_1) - \sin(\beta+\alpha_1-\frac{\pi}{2}\delta_1) \right. \right.$$

$$\left. + \sin(\Delta\omega T_b+\beta+\alpha_1) - \sin(\Delta\omega\epsilon+\beta+\alpha_1) \right] \bar{a}_x$$

$$+ \left[\cos(\beta+\alpha_1-\frac{\pi}{2}\delta_1) - \cos(\Delta\omega\epsilon+\beta+\alpha_1-\frac{\pi}{2}\delta_1) \right.$$

$$\left. \left. + \cos(\Delta\omega\epsilon+\beta+\alpha_1) - \cos(\Delta\omega T_b+\beta+\alpha_1) \right] \bar{a}_y \right\} \quad . \tag{29}$$

For $-T_b < \epsilon < 0$,

$$\bar{S}_1 = \frac{2\sqrt{E_b}}{T_b} \left\{ \left[\int_0^{T_b+\epsilon} \sin([\omega_0+\Delta\omega_0]t+\alpha_1+\alpha_r)\sin(\omega_d t+\gamma)dt \right. \right.$$

$$\left. + \int_{T_b+\epsilon}^{T_b} \sin([\omega_0+\Delta\omega_0]t+\alpha_1+\frac{\pi}{2}\delta_2+\alpha_r)\sin(\omega_d t+\gamma)dt \right] \bar{a}_x$$

$$+ \left[\int_0^{T_b+\epsilon} \sin([\omega_0+\Delta\omega_0]t+\alpha_1+\alpha_r)\cos(\omega_d t+\gamma)dt \right.$$

$$\left. \left. + \int_{T_b+\epsilon}^{T_b} \sin([\omega_0+\Delta\omega_0]t+\alpha_1+\frac{\pi}{2}\delta_2+\alpha_r)\cos(\omega_d t+\gamma)dt \right] \bar{a}_y \right\} \quad . \tag{30}$$

Following the same procedure as for positive ϵ, it is determined that

$$\bar{S}_1 = \frac{\sqrt{E_b}}{\Delta\omega T_b} \left\{ \left[\sin(\Delta\omega(T_b+\epsilon)+\beta+\alpha_1) - \sin(\beta+\alpha_1) \right. \right.$$

$$\left. + \sin(\Delta\omega T_b+\beta+\alpha_1+\frac{\pi}{2}\delta_2) - \sin(\Delta\omega(T_b+\epsilon)+\beta+\alpha_1+\frac{\pi}{2}\delta_2) \right] \bar{a}_x$$

$$+ \left[\cos(\beta+\alpha_1) - \cos(\Delta\omega(T_b+\epsilon)+\beta+\alpha_1) \right.$$

$$\left. \left. + \cos(\Delta\omega(T_b+\epsilon)+\beta+\alpha_1+\frac{\pi}{2}\delta_2) - \cos(\Delta\omega T_b+\beta+\alpha_1+\frac{\pi}{2}\delta_2) \right] \bar{a}_y \right\} \quad . \tag{31}$$

9

Although Eqs. (29) and (31) are correct, they cannot be readily interpreted as to the process involved in their determination. Another method to calculate the signal vector $\bar{S}_1$ is to consider the results shown in [2]. With frequency offset, $\Delta\omega$, alone, the resultant signal vector is reduced in magnitude by

$$H = \frac{\sin(\Delta\omega t_p/2)}{\Delta\omega t_p/2} \quad , \tag{32}$$

where t_p is the duration of the integrated signal. The resultant signal vector is also increased in phase by

$$\theta = \Delta\omega t_{avg} \quad , \tag{33}$$

where t_{avg} is the average t of the signal, where t is zero at the reference phase angle (i.e., t_{avg} = (start time + stop time)/2). Thus, the signal vector $\bar{S}_1$ can be considered to be the sum of three appropriately modified (in amplitude and phase) signal vectors; the desired ($\varepsilon=0$)m=1 signal vector, minus the portion of the m=1 signal not integrated due to timing error, plus the portion of the adjacent bit (i.e., bit m=0 if $\varepsilon>0$, bit m=2 if $\varepsilon<0$) integrated due to timing error. The resultant signal vector is, therefore, given by

$$
\begin{aligned}
\bar{S}_1 = \sqrt{E_b} \Bigg\{ &\frac{\sin(\Delta\omega T_b/2)}{(\Delta\omega T_b/2)} \left[\cos\left(\frac{\Delta\omega T_b}{2}+\beta+\alpha_1\right) \bar{a}_x \right. \\
&\left. + \sin\left(\frac{\Delta\omega T_b}{2}+\beta+\alpha_1\right) \bar{a}_y \right] \\
-&\frac{|\varepsilon|}{T_b} \frac{\sin(\Delta\omega|\varepsilon|/2)}{(\Delta\omega|\varepsilon|/2)} \left[\cos\left(\Delta\omega\left(\frac{T_b}{2}-\text{sgn}(\varepsilon)\left(\frac{T_b}{2}-\frac{|\varepsilon|}{2}\right)\right)+\beta+\alpha_1\right) \bar{a}_x \right. \\
&\left. + \sin\left(\Delta\omega\left(\frac{T_b}{2}-\text{sgn}(\varepsilon)\left(\frac{T_b}{2}-\frac{|\varepsilon|}{2}\right)\right)+\beta+\alpha_1\right) \bar{a}_y \right] \\
+&\frac{|\varepsilon|}{T_b} \frac{\sin(\Delta\omega|\varepsilon|/2)}{(\Delta\omega|\varepsilon|/2)} \left[\cos\left(\Delta\omega\left(\frac{T_b}{2}-\text{sgn}(\varepsilon)\left(\frac{T_b}{2}-\frac{|\varepsilon|}{2}\right)\right)+\beta+\alpha_1\right. \right. \\
&\left. -\text{sgn}(\varepsilon)\frac{\pi}{2}\delta_a\right) \bar{a}_x \\
&\left. + \sin\left(\Delta\omega\left(\frac{T_b}{2}-\text{sgn}(\varepsilon)\left(\frac{T_b}{2}-\frac{|\varepsilon|}{2}\right)\right)+\beta+\alpha_1-\text{sgn}(\varepsilon)\frac{\pi}{2}\delta_a\right) \bar{a}_y \right] \Bigg\} \quad .
\end{aligned}
\tag{34}
$$

10

where,

$$\delta_a = \begin{cases} \delta_1 , & \text{if } \epsilon \geq 0 \\ \delta_2 , & \text{if } \epsilon < 0 \end{cases} .$$ (35)

Figure 2 illustrates an example of the signal vector generated from Eq. (34). Note that if there is no phase shift between bits (CDD case only), the last two terms of Eq. (34) cancel, independent of timing error.

By a long, but straightforward procedure Eq. (34) may also be derived from Eqs. (29) and (31).

For $\overline{S}_2$, the vector equation is that of Eq. (34) with an increase in phase of $\Delta\omega T_b$, α_2 substituted for α_1, and

$$\delta_a = \begin{cases} \delta_2 , & \text{if } \epsilon \geq 0 \\ \delta_3 , & \text{if } \epsilon < 0 \end{cases} .$$ (36)

In the decision circuitry the process involved is differential detection. Thus, one of the parameters needed in determining the BEP of the receiver in the presence of noise is the relative angles of the vectors $\overline{S}_1$ and $\overline{S}_2$, not their absolute angles. Note that this angle is independent of β and α_1. The parameters of interest from the signal vectors are, therefore,

$$L_1(\epsilon, \Delta\omega, \{\delta\}) \triangleq |\overline{S}_1| ,$$ (37)

$$L_2(\epsilon, \Delta\omega, \{\delta\}) \triangleq |\overline{S}_2| ,$$ (38)

and

$$\Delta\phi(\epsilon, \Delta\omega, \{\delta\}) \triangleq \underline{/\overline{S}_2} - \underline{/\overline{S}_1} .$$ (39)

Note that for a given system (E_b and T_b fixed), these parameters are explicit functions of ϵ, $\Delta\omega$, and $\{\delta\}$ alone, where $\{\delta\}$ is the sequence $\delta_1 \delta_2 \delta_3$, for δ_m as defined in Eqs. (3) and (4). In the analysis to follow this dependence is not shown for notational convenience.

11

$\bar{S}_1$ FOR $\epsilon = 0$

CHANGE IN $\bar{S}_1$ DUE TO LOSS OF PORTION OF m = 1 BIT

CHANGE IN $\bar{S}_1$ DUE TO INTEGRATION OF PORTION OF ADJACENT BIT

$\delta_1 = 1$

$\dfrac{\Delta\omega|\epsilon|}{2} + \beta$

$\Delta\omega\left(T_b - \dfrac{|\epsilon|}{2}\right) + \beta$

$\delta_1 = 0$

$\delta_1 = 2$

$\epsilon < 0$

$\epsilon > 0$

$\bar{S}_1$ FOR $\epsilon > 0$ $\delta_1 = 2$

$\delta_2 = 0$

$\delta_2 = -1$

$\delta_2 = 1$

$\delta_1 = -1$

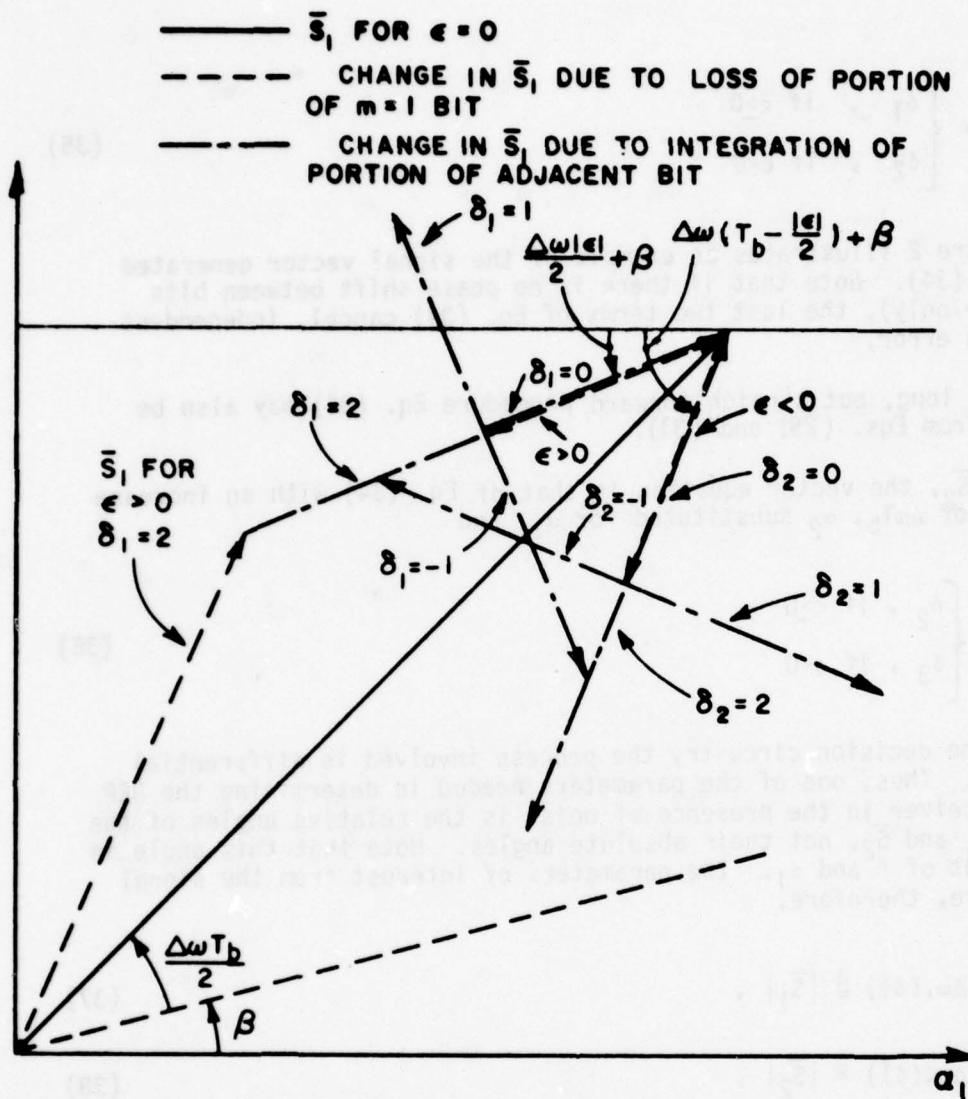$\delta_2 = 2$

$\dfrac{\Delta\omega T_b}{2}$

β

a_1

Figure 2. Received signal vectors of interest for $\Delta\omega T_b = \pi/3$ and $|\epsilon| = .25 T_b$. $\bar{S}_1$ for $\epsilon > 0$ and $\delta_1 = 2$ shown.

C. Bit Error Probability for Differential Detection in the Presence of Noise

1. General bit error probability expression

The calculation of the BEP will follow that of [1]. A new co-ordinate frame, (x',y'), in which $\bar{S}_1$ is aligned with the x' axis can be obtained by rotating the (x,y) frame by $\underline{/S}_1$. In this new frame

$$\bar{S}_1 = L_1 \bar{a}_{x'} \quad , \tag{40}$$

and

$$\bar{S}_2 = L_2(\cos \Delta\phi \ \bar{a}_{x'} + \sin \Delta\phi \ \bar{a}_{y'}) \quad , \tag{41}$$

where $\bar{a}_{x'}$ and $\bar{a}_{y'}$ are unit vectors in the plus x' and plus y' direction, respectively.

In the (x',y') frame, the vectors $\bar{Z}_1$ and $\bar{Z}_2$ are expressible as

$$\bar{Z}_1 = e_{x'1} \ \bar{a}_{x'} + e_{y'1} \ \bar{a}_{y'} \quad , \tag{42}$$

and

$$\bar{Z}_2 = e_{x'2} \ \bar{a}_{x'} + e_{y'2} \ \bar{a}_{y'} \quad , \tag{43}$$

where

$$e_{x'1} = L_1 + n_{x'1} \quad , \tag{44}$$

$$e_{y'1} = n_{y'1} \quad , \tag{45}$$

$$e_{x'2} = L_2 \cos \Delta\phi + n_{x'2} \quad , \tag{46}$$

and

$$e_{y'2} = L_2 \sin \Delta\phi + n_{y'2} \tag{47}$$

13

Now, n_{x_m} and n_{y_m} (m=1,2) are orthogonal components of the noise which is Gaussian with mean, 0, variance, $N_0/2$. Thus, it can be shown that $n_{x'_m}$ and $n_{y'_m}$ are also Gaussian with mean, 0, variance, $N_0/2$. The conditional joint density function for $e_{x'_1}$ and $e_{y'_1}$ can, therefore, be written as

$$p(e_{x'_1}, e_{y'_1}/L_1) = \frac{1}{\pi N_0} \exp\left\{-\frac{(e_{x'_1}-L_1)^2 + e_{y'_1}^2}{N_0}\right\} \quad . \tag{48}$$

Let

$$\psi_1 \equiv \underline{/\bar{Z}_1} - \underline{/\bar{S}_1} \tag{49}$$

The signal components $e_{x'_1}$ and $e_{y'_1}$ can be written in terms of $\bar{Z}_1$ and ψ_1 as

$$\left.\begin{aligned}e_{x'_1} &= |\bar{Z}_1| \cos \psi_1 \\ \text{and} \\ e_{y'_1} &= |\bar{Z}_1| \sin \psi_1\end{aligned}\right\} \quad -\pi < \psi_1 < \pi \tag{50}$$
$$\tag{51}$$

The conditional probability density function of ψ_1, given L_1, is, therefore [2],

$$P(\psi_1/L_1) = \frac{1}{2\pi} \exp\left[-\frac{L_1^2}{N_0}\right] + \frac{1}{\sqrt{2\pi}} \exp\left[-\frac{L_1^2 \sin^2\psi_1}{N_0}\right]$$
$$\cdot L_1 \sqrt{\frac{2}{N_0}} \cos \psi_1 \left[\frac{1}{2} + Q(L_1, \psi_1)\right] \quad , \tag{52}$$

where

$$Q(L_1, \psi_1) = \frac{1}{\sqrt{2\pi}} \int_0^{L_1\sqrt{2/N_0} \cos\psi_1} \exp\left(-\frac{u^2}{2}\right) du \quad . \tag{53}$$

Next, assuming ψ_1 given, a new $(\bar{x}, \bar{y})$ coordinate frame is formed by rotating the (x', y') frame counterclockwise by ψ_1 radians, so that signal vector $\bar{Z}_1$ is aligned with the positive $\bar{x}$ axis (see Fig. 3). In this frame

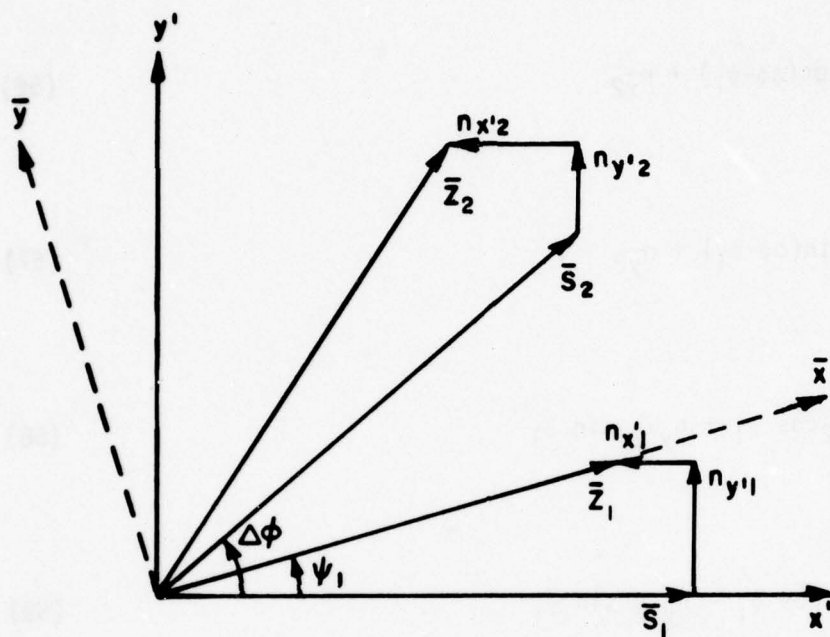$$e_{\bar{x}2} = L_2 \cos \Delta\phi \cos \psi_1 + L_2 \sin \Delta\phi \sin \psi_1 + n_{\bar{x}2} \tag{54}$$

14

Figure 3. Relationship of the signal vectors $\bar{Z}_1$ and $\bar{Z}_2$ to the (x',y') and $(\bar{x},\bar{y})$ coordinate reference frames.

and

$$e_{\overline{y}2} = L_2 \sin \Delta\phi \cos \psi_1 - L_2 \cos \Delta\phi \sin \psi_1 + n_{\overline{y}2} \quad , \tag{55}$$

which reduces to

$$e_{\overline{x}2} = L_2 \cos(\Delta\phi - \psi_1) + n_{\overline{x}2} \tag{56}$$

and

$$e_{\overline{y}2} = L_2 \sin(\Delta\phi - \psi_1) + n_{\overline{y}2} \quad , \tag{57}$$

where

$$n_{\overline{x}2} = n_{x'2} \cos \psi_1 + n_{y'2} \sin \psi_1 \tag{58}$$

and

$$n_{\overline{y}2} = n_{y'2} \cos \psi_1 - n_{y'2} \sin \psi_1 \quad . \tag{59}$$

Examination of the vector components of $\overline{Z}_2$ and $\overline{Z}_1$ in the $(\overline{x}.\overline{y})$ frame shows that for CDD, $e_{\overline{x}2}$ is proportional to the dot product, $\overline{Z}_1 \cdot \overline{Z}_2$ Thus, (see Eqs. (8) and (9))

$$P_o = P_r(e_{\overline{x}2} < 0/\delta_2 = 0) \quad , \tag{60}$$

and

$$P_1 = P_r(e_{\overline{x}2} > 0/\delta_2 = 2) \quad , \tag{61}$$

where P_o and P_1 are the probability of error given that a "0" and a "1", respectively, were transmitted.

For SDD, $e_{\overline{y}2}$ is proportional to the coefficient of the cross product $(\overline{Z}_1 X \overline{Z}_2)$ vector. Thus, (see Eqs. (10) and (11))

$$P_o = P_r(e_{\overline{y}2} > 0/\delta_2 = -1),$$ (62)

and

$$P_1 = P_r(e_{\overline{y}2} < 0/\delta_2 = 1) \quad .$$ (63)

From Eq. (56), the conditional density function for $e_{\overline{x}2}$ (the variable of interest for CDD) can be written as (note again that $n_{\overline{x}2}$ and $n_{\overline{y}2}$ are Gaussian distributed, mean equal 0, variance equal $N_o/2$)

$$p(e_{\overline{x}2}/\psi_1, L_2, \Delta\phi) = \frac{1}{\sqrt{\pi N_o}} \exp\left[-\frac{1}{N_o}\left[e_{\overline{x}2} - L_2 \cos(\Delta\phi - \psi_1)\right]^2\right] .$$ (64)

From Eq. (57) the conditional density function for $e_{\overline{y}2}$ (the variable of interest in SDD) can be written as

$$p(e_{\overline{y}2}/\psi_1, L_2, \Delta\phi) = \frac{1}{\sqrt{\pi N_o}} \exp\left[-\frac{1}{N_o}\left[e_{\overline{y}2} - L_2 \sin(\Delta\phi - \psi_1)\right]^2\right] .$$ (65)

Equations (64) and (65) are similar in form and differ due to $\Delta\phi$. $\Delta\phi$ may be considered to have two components, one the desired phase shift, and the other due to imperfections in the receiver. Thus,

$$\Delta\phi = \Delta\phi_\epsilon + \frac{\pi}{2}\delta_2 \quad ,$$ (66)

where $\Delta\phi_\epsilon$ is the error in the phase.

Substituting Eq. (66) into Eqs. (64) and (65), respectively, and noting the symmetry in the equations of ψ_1 with respect to 0, the conditional probability density functions of interest become (noting that L_2 and $\Delta\phi_\epsilon$ are functions of ϵ, $\{\delta\}$, and $\Delta\omega$)

$$p(e_a/\psi_1, \epsilon, \{\delta\}, \Delta\omega) = \frac{1}{\sqrt{\pi N_o}} \exp\left\{-\frac{1}{N_o}\left[e_a \pm L_2 \cos(\Delta\phi_\epsilon - \psi_1)\right]^2\right\} .$$ (67)

where

$$e_a = \begin{cases} e_{\overline{x}2} , & \text{for CDD} \\ e_{\overline{y}2} , & \text{for SDD} \end{cases} \quad ,$$ (68)

17

and the plus sign (case 1) is employed for $\delta=2$ or -1, and the minus sign (case 2) for $\delta=0$ or 1. Thus the probability density function (pdf) of the error component is the same for CDD and SDD when L_2 and $\Delta\phi_\varepsilon$ are identical.

The pdf of interest to determine the BEP, $p(e_a/\{\delta\},\Delta\omega)$, can be derived as follows.

$$p(e_a/\{\delta\},\Delta\omega) = \int_\varepsilon \int_{\psi_1} p(e_a/\psi_1,\varepsilon,\{\delta\},\Delta\omega)$$
$$\cdot\ p(\psi_1/\varepsilon,\{\delta\},\Delta\omega)$$
$$\cdot\ p(\varepsilon/\{\delta\},\Delta\omega)d\psi_1 d\varepsilon \quad . \tag{69}$$

Eliminating unnecessary conditions, the pdf is given by

$$p(e_a/\{\delta\},\Delta\omega) = \int_\varepsilon \int_{\psi_1} p(e_a/\psi_1,\varepsilon,\{\delta\},\Delta\omega)$$
$$\cdot\ p(\psi_1/\varepsilon,\{\delta\},\Delta\omega) \cdot p(\varepsilon)d\psi_1 d\varepsilon \quad . \tag{70}$$

Let

$$K_1(L_1,L_2,\Delta\phi_\varepsilon/\varepsilon,\Delta\omega,\{\delta\}) \triangleq \left. P_0\right|_\varepsilon \text{ for CDD} = \left. P_1\right|_\varepsilon \text{ for SDD}$$
$$= \int_{-\infty}^0 \int_{\psi_1} p(e_a/\psi_1,\varepsilon,\{\delta\},\Delta\omega)p(\psi_1/\varepsilon,\{\delta\},\Delta\omega)$$
$$d\psi_1 de_a \quad . \tag{71}$$

and

$$K_2(L_1,L_2,\Delta\phi_\varepsilon/\varepsilon,\Delta\omega,\{\delta\}) \triangleq \left. P_1\right|_\varepsilon \text{ for CDD} = \left. P_0\right|_\varepsilon \text{ for SDD}$$
$$= \int_0^\infty \int_{\psi_1} p(e_a/\psi_1,\varepsilon,\{\delta\},\Delta\omega)p(\psi_1/\varepsilon,\{\delta\},\Delta\omega)$$
$$d\psi_1 de_a \quad . \tag{72}$$

Following the procedure in [2], it is found that

18

$$K_1(L_1,L_2,\Delta\phi_\varepsilon/\varepsilon,\Delta\omega,\{\delta\}) = K_2(L_1,L_2,\Delta\phi_\varepsilon/\varepsilon,\Delta\omega,\{\delta\})$$
$$\triangleq K(L_1,L_2,\Delta\phi_\varepsilon/\varepsilon,\Delta\omega,\{\delta\}) \quad , \tag{73}$$

where

$$K(L_1,L_2,\Delta\phi_\varepsilon/\varepsilon,\Delta\omega,\{\delta\}) =$$

$$\frac{1}{\pi}\int_0^{\pi/2} \exp\left[-\frac{L_1^2 L_2^2 \cos^2\Delta\phi_\varepsilon/N_0}{L_1^2\cos^2\theta + L_2^2\cos^2\Delta\phi_\varepsilon \sin^2\theta}\right] d\theta$$

$$+ \frac{L_1}{\pi\sqrt{2N_0}}\int_{-\pi/2}^{\pi/2}\left\{\int_{L_1\sqrt{2/N_0}\cos(x+\Delta\phi_\varepsilon)}^{L_1\sqrt{2/N_0}\cos x \cos\Delta\phi_\varepsilon}\exp(-u^2/2)du\right\}$$

$$\cdot \exp\left[-\frac{L_1^2\sin^2 x}{N_0}\right]\cos x\, dx \quad . \tag{74}$$

The dependence of L_1, L_2, and $\Delta\phi_\varepsilon$ on ε, $\Delta\omega$, $\{\delta\}$ is implied in the above equations.

Therefore the BEP for a bit, given the encoded data stream $\{\delta\}$ and $\Delta\omega$ is given by

$$P_E|\{\delta\} = \int_\varepsilon K(L_1,L_2,\Delta\phi_\varepsilon/\varepsilon,\Delta\omega,\{\delta\})p(\varepsilon)d\varepsilon \quad . \tag{75}$$

As stated before ε is assumed to have a Gaussian distribution (see Chapter VI), which may be given by

$$p(\varepsilon) = \frac{1}{\sqrt{2\pi}\sigma_\varepsilon}\exp\left[-\frac{(\varepsilon-\bar\varepsilon)^2}{2\sigma_\varepsilon^2}\right] \quad , \tag{76}$$

where $\bar\varepsilon$ is the mean and σ_ε^2 the variance of the timing jitter. The average BEP for a given $\Delta\omega$ can now be calculated as the average of the BEP's for each of the eight possible encoded data streams, $\{\delta\}_i$, i=1, $\cdots$,8, for a given type of detector (CDD or SDD). Assuming equally probable and independent input data, the average BEP is, therefore

$$P_E = \frac{1}{8}\sum_{i=1}^8 \int_\varepsilon K(L_1,L_2,\Delta\phi_\varepsilon/\varepsilon,\Delta\omega,\{\delta\}_i)p(\varepsilon)d\varepsilon \quad . \tag{77}$$

19

The required parameters for the above BEP calculation are, therefore, E_b, T_b, N_o, $\Delta\omega$, $\bar{\varepsilon}$, σ_ε, and the type of detection (CDD or SDD) involved.

2. Numerical results

a. Computer program structure

Equation (77) has been analyzed using numerical techniques. Simpson's one-third rule was employed in evaluating all integrals. The number of iterations for each integral was determined to produce a total error on the order of 1%. To achieve this goal, the number of equal length increments in each calculation was 4 for u (Eq. (74)), 40 for x (Eq. (74)), 30 for θ (Eq. (74)) and 150 for ε (Eq. (77)).

To verify the validity of the equations developed, a comparison of computer program results to those obtained both analytically and experimentally in [1] and [2] was performed. In these two references only CDPSK was considered. It can be demonstrated that with $\Delta\omega=0$, Eq. (77) reduces to that in [1] with timing jitter alone. With $\varepsilon=0$, Eq. (77) reduces to the equation derived in [2] for frequency offset only. Thus, computer analysis of Eq. (77) for the independent effects of timing jitter and frequency offset yield identical BEP values as those presented in [1] and [2]. Also in [2], experimental results are shown to be in good agreement with the numerical evaluation of the above two equations.

For the joint effect on the BEP of both timing jitter and frequency offset, experimental results were presented in [2]. In Figs. 4 and 5 a comparison has been made between these experimental results and the analytical results from Eq. (77).

b. Computer generated results

Equation (77) will now be investigated to make a comparison in performance of CDPSK and SDPSK at the receiver. To be considered is the performance of the two techniques with frequency offset alone, timing error alone, and both frequency offset and timing error in the differential detector.

With frequency offset alone, it can be demonstrated that Eq. (77) reduces to the same equation for both techniques (see [2]). Therefore, the two techniques have the same BEP performance with frequency offset.

With timing error alone, Fig. 6 illustrates the difference in performance of the two methods for various values of the normalized

20

Figure 4. The bit error probability versus the bit energy to noise density ratio of the imperfectly-timed differential detector for selected values of frequency offset; experimental results as presented in [2], Fig. 26, with theoretical values from computer analysis of Eq. (77), for CDPSK.

21

Figure 5.   The bit error probability versus the bit energy to
noise density ratio of the imperfectly-timed dif-
ferential detector for selected values of frequency
offset; experimental results as presented in [2],
Fig. 27, with theoretical values from computer
analysis of Eq. (77), for CDPSK.

22
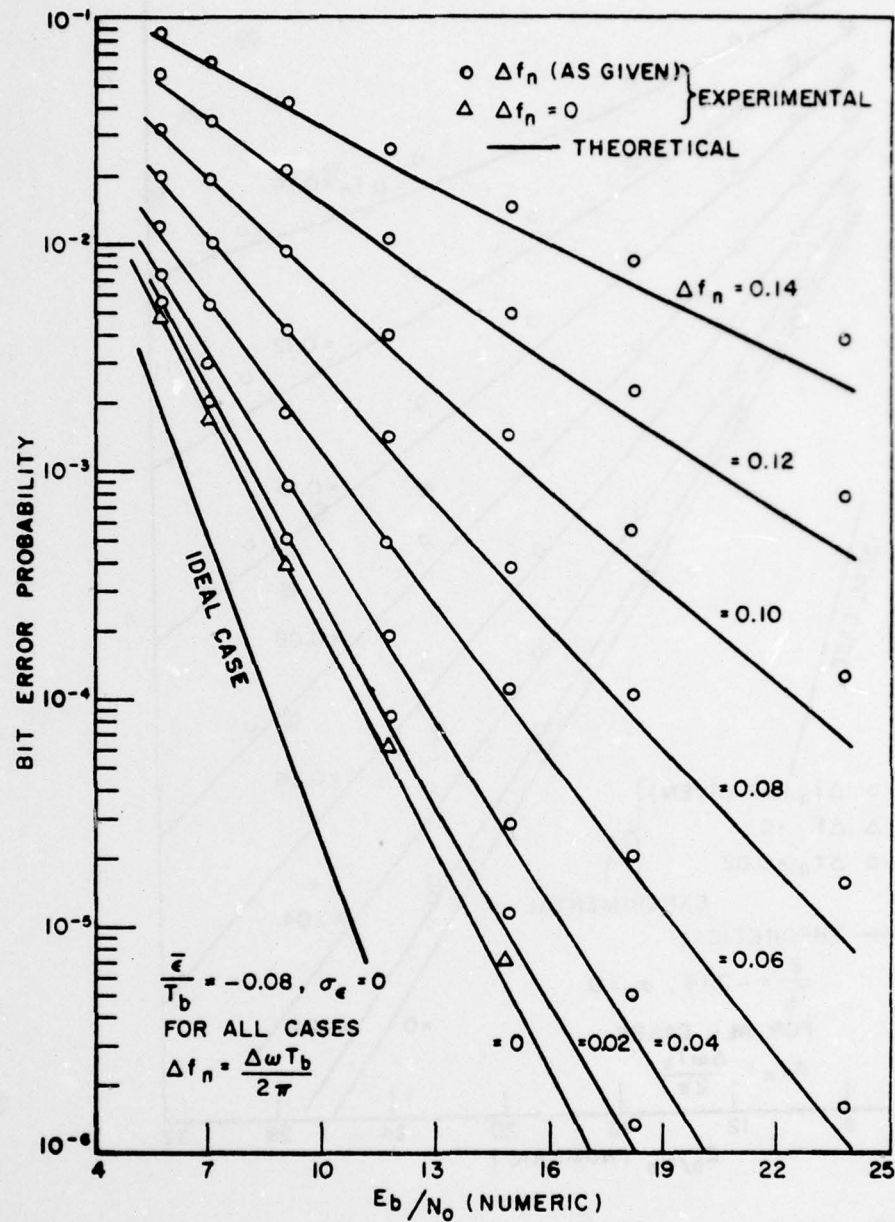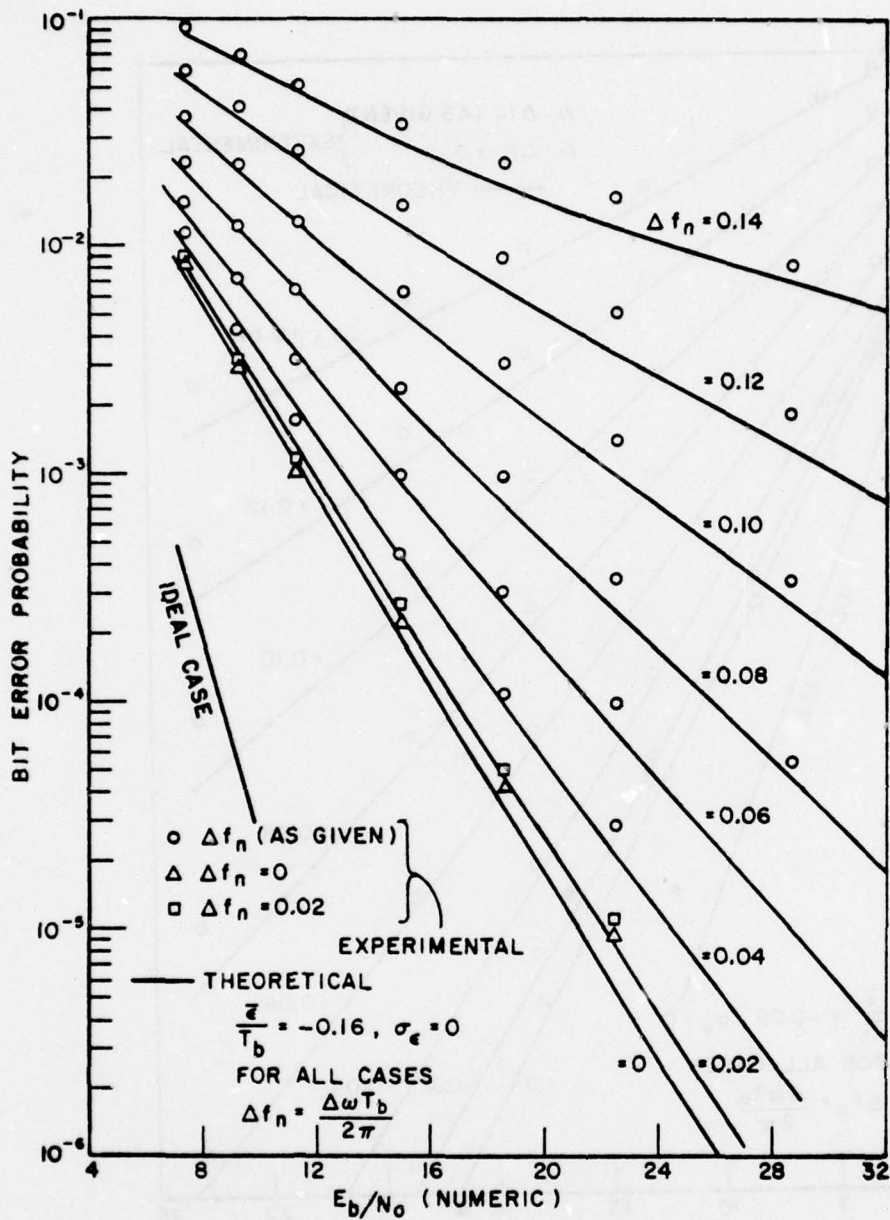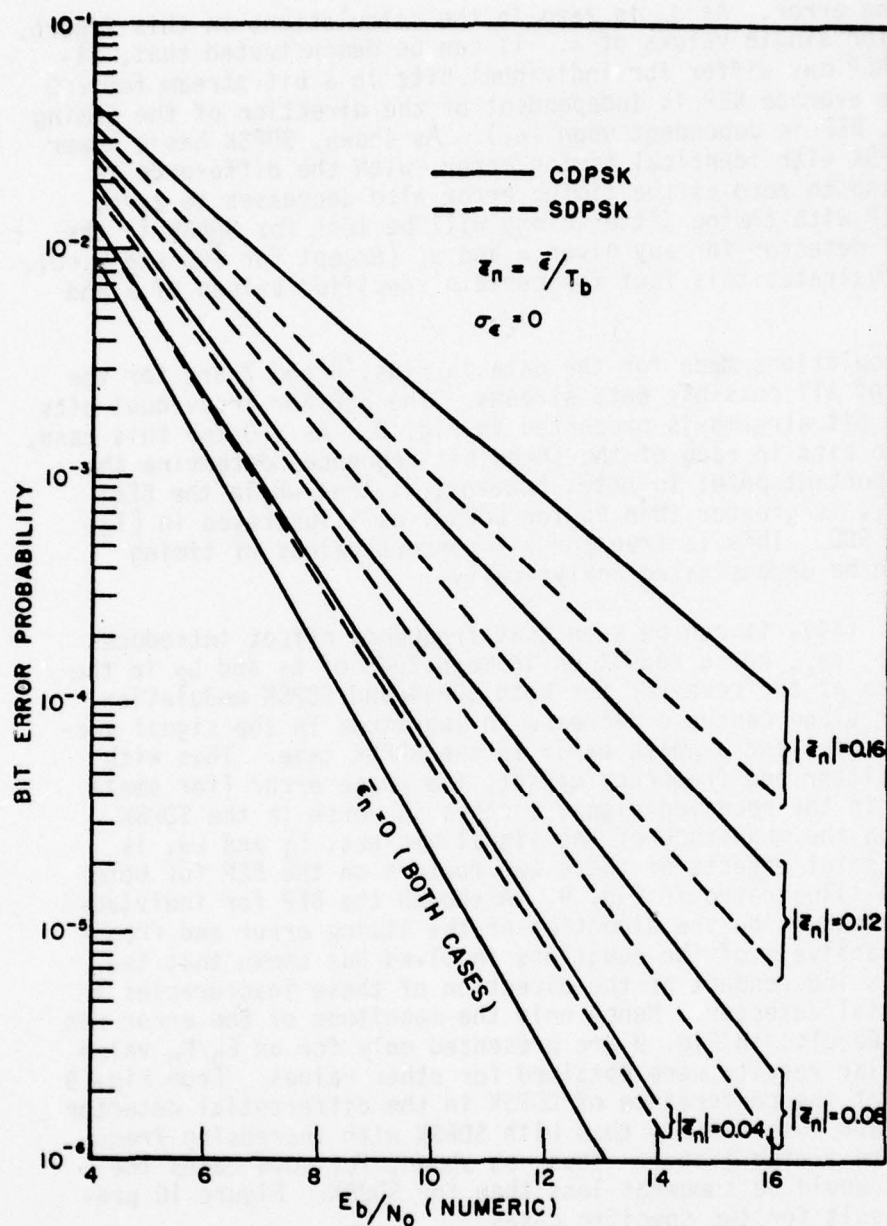
Figure 6. The average bit error probability versus the bit energy to noise density ratio of differential detector with selected values of timing error; comparison of CDPSK versus SDPSK.

23

(ϵ/T_b) timing error. As σ_ϵ is zero in the calculations in this figure, the BEP is for single values of ϵ. It can be demonstrated that, although the BEP may differ for individual bits in a bit stream for $\epsilon > 0$ and $\epsilon < 0$, the average BEP is independent of the direction of the timing error (i.e., BEP is dependent upon $|\epsilon|$). As shown, SDPSK has a lower BEP than CDPSK with identical timing error, with the difference in BEP decreasing to zero as the timing error also decreases to zero. Thus, the BEP with timing jitter alone will be less for SDPSK in the differential detector for any given $\bar{\epsilon}$ and σ_ϵ (except for $\bar{\epsilon}=0$ and $\sigma_\epsilon=0$). Figure 7 illustrates this fact for certain specified values of $\bar{\epsilon}$ and σ_ϵ.

The calculations made for the data in Figs. 6 and 7 are for the average BEP of all possible data streams. The BEP for individual bits in different bit streams is presented in Fig. 8. As $\epsilon > 0$ for this case, the first two bits in each of the three bit sequences determine the BEP. The important point to note, however, is that while the BEP for a "1", P_1, is greater than P_0 for CDPSK, as illustrated in [1], $P_1=P_0$ in the SDD. This is true for all nonzero values of timing error, as can be demonstrated analytically.

From Eq. (34), it can be seen that frequency offset introduces a phase error, $\Delta\phi_\epsilon$, and a reduction in magnitude of L_1 and L_2 in the signal vectors at the receiver for both SDPSK and SDPSK modulation. Timing jitter alone causes a decrease in magnitude in the signal vectors in both cases and a phase error in the SDPSK case. Thus with both timing jitter and frequency offset, the phase error (for small $\Delta\omega/T_b$), $\Delta\phi_\epsilon$, in the received signal vectors is worse in the SDPSK case, although the magnitude of the signal vectors, L_1 and L_2, is larger. The joint effects of these two factors on the BEP for both techniques is illustrated in Fig. 9. Although the BEP for individual bits is dependent on the direction of the timing error and frequency offset, analysis of the equations involved has shown that the average BEP is independent of the direction of these inaccuracies in the differential detector. Hence only the magnitude of the error was considered. Results in Fig. 9 are presented only for an E_b/N_0 value of 10 as similar results were obtained for other values. From Fig. 9 it is seen that the performance of CDPSK in the differential detector tends to degrade less rapidly than with SDPSK with increasing frequency offset and timing jitter. Thus, as shown, for some cases the BEP for CDPSK would be somewhat less than for SDPSK. Figure 10 presents this result for two specific cases.

At this point a detailed analysis could be made to determine the 3-parameter (ϵ, $\Delta\omega$, and E_b/N_0) BEP surface for both SDPSK and CDPSK. However, such a study shall not be undertaken for the following reasons. The above comparison has been made for the case where $\Delta\omega$ and ϵ are equal for both techniques. In an actual transmission system $\Delta\omega$ could be assumed to be basically the same whether SDPSK or CDPSK was implemented because $\Delta\omega$ is dependent upon the system geometry. The

bit timing information (and hence the timing jitter) is derived from the modulation itself, however. Hence the timing jitter characteristics will be different for SDPSK and CDPSK using the same channel. The difference in timing error for the two techniques is studied in detail in Section V.B. Let it suffice for now that differential detection with SDPSK has a lower BEP with timing jitter and frequency offset at the receiver, except for large frequency offset, if the timing jitter is the same.

Figure 7. The average bit error probability versus the bit energy to noise density ratio of the differential detector for certain values of timing jitter mean and variance, comparison of CDPSK versus SDPSK.
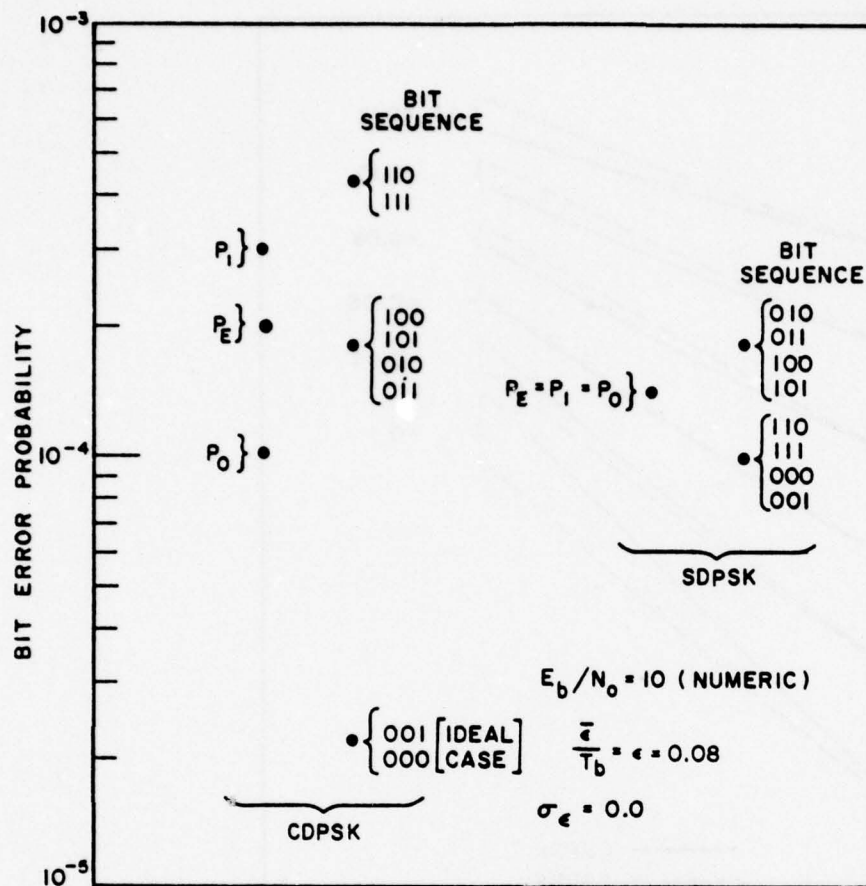
Figure 8. The BEP for the middle bit in all possible three bit sequences and the average BEP for each bit; CDPSK versus SDPSK in the differential detector.
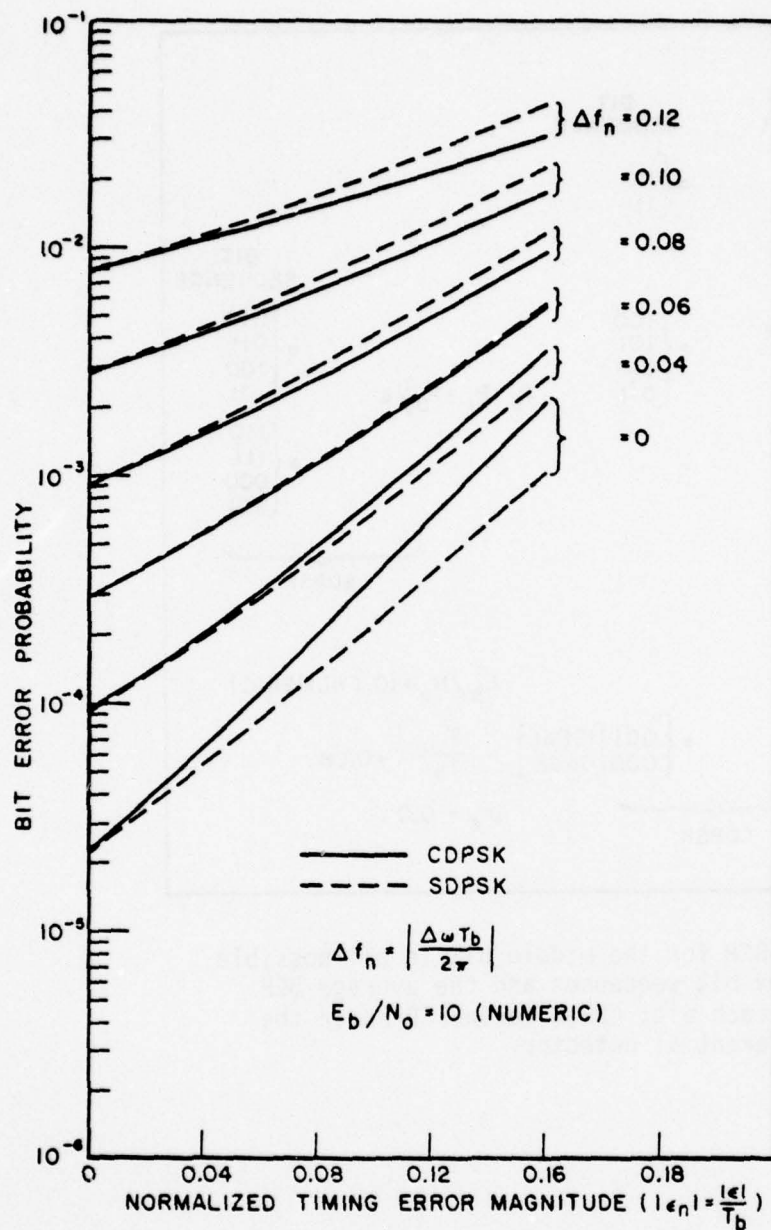
Figure 9. The average bit error probability versus the magnitude
of the normalized bit timing error for selected values
of the magnitude of the normalized $(\Delta\omega T_b/2\pi)$ frequency
offset in the differential detector; comparison of
CDPSK to SDPSK.

28
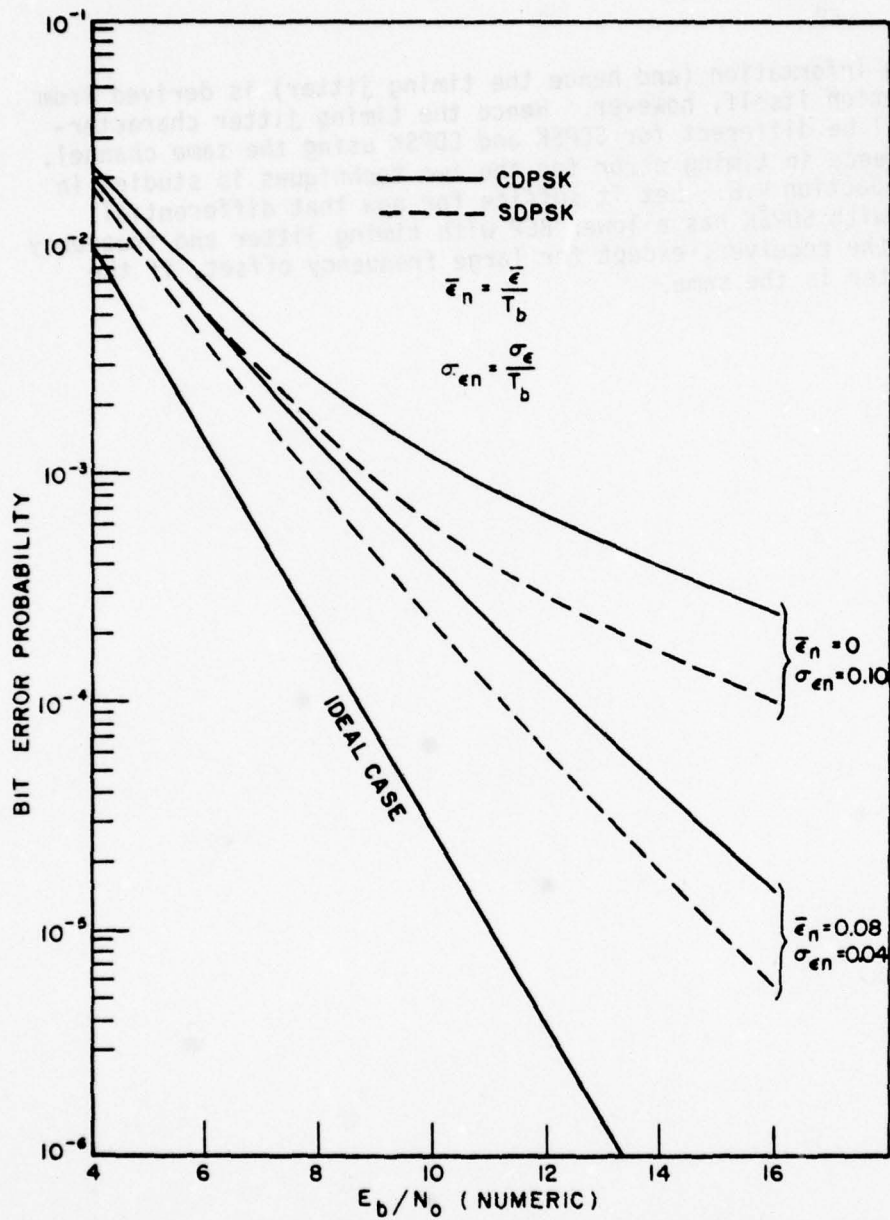
Figure 10. The average bit error probability versus the bit
energy to noise density ratio for selected values
of timing jitter and frequency offset; comparison
of CDPSK to SDPSK.

CHAPTER III
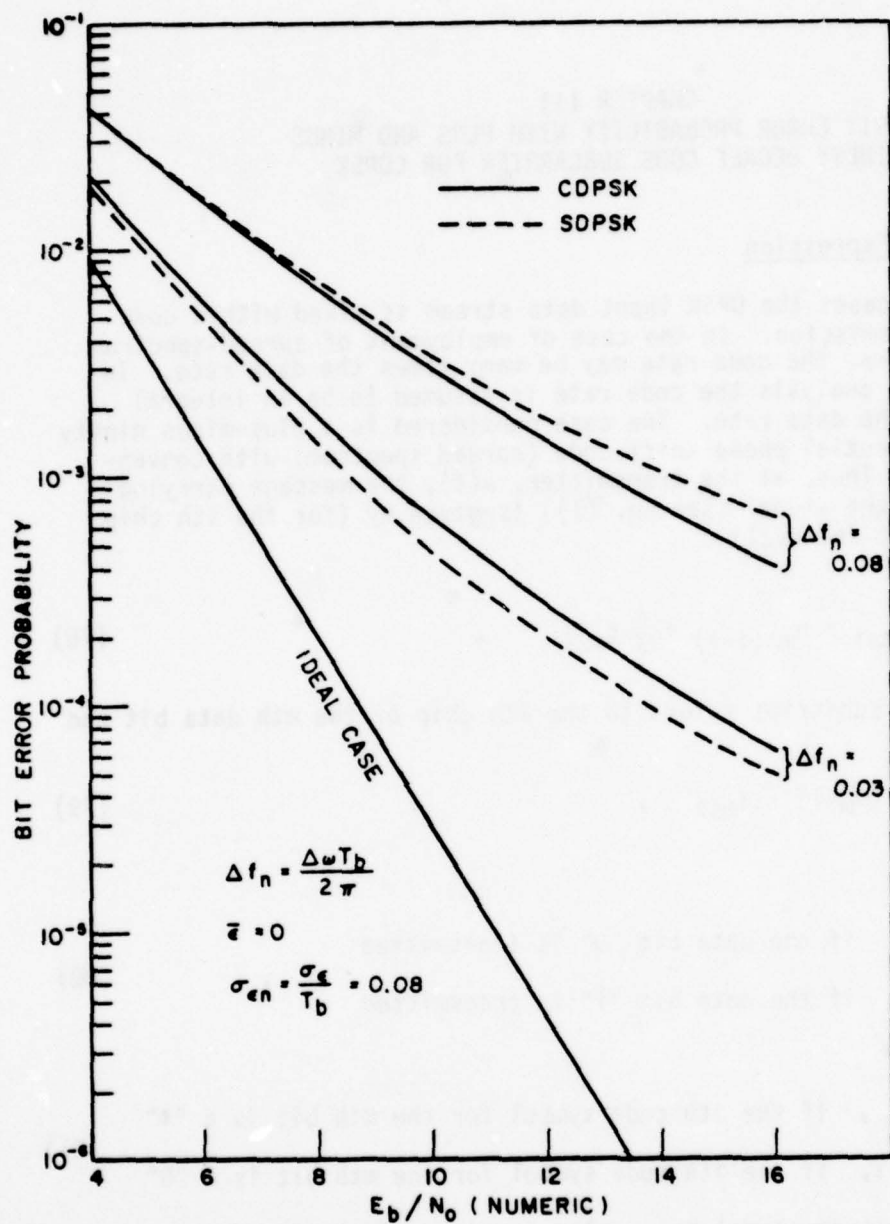## THE BIT ERROR PROBABILITY WITH PLUS AND MINUS
NINETY DEGREE CODE SUBCARRIER FOR CDPSK

A.   General Expression

In many cases the DPSK input data stream is mixed with a code prior to transmission. In the case of employment of spread-spectrum (SS) techniques, the code rate may be many times the data rate. In the following analysis the code rate is assumed to be an integral multiple of the data rate. The case considered is a plus-minus ninety degree differential phase shift code (spread spectrum) with conventional DPSK. Thus, at the transmitter, $\alpha(t)$, the message carrying parameter of the signal (see Eq. (1)) is given by (for the ith chip of the mth bit interval)

$$\alpha(t) = \alpha_{m\Delta i} = \alpha_{m\Delta(i-1)} + \frac{\pi}{2} \delta'_{m\Delta i} \quad , \tag{78}$$

where the $m\Delta i$ subscript refers to the ith chip of the mth data bit and

$$\delta'_{m\Delta i} = - (\delta_m - 1) \cdot \delta_{m\Delta i} \quad , \tag{79}$$

where

$$\delta_m = \begin{cases} 0 \ , & \text{if the data bit "0" is transmitted} \\ 2 \ , & \text{if the data bit "1" is transmitted} \end{cases} \quad , \tag{80}$$

and

$$\delta_{m\Delta i} = \begin{cases} 1 \ , & \text{if the ith code symbol for the mth bit is a "1"} \\ -1, & \text{if the ith code symbol for the mth bit is a "0"} \end{cases} \quad . \tag{81}$$

Thus, the resulting signal has a plus or minus ninety degree phase shift at each chip. The analysis is performed to determine the performance of this signal in the differential detector when white, Gaussian noise is present at the receiver which is imperfectly timed. The effect of frequency offset has been assumed to be negligible for the code subcarrier case. The analysis parallels that in [1] for CDPSK with zero and one hundred eighty degree spread spectrum.

30

Due to the nature of the problem, the BEP expression will be similar in form to Eq. (77). Since the code is present, however, signal phase transitions between bits will not necessarily correspond to whether a data bit "1" or "0" is transmitted. Thus the probability of error is the same for all bits in the eight different δ_{m-1} δ_m δ_{m+1} sequences. The essential difference between the coded and uncoded case, though, is that, with timing error, the bit signal vectors are different. With coding the mth bit signal vector, $\overline{S}_m$, consists of the vector sum of the properly orientated chip signal vectors, $\overline{S}_{m\Delta i}$, during that bit. That is,

$$\overline{S}_m = \sum_{i=1}^{k} \overline{S}'_{m\Delta i} \quad , \tag{82}$$

where $\overline{S}'_{m\Delta i}$ is $\overline{S}_{m\Delta i}$ shifted by an angle

$$\theta = -\frac{\pi}{2} \sum_{j=1}^{i} \delta_{m\Delta j} \quad , \tag{83}$$

and k is the number of chips per bit.

With imperfectly timed demodulation, the resultant chip signal vectors have different magnitude and phase errors. Using the procedure of Section II.B, the chip signal vector may be found to be, for $T_{b/k} > \epsilon \geq 0$,

$$\overline{S}'_{m\Delta i} = \frac{\sqrt{E_b}}{T_b} \left[\left(\frac{T_b}{k} - \epsilon \right) \overline{a}_{x'} + \delta_{m\Delta i} \epsilon \overline{a}_{y'} \right] \quad , \tag{84}$$

where $\overline{a}_{x'}$ is coincident with the mth bit signal vector, $\overline{S}_m$, for $\epsilon = 0$ and coding not present (i.e., the (x,y) coordinate frame shifted by an angle β).

For $\frac{T_b}{k} < \epsilon < 0$,

$$\overline{S}'_{m\Delta i} = \frac{\sqrt{E_b}}{T_b} \left[\left(\frac{T_b}{k} - |\epsilon| \right) \overline{a}_{x'} + \delta'_{m\Delta(i+1)} \epsilon \overline{a}_{y'} \right] \quad . \tag{85}$$

Therefore, the mth bit signal vector, given by Eq. (82) is

$$\overline{S}_m = \frac{\sqrt{E_b}}{T_b} \left[\left(\frac{T_b}{k} - |\epsilon| \right) k \overline{a}_{x'} + \epsilon(2 k_m - k) \overline{a}_{y'} \right] \quad , \tag{86}$$

31

where k_m is the number of $\delta_{m\Delta i}$ equal to minus one during the mth bit interval. An example signal vector is shown in Fig. 11.
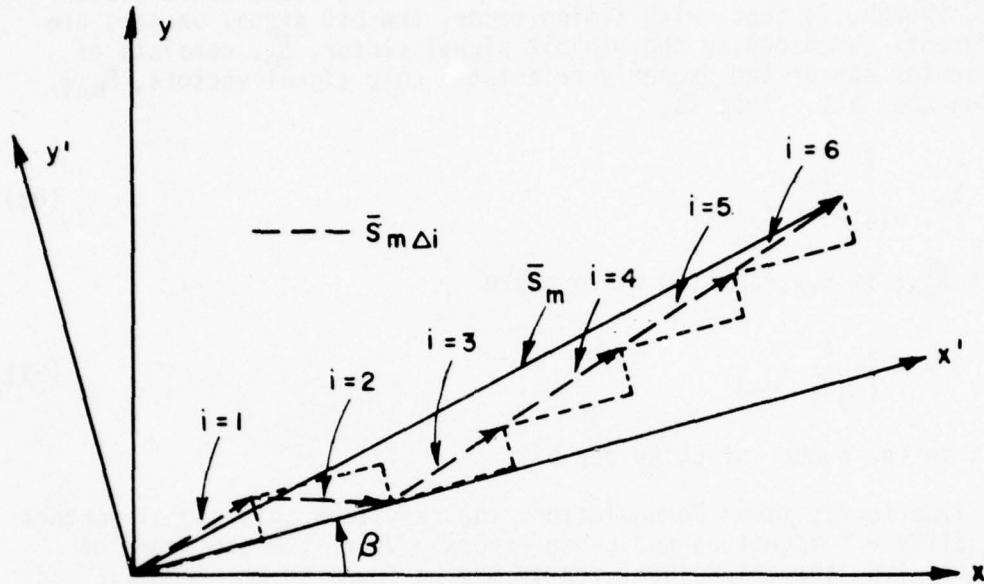
Figure 11.   The mth bit signal vector for k=6, $\varepsilon=.25T_b$, and:
$\delta_{m\Delta 1}=-1$; $\delta_{m\Delta 2}=1$; $\delta_{m\Delta 3}=-1$; $\delta_{m\Delta 4}=-1$; $\delta_{m\Delta 5}=-1$;
$\delta_{m\Delta 6}=-1$.

Let

$$\varepsilon_n \triangleq \frac{\varepsilon}{T_b} \qquad . \tag{87}$$

Equation (86) may, therefore, also be stated as

$$\bar{S}_m = \sqrt{E_b} \left[(1-k|\varepsilon_n|)\bar{a}_{x'} + |\varepsilon_n|(2\,k_m - k)\bar{a}_{y'} \right] \quad . \tag{88}$$

Thus, the value of L_1 can be calculated to be

$$L_1 = \sqrt{E_b} \left[(1-k|\varepsilon_n|)^2 + (|\varepsilon_n|(2\,k_1-k))^2 \right]^{1/2} \tag{89}$$

$$= \sqrt{E_b} \left[1-2k|\varepsilon_n| + 2|\varepsilon_n|^2 (k^2 + 2k_1^2 - 2k_1 k) \right]^{1/2} \quad . \tag{90}$$

32

Likewise for L_2,

$$L_2 = \sqrt{E_b} \left[1-2k|\epsilon_n|+2|\epsilon_n|^2(k^2+2k_2^2-2k_2k)\right]^{1/2} \tag{91}$$

Also, for $\Delta\phi_\epsilon$,

$$\Delta\phi_\epsilon = \tan^{-1}\left[\frac{2k_2-k}{|\epsilon_n|-k}\right] - \tan^{-1}\left[\frac{2k_1-k}{|\epsilon_n|-k}\right] \qquad . \tag{92}$$

Thus L_1, L_2, and $\Delta\phi_\epsilon$ depend on the parameters k, k_1, k_2, and ϵ, rather than ϵ, $\Delta\omega$, and $\{\delta\}$ as in Section II.B. The BEP given these parameters is, therefore (with the dependence on k implied),

$$P_E\Big|_{k_1,k_2} = \int_\epsilon K(L_1,L_2,\Delta\phi_\epsilon/k_1,k_2,\epsilon)p(\epsilon)d\epsilon \qquad , \tag{93}$$

where $K(L_1,L_2,\Delta\phi_\epsilon/k_1,k_2,\epsilon)$ is defined Eq. (74), although the dependence of L_1, L_2, $\Delta\phi_\epsilon$ on k_1 and k_2 is now shown. Eliminating the k_1 and k_2 conditions of the BEP expression

$$P_E = \int_{k_1}\int_{k_2}\int_\epsilon K(L_1,L_2,\Delta\phi_\epsilon/k_1,k_2,\epsilon)p(\epsilon)p(k_1)p(k_2)d\epsilon dk_1 dk_2 \quad . \tag{94}$$

As the probability density functions for k_1 and k_2 are discrete, Eq. (94) may be written as [1],

$$P_E = \sum_{k_1=0}^{k}\sum_{k_2=0}^{k} P_k(k_1)P_k(k_2) \int_\epsilon K(L_1,L_2,\Delta\phi_\epsilon/k_1,k_2,\epsilon)p(\epsilon)d\epsilon , \tag{95}$$

where

$$P_k(x) \triangleq \left(\frac{1}{2}\right)^k \frac{k!}{x!(k-x)!} \qquad . \tag{96}$$

B. Approximate Expression

For k large, the binomial distribution can be approximated by normal distribution with a mean of k/2 and a variance of k/4. Thus the probability density function of k_1 and k_2 may be written as

33

$$p(k_1) = \frac{1}{\sqrt{2\pi k/4}} \quad \exp\left[-\frac{(k_1 - k/2)^2}{2k/4}\right] \tag{97}$$

and

$$p(k_2) = \frac{1}{\sqrt{2\pi k/4}} \quad \exp\left[-\frac{(k_2 - k/2)^2}{2k/4}\right] \quad . \tag{98}$$

As k approaches infinity

$$p(k_1) \rightarrow \delta(k_1 - k/2) \tag{99}$$

and

$$p(k_2) \rightarrow \delta(k_2 - k/2) \quad , \tag{100}$$

where $\delta(\cdot)$ is the Dirac-delta function.

Thus, k_1 approaches $k/2$, as does k_2. In the limit L_1, L_2 and $\Delta\phi_\varepsilon$ become

$$L_1 = L_2 = \sqrt{E_b} \ (1 - k|\varepsilon_n|) \tag{101}$$

and

$$\Delta\phi_\varepsilon = 0 \quad . \tag{102}$$

Substituting this result into the bit error probability equations, produces the equation

$$P_E = \frac{1}{2} \int_{-\infty}^{\infty} \exp(-L^2/N_0) p(\varepsilon) d\varepsilon \quad , \tag{103}$$

where

$$L = (1 - k|\varepsilon_n|) \ \sqrt{E_b} \quad . \tag{104}$$

34

C.   Numerical Results

Equations (95) and (103) have been analyzed using numerical techniques. $K(L_1, L_2, \Delta\phi_\epsilon/k, k_1, k_2, \epsilon)$ as given in Eq. (74) was computed by using Simpson's one-third rule for integration with the same number of equal length increments as specified in the computer program described in Section II.C. The integral over ϵ was computed using Simpson's one-third rule with 150 equal length increments.

As Eq. (103) is identical to the equation developed in [1] for CDPSK with zero and one hundred eighty degree spread spectrum with k large, the BEP in the DD is identical with either plus and minus ninety degree or zero and one hundred eighty degree coding for a large code-to-data rate. For k equal to one, the average BEP is the same for the case studied as for SDD without coding, and the same for the case studied in [1] as for CDD without coding.

Thus, from the results of Chapter II, the BEP for differential detection with plus and minus ninety degree spread spectrum will be less than the BEP for zero and one hundred eighty degree spread spectrum for k equal to one.

Figure 12 illustrates these points for a particular value of timing error. The BEP values in both cases are seen to rapidly converge to their limiting values with increasing k. Thus CDPSK with plus and minus ninety degree spread spectrum has a lower BEP with timing jitter than CDPSK with zero and one hundred eighty degree spread spectrum for small code-to-data rate ratios.

Figures 13 and 14 illustrate the improved BEP performance with spread spectrum techniques. It should again be emphasized that in the above comparison the normalized timing jitter is assumed to be equal in both cases.

Figure 12. The average bit error probability versus the bit
energy to noise density ratio for selected
values of the code-to-data rate; comparison of
0-180° spread spectrum [1] to ±90° spread
spectrum with CDPSK in the differential detector.

36

Figure 13. The bit error probability versus the bit energy to noise density ratio for selected values of bit timing error; comparison of the improvement in performance with coding for 0-180° spread spectrum and ±90° spread spectrum with CDPSK in the differential detector.

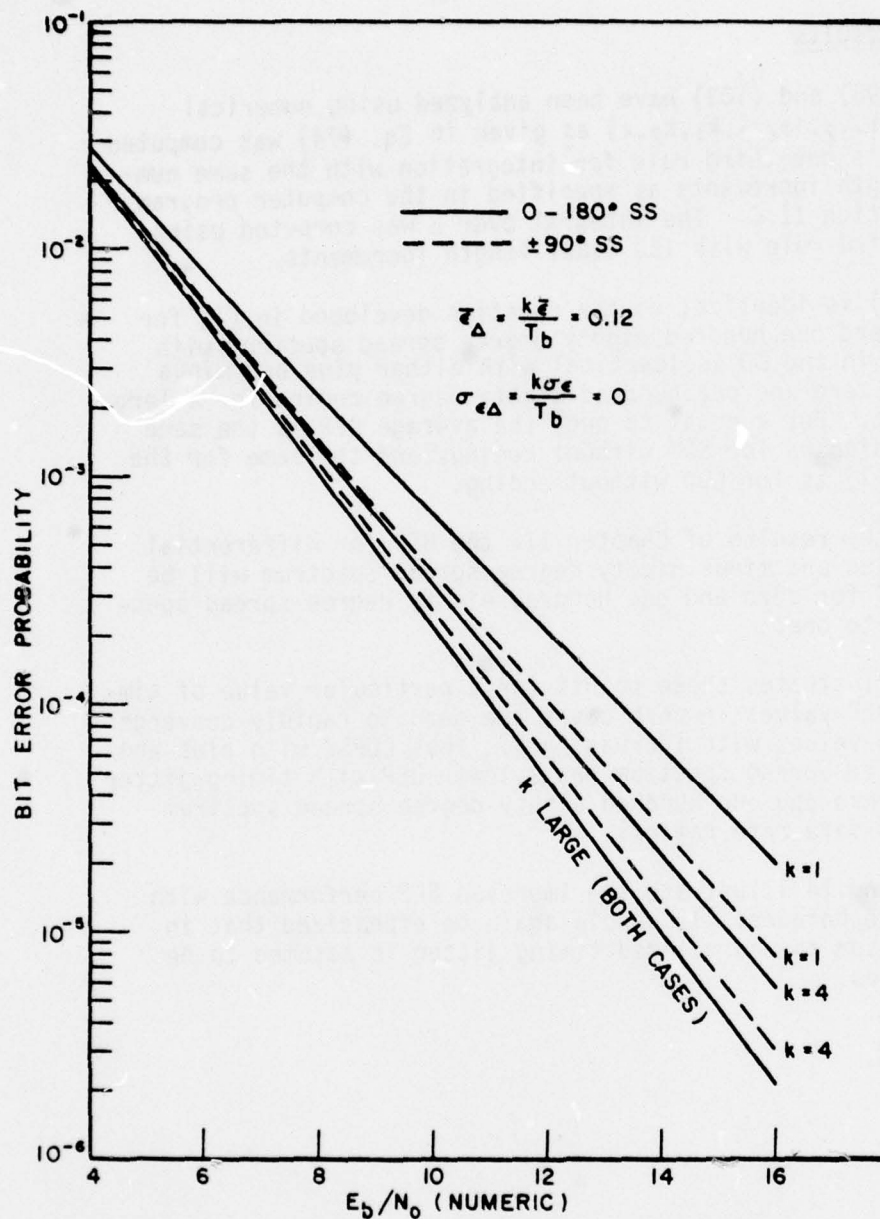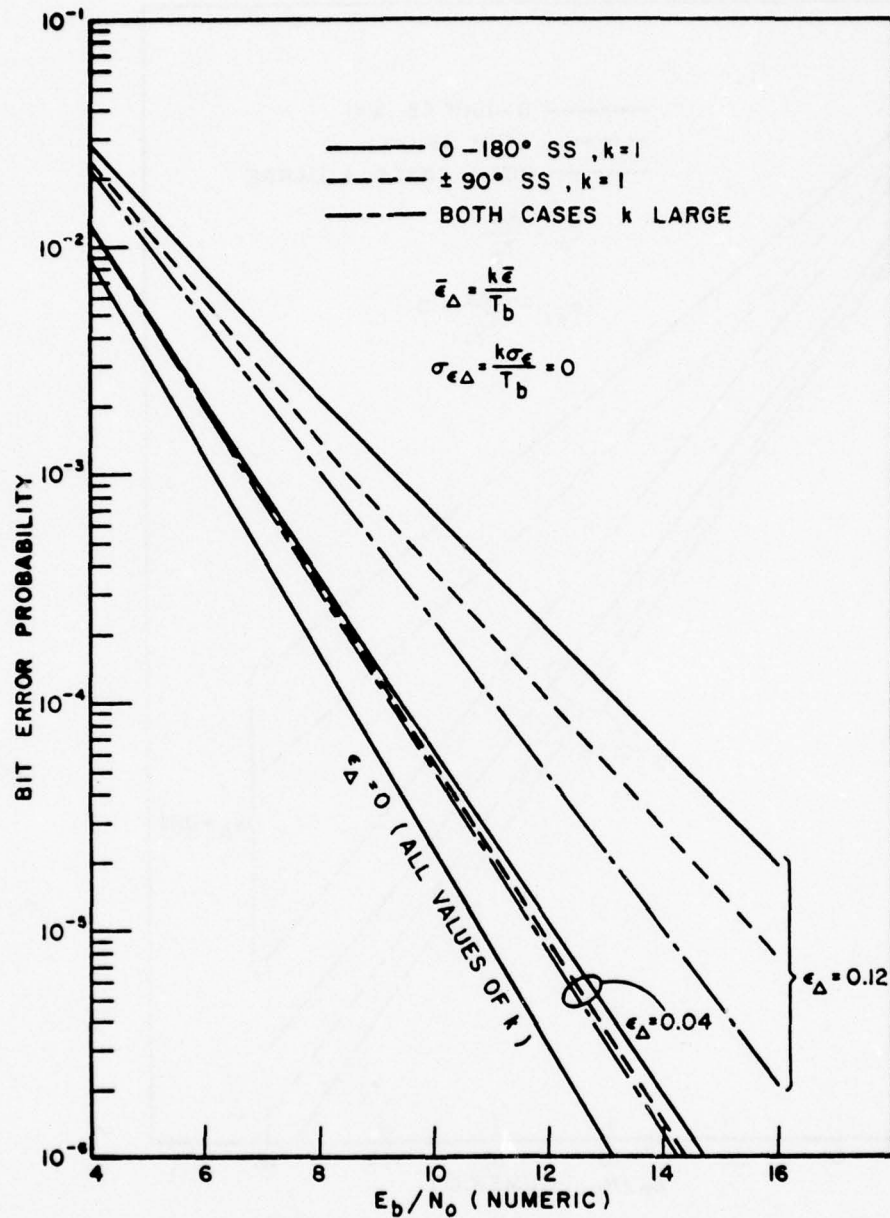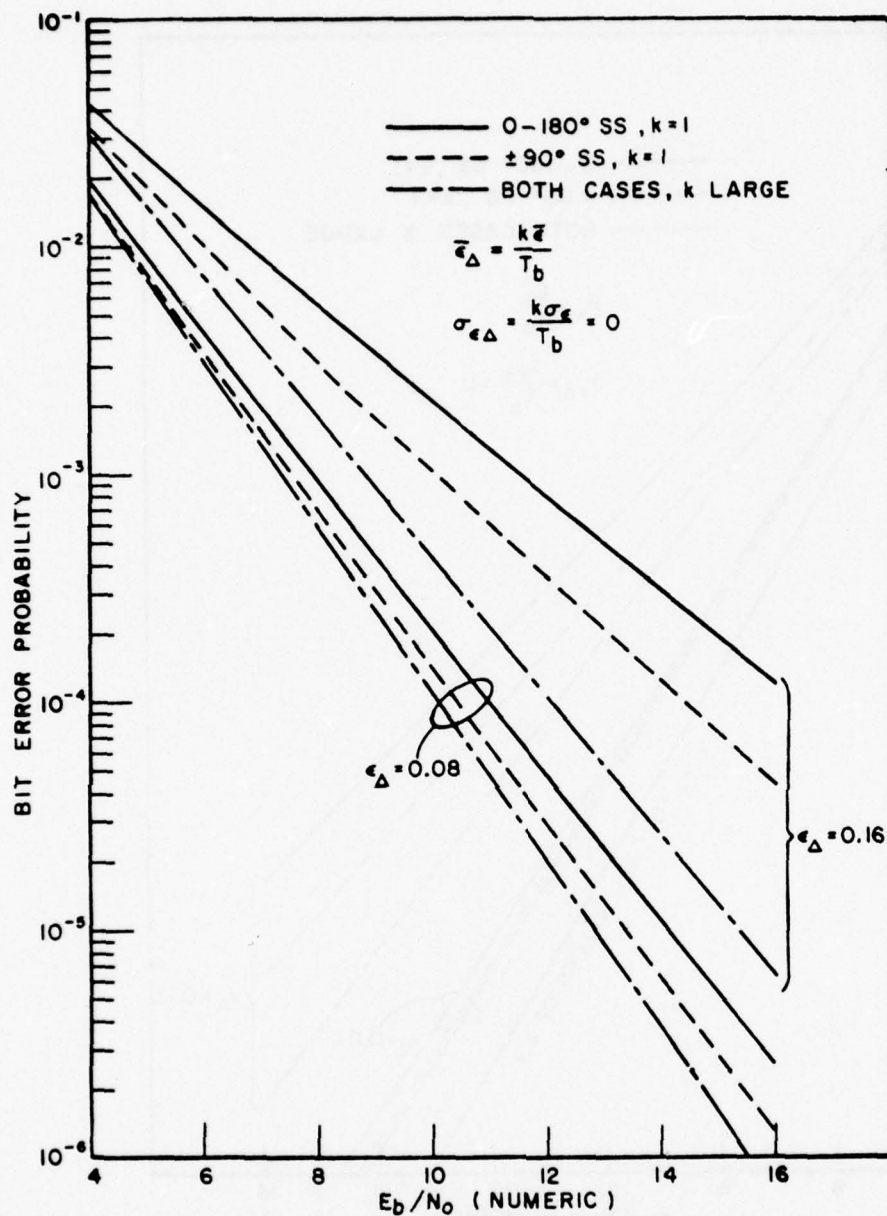Figure 14. The bit error probability versus the bit energy to
noise density ratio for selected values of bit
timing error; comparison of the improvement in
performance with coding for 0-180° spread spectrum
and ±90° spread spectrum with CDPSK in the
differential detector.

38

CHAPTER IV
BANDLIMITING AND HARDLIMITING OF DPSK

A. Introduction

In practical DPSK communication systems the received signal must
be bandlimited before demodulation. To be considered in this chapter
is the performance of CDPSK and SDPSK in the differential detector
when the bandlimited signal is demodulated. With bandlimiting, the
signal experiences both a reduction in energy and a phase shift, and
the noise at the receiver is correlated. An exact analysis of the
receiver BEP performance in the presence of noise is thus difficult
to determine. Hence, only the effect of bandlimiting on the signal
without noise has been studied in the following analysis. In Section
IV.B, the filtered signal envelope and resulting signal vectors
employed in the differential detector are derived for both CDPSK and
SDPSK. A rough comparison of performance in the differential detector
with noise present can be deduced from the signal vectors, and this is
also presented in Section IV.B.

In a DPSK communication system, the signal may be bandpass filter-
ed and hardlimited (e.g., in an active repeater in a satellite) during
transmission. When severe bandlimiting is effected it is very desir-
able to have a minimal regeneration of sidelobes when the signal is
hardlimited. A comparison of this regeneration for SDPSK and CDPSK
is presented in Section IV.C.

B. Differential Detection of a
Bandlimited Signal

1. Signal analysis

In Fig. 15, a block diagram of a differential detector preceded
by a bandpass filter is presented. As stated previously, the filter
produces both a decrease in amplitude and a time delay (i.e., a shift
in the occurence of minimum signal envelope) in the received signal.
Thus, filtering causes intersymbol interference whereby the mth bit
signal vector, $\overline{S}_m$, will be effected by δ_{m+1}, δ_{m-1}, δ_{m-2}, etc. (when
the time delay is less than one bit interval). In the subsequent
analysis it has been assumed that the effect on $\overline{S}_m$ of the δ_i's for i
less than m-2 is negligible, although the analysis could easily be
extended to such a case. The received signal under consideration is,
therefore (from Eq. (5) with $\Delta\omega=\epsilon=0$),
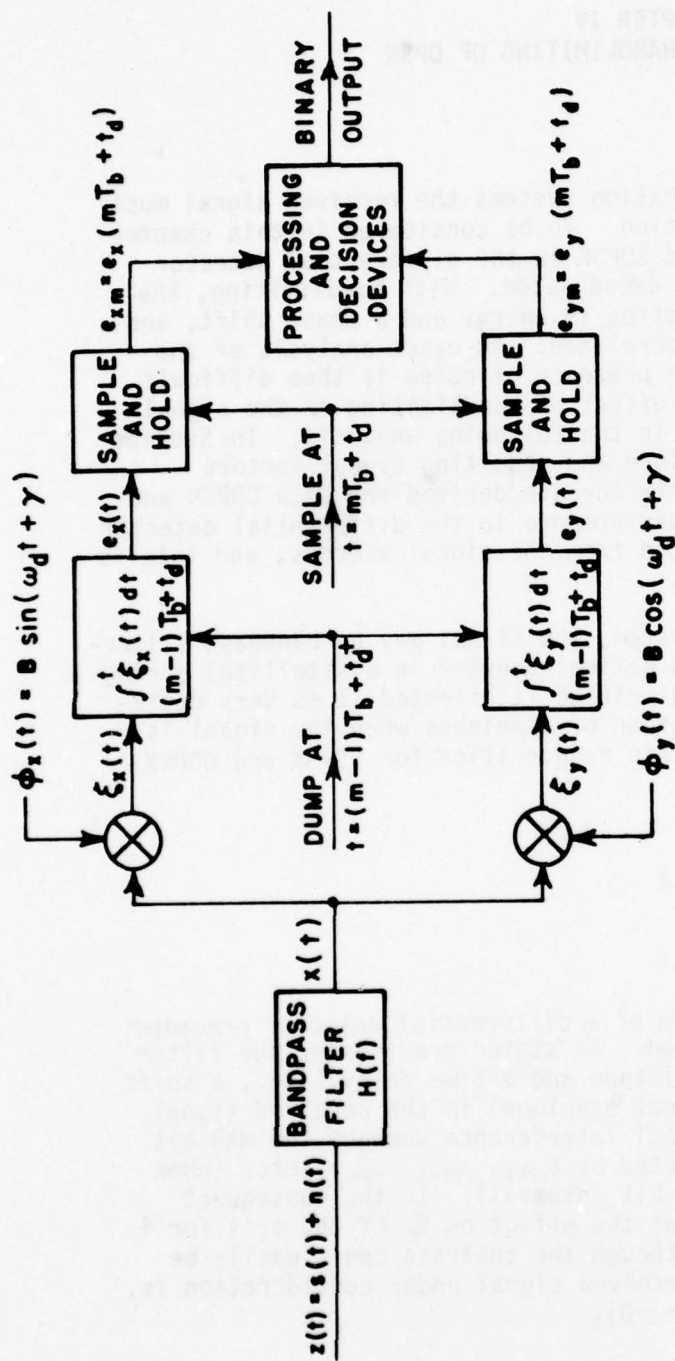
Figure 15. A differential detector preceded by a bandpass filter.

$$s(t) = A(t) \sin(\omega_d t + \alpha(t) + \alpha_r) \quad , \tag{105}$$

for $(m-3)T_b < t < (m+1)T_b$. As the effect of the signal for t less than $(m-3)T_b$ on $s(t)$ defined in Eq. (105) has been assumed negligible, a periodic $s(t)$ can be considered and a Fourier Series expansion of the signal developed. In this case (with $(m-3)T_b$ set equal to zero)

$$s(t) = \sum_{n=-\infty}^{\infty} S_n e^{jn\omega_0 t} \quad , \tag{106}$$

for $0 < t < 4T_b$, where

$$S_n = \frac{1}{4T_b} \int_0^{4T_b} s(t) e^{-jn\omega_0 t} dt \quad , \tag{107}$$

and

$$\omega_0 = \frac{2\pi}{4T_b} \quad . \tag{108}$$

The signal at the output of the filter, $x(t)$, is, therefore,

$$x(t) = \sum_{n=-\infty}^{\infty} X_n e^{jn\omega_0 t} \tag{109}$$

where

$$X_n = S_n \cdot H(n\omega_0) \quad , \tag{110}$$

where $H(\cdot)$ is the radian frequency response of the filter. To be considered in this chapter are both Butterworth and Chebyshev filters, and their transfer functions are provided below.

For a Butterworth filter,

$$|H(\omega)| = \frac{1}{\sqrt{1+(p)^{2n}}} \tag{111}$$

and

41

$$\underline{/H(\omega)} = \begin{cases} -\displaystyle\sum_{i=-n/2}^{n/2} \tan^{-1}\left[\dfrac{p-\sin\left(\frac{\pi}{2n} + \frac{i\pi}{n}\right)}{\cos\left(\frac{\pi}{2n} + \frac{i\pi}{n}\right)}\right] & \text{, for n even} \\[4mm] -\displaystyle\sum_{i=-(n-1)/2}^{(n-1)/2} \tan^{-1}\left[\dfrac{p-\sin\left(\frac{i\pi}{n}\right)}{\cos(i\pi/n)}\right] & \text{, for n odd,} \end{cases} \tag{112}$$

where n is the number of poles of the filter and p is the transform variable defined in Eq. (119) [3].

For a Chebyshev filter,

$$|H(\omega)| = \frac{1}{\sqrt{1+\varepsilon^2 C_n^2(\omega)}} \tag{113}$$

where

$$C_n(\omega) = \begin{cases} 2p\ C_n(\omega)-C_{n-2}(\omega) & \text{, } n=2,3,\cdots \\[2mm] p & \text{, } n=1 \\[2mm] 1 & \text{, } n=0 \end{cases} \tag{114}$$

and

$$\varepsilon = \sqrt{10\frac{AMAX}{5} - 1} \tag{115}$$

where AMAX is the peak-to-peak amplitude ripple in dB [3,4], and

$$\underline{/H(\omega)} = \begin{cases} -\displaystyle\sum_{i=-n/2}^{n/2} \tan^{-1}\left[\dfrac{p-b\ \sin\left(\frac{\pi}{2n} + \frac{i\pi}{n}\right)}{a\ \cos\left(\frac{\pi}{2n} + \frac{i\pi}{n}\right)}\right] & \text{, for n even} \\[4mm] -\displaystyle\sum_{i=-(n-1)/2}^{(n-1)/2} \tan^{-1}\left[\dfrac{p-b\ \sin\left(\frac{i\pi}{n}\right)}{a\ \cos\left(\frac{i\pi}{n}\right)}\right] & \text{, for n odd,} \end{cases} \tag{116}$$

where n and p are defined as before and

42

$$b = \frac{1}{2}\left[\left(\sqrt{\epsilon^{-2}+1}+\epsilon^{-1}\right)^{1/n} + \left(\sqrt{\epsilon^{-2}+1}+\epsilon^{-1}\right)^{-1/n}\right] \quad . \tag{117}$$

and

$$a = \frac{1}{2}\left[\left(\sqrt{\epsilon^{-2}+1}+\epsilon^{-1}\right)^{1/n} - \left(\sqrt{\epsilon^{-2}+1}+\epsilon^{-1}\right)^{1/n}\right] \quad . \tag{118}$$

In the above equations, with p equal to ω/ω_ℓ where ω is the frequency in radians per second and ω_ℓ is the filter cutoff frequency in radians per second, the filter is lowpass. For a bandpass filter, a geometric transform of the filter from a low pass to bandpass can be obtained by [4]:

$$p = \frac{\omega^2 - \omega_2^2}{\omega \cdot BW} \quad , \tag{119}$$

where ω_2 is the center radian frequency of the filter and BW is its bandwidth in radians per second. As this is a geometric transform, the filter characteristics are geometrically symmetric about the center frequency. This has an impact on the response of the filter to plus and minus ninety degree phase shifts in the carrier as explained in Section IV.B.2.

Let $w'(t)$ be the output of the mixers shown in Fig. 15, defined as

$$w'(t) \triangleq \mathcal{E}_x(t) + j\mathcal{E}_y(t) \tag{120}$$

$$= x(t)\{\sin(\omega_d t+\gamma) + j\cos(\omega_d t+\gamma)\} \quad . \tag{121}$$

From Eqs. (109) and (110) it follows that

$$w'(t) = \sum_{n=-\infty}^{\infty} H(n\omega_0)S_n e^{jn\omega_0 t}(j e^{-j(\omega_d t+\gamma)}) \quad . \tag{122}$$

If ω_d equals $i\omega_0$, where i is a positive integer (i.e., the carrier frequency is an integral multiple of one-quarter the data rate), then

$$w'(t) = \sum_{n=-\infty}^{\infty} H((n+i)\omega_0)S_{n+i} j e^{j(n\omega_0 t+\gamma)} \quad . \tag{123}$$

43

The signal, $w'(t)$ contains both baseband and double frequency components. As $w'(t)$ is integrated, only the baseband component, $w(t)$, defined as

$$w(t) \triangleq \mathcal{E}'_x(t) + \mathcal{E}'_y(t) \quad , \tag{124}$$

where $\mathcal{E}'_x(t)$ and $\mathcal{E}'_y(t)$ are the baseband components of $\mathcal{E}_x(t)$ and $\mathcal{E}_y(t)$, respectively, is of interest. It can easily be shown that $w(t)$ is given by (with a $-\beta$ degree phase shift)

$$w(t) = \sum_{n=-\infty}^{\infty} H((n+i)\omega_0) \, Y_n \, e^{jn\omega_0 t} \quad , \tag{125}$$

where

$$Y_n = \frac{1}{4T_b} \int_0^{4T_b} y(t) e^{-jn\omega_0 t} \, dt \quad , \tag{126}$$

and $y(t)$ is the baseband signal of $s(t)$, defined as

$$y(t) \triangleq \sqrt{E_b} \, [\cos(\alpha(t)) + j \sin(\alpha(t))] \quad . \tag{127}$$

The signal vector, $\overline{S}_m$, is, therefore,

$$\overline{S}_m = \int_{2T_b + t_d}^{3T_b + t_d} \operatorname{Re}[w(t)]dt \, \overline{a}_{x'} + \int_{2T_b + t_d}^{3T_b + t_d} \operatorname{Im}[w(t)]dt \, \overline{a}_{y'} \quad , \tag{128}$$

where t_d is the time delay in the occurence of minimum signal envelope in the filtered signal.

2. Numerical and Experimental Results

To verify the accuracy of Eqs. (125) through (127), numerical results were compared to experimental results obtained by filtering the SDPSK signal and CDPSK signal produced using the circuitry described in Chapter V. The filter employed in the circuit had a center frequency of 70 MHz and a bandwidth of 10 MHz. The filter was a five section Chebyshev with a peak-to-peak passband ripple of 0.05 dB.

In Figs. 16 through 27 experimental and theoretical results are given for both SDPSK and CDPSK. In the theoretical results, $|w(t)|$ has been plotted. For the experimental results, the modulated signal whose envelope has a magnitude, $|w(t)|$, is shown.

44

Figure 16. Theoretical filtered baseband signal

Modulation : SDPSK
Periodic input data {δ} : -1 1
Carrier freq. to data rate ratio: 56.0
Filter : Chebyshev
   No. of sections : 5
   Bandwidth to data rate ratio : 8.0
   Peak-to-peak passband ripple : 0.05 dB

$-\cdot\cdot-$ $\mathcal{E}'_x(t)$

$----$ $\mathcal{E}'_y(t)$

$———$ $|w(t)| = \sqrt{\mathcal{E}'^2_x(t) + \mathcal{E}'^2_y(t)}$

45

Figure 17. Experimental filtered signal envelope
              Modulation   : SDPSK
              Input data   : Pseudo-random
              Carrier freq.   : 70 MHz
              Data rate   : 1.25 MHz
              (Carrier freq. to data rate ratio: 56.0)
              Filter   : Chebyshev
                No. of sections   : 5
                Bandwidth   : 10 MHz
                (Bandwidth to data rate ratio : 8.0)
                Peak-to-peak passband ripple : 0.05 dB

46

Figure 18. Theoretical filtered baseband signal
Modulation : SDPSK
Periodic input data {δ} : -1 1
Carrier Freq. to data rate ratio: 28.0
Filter : Chebyshev
No. of sections : 5
Bandwidth to data rate ratio : 4.0
Peak-to-peak passband ripple : 0.05 dB

$-\cdot-$ $\mathcal{E}'_x(t)$

$----$ $\mathcal{E}'_y(t)$

$-----$ $|w(t)| = \sqrt{\mathcal{E}'^2_x(t) + \mathcal{E}'^2_y(t)}$

47

Figure 19.   Experimental filtered signal envelope
             Modulation   : SDPSK
             Input data   : Pseudo-random
             Carrier freq.   : 70 MHz
             Data rate   : 2.5 MHz
             (Carrier freq. to data rate ratio: 28.0)
             Filter   : Chebyshev
               No. of sections   : 5
               Bandwidth   : 10 MHz
               (Bandwidth to data rate ratio   : 4.0)
               Peak-to-peak passband ripple   : 0.05 dB

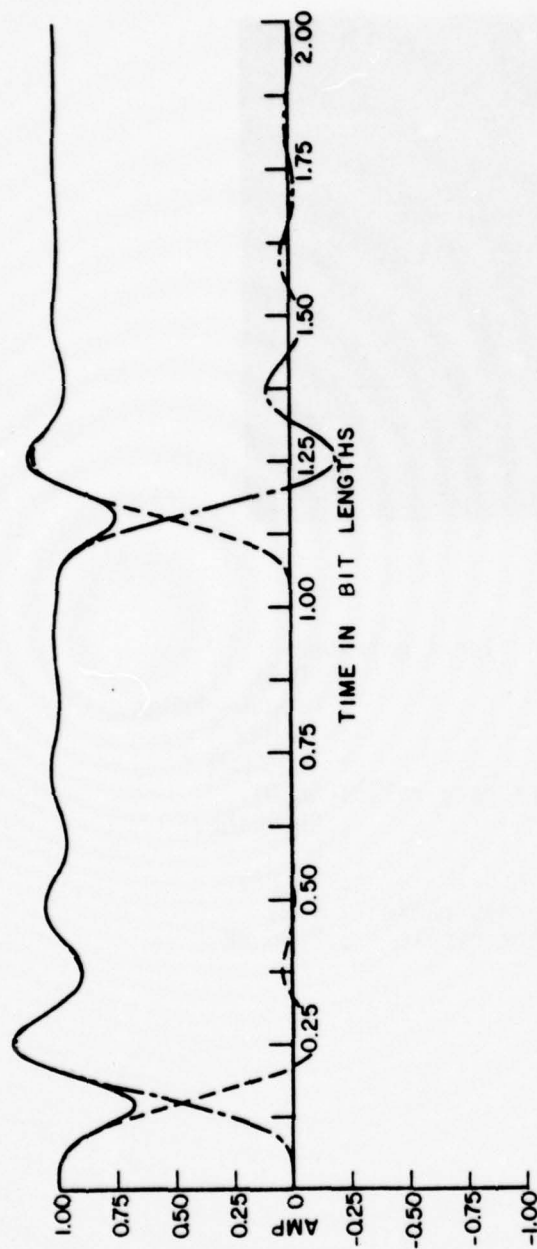Figure 20. Theoretical filtered baseband signal

Modulation : SDPSK
Periodic input data {δ} : -1 1
Carrier freq. to data rate ratio : 17.5
Filter : Chebyshev
No. of sections : 5
Bandwidth to data rate ratio : 2.5
Peak-to-peak passband ripple : 0.05 dB

$--\ \mathcal{E}'_x(t)$

$---\ \mathcal{E}'_y(t)$

$---\ |w(t)| = \sqrt{\mathcal{E}'^2_x(t) + \mathcal{E}'^2_y(t)}$

49

1 3 2 4

Figure 21. Experimental filtered signal envelope
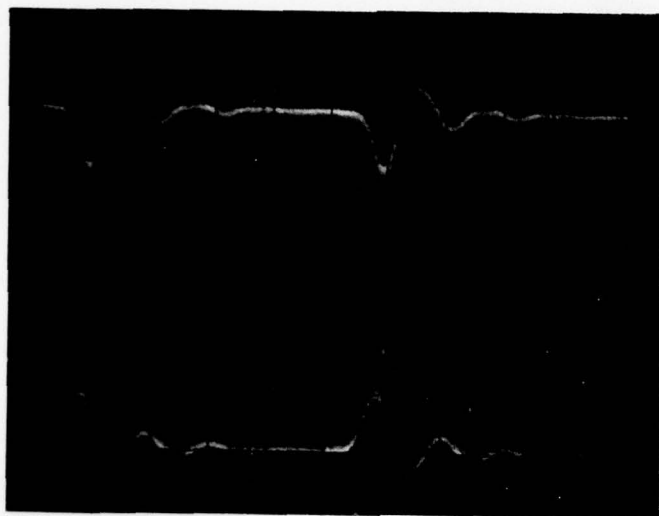   Modulation   : SDPSK
         Input data   : Pseudo-random
         Carrier freq.   : 70 MHz
         Data rate   : 4.0 MHz
         (Carrier freq. to data rate ratio: 17.5)
         Filter   : Chebyshev
           No. of sections   : 5
           Bandwidth   : 10 MHz
           (Bandwidth to data rate ratio   : 2.5)
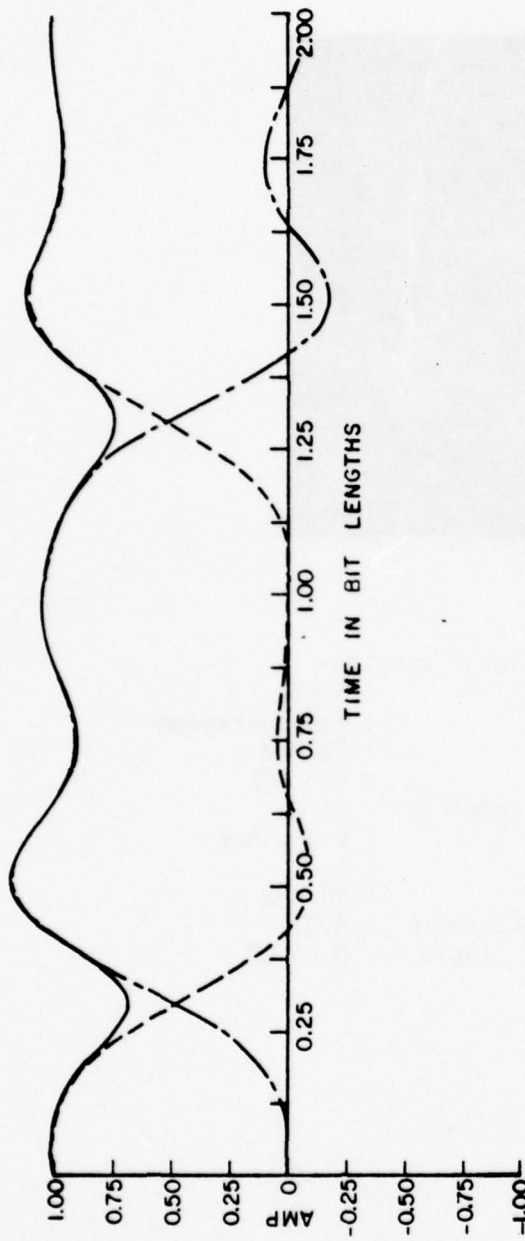   Peak-to-peak passband ripple   : 0.05 dB

Figure 22. Theoretical filtered baseband signal
Modulation : CDPSK
Periodic input data {δ} : 2 2
Carrier freq. to data rate ratio: 56.0
Filter : Chebyshev
No. of sections : 5
Bandwidth to data rate ratio : 8.0
Peak-to-peak passband ripple : 0.05 dB

$$—\cdot— \quad \mathcal{E}_x'(t)$$

$$——— \quad \mathcal{E}_y'(t)$$

$$\underline{\quad\quad} \quad |w(t)| = \sqrt{\mathcal{E}_x'^2(t) + \mathcal{E}_v'^2(t)}$$

TIME IN BIT LENGTHS

AMP

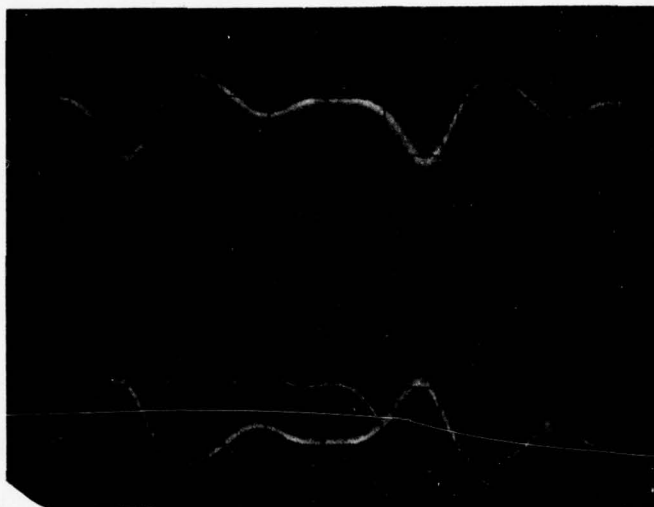Figure 23.   Experimental filtered signal envelope
            Modulation   : CDPSK
            Input data   : Pseudo-random
            Carrier freq.   : 70 MHz
            Data rate   : 1.25 MHz
            (Carrier freq. to data rate ratio: 56.0)
            Filter   : Chebyshev
              No. of sections   : 5
              Bandwidth   : 10 MHz
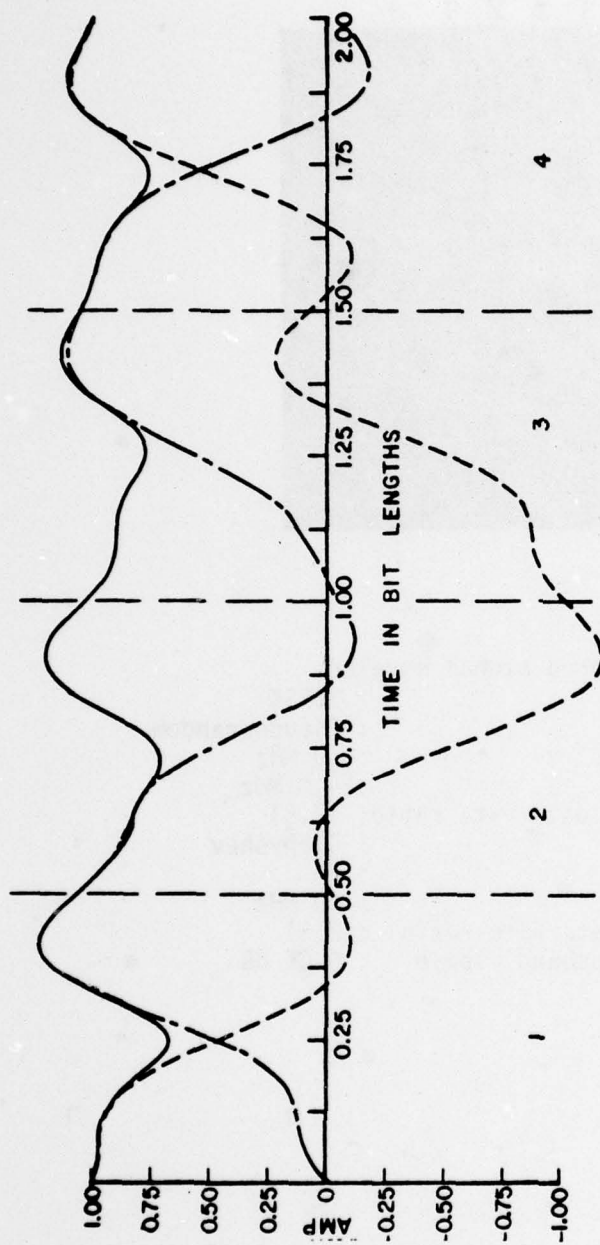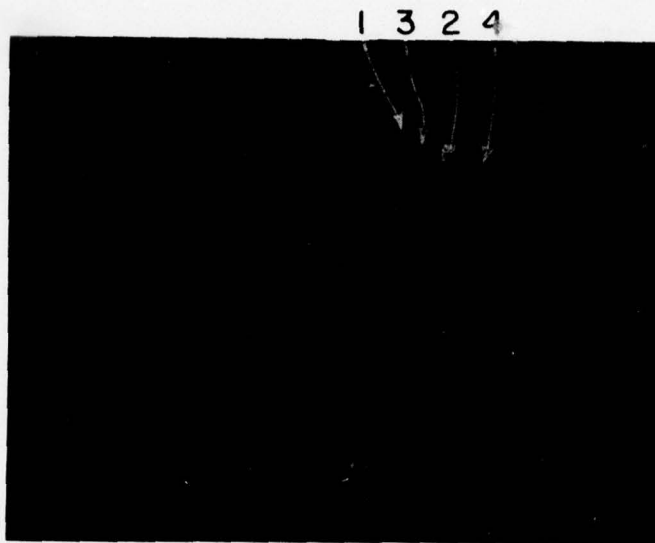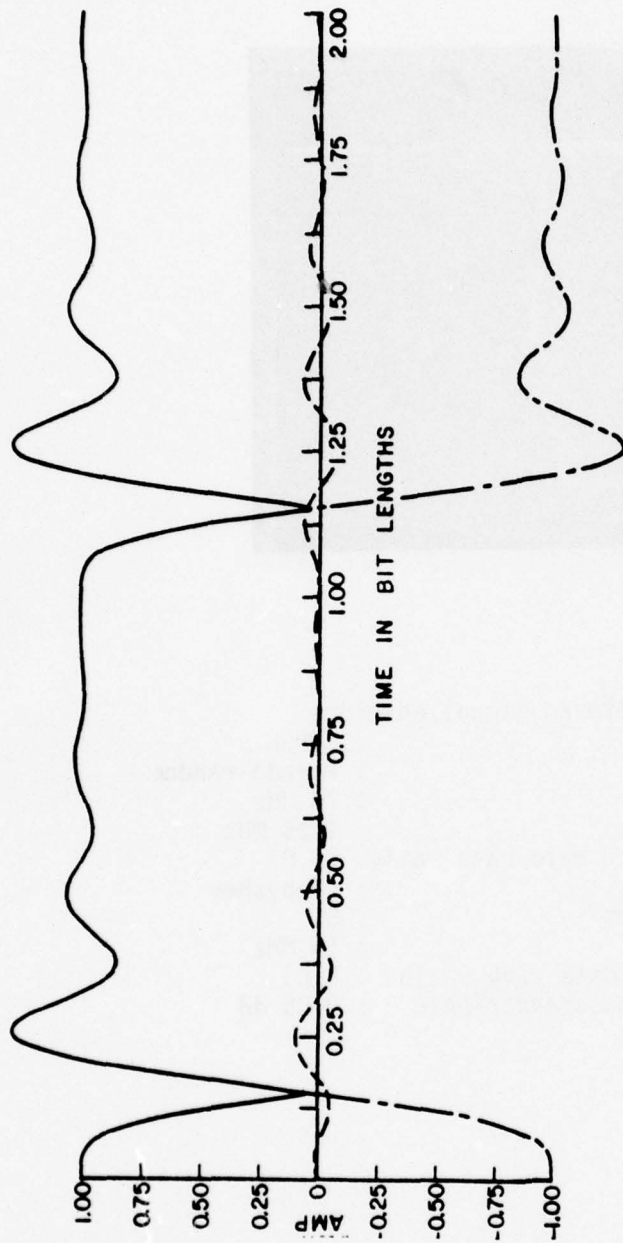   (Bandwidth to data rate ratio : 8.0)
              Peak-to-peak passband ripple   : 0.05 dB

Figure 24. Theoretical filtered baseband signal

Modulation	: CDPSK
Periodic input data {δ}	: 2 2
Carrier freq. to data rate ratio:	28.0
Filter	: Chebyshev
No. of sections	: 5
Bandwidth to data rate ratio	: 4.0
Peak to peak passband ripple	: 0.05 dB

—··— $\xi'_x(t)$

——— $\xi'_y(t)$

——— $|w(t)| = \sqrt{\xi'^2_x(t) + \xi'^2_y(t)}$

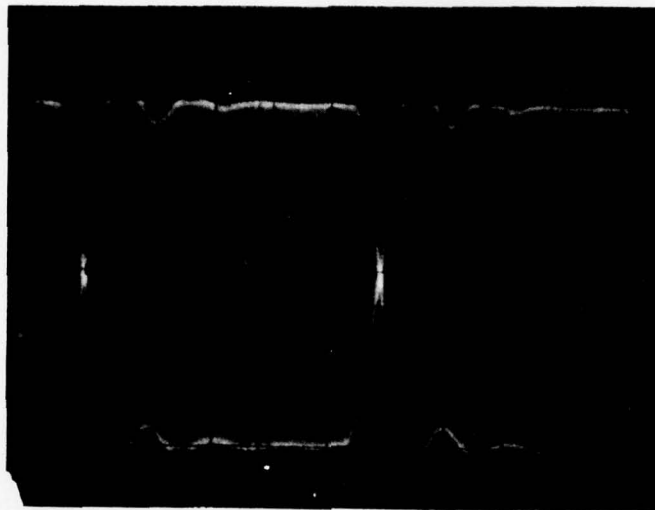Figure 25.   Experimental filtered signal envelope
            Modulation   : CDPSK
            Input data   : Pseudo-random
            Carrier freq.   : 70 MHz
            Data rate   : 2.5 MHz
            (Carrier freq. to data rate ratio: 28.0)
            Filter   : Chebyshev
              No. of sections   : 5
              Bandwidth   : 10 MHz
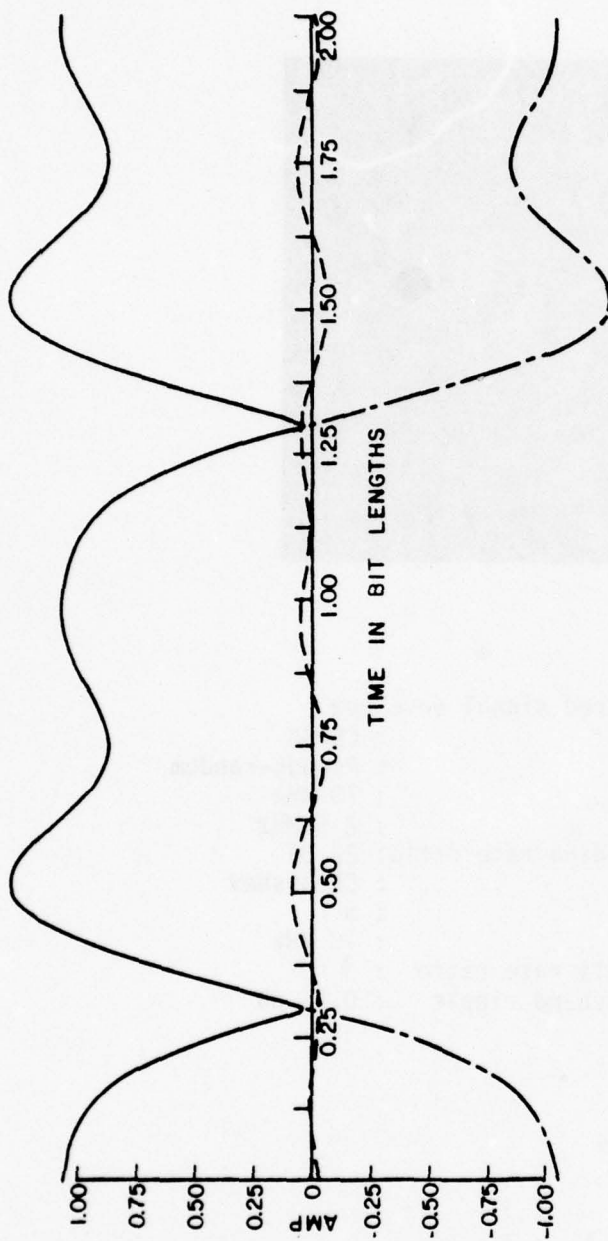   (Bandwidth to data rate ratio   : 4.0)
              Peak-to-peak passband ripple   : 0.05 dB

54

Figure 26. Theoretical filtered baseband signal

Modulation	: CDPSK
Periodic input data $\{\delta\}$	: 0 2 2 0
Carrier freq. to data rate ratio:	17.5
Filter	: Chebyshev
No. of sections	: 5
Bandwidth to data rate ratio	: 2.5
Peak-to-peak passband ripple	: 0.05 dB

$$-\cdot-\cdot- \quad \xi'_x(t)$$
$$----- \quad \xi'_y(t)$$
$$——— \quad |w(t)| = \sqrt{\xi'^2_x(t) + \xi'^2_y(t)}$$

55

2 1 4 3
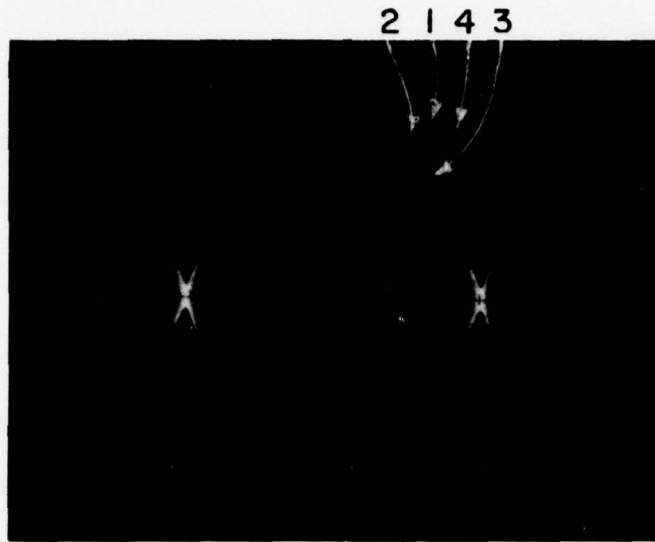
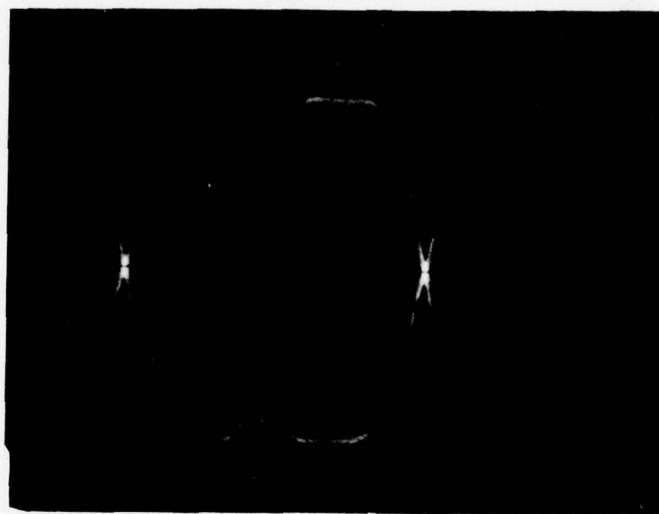Figure 27. Experimental filtered signal envelope
            Modulation   : CDPSK
            Input data   : Pseudo-random
            Carrier freq.   : 70 MHz
            Data rate   : 4.0 MHz
            (Carrier freq. to data rate ratio: 17.5)
            Filter   : Chebyshev
              No. of sections   : 5
              Bandwidth   : 10 MHz
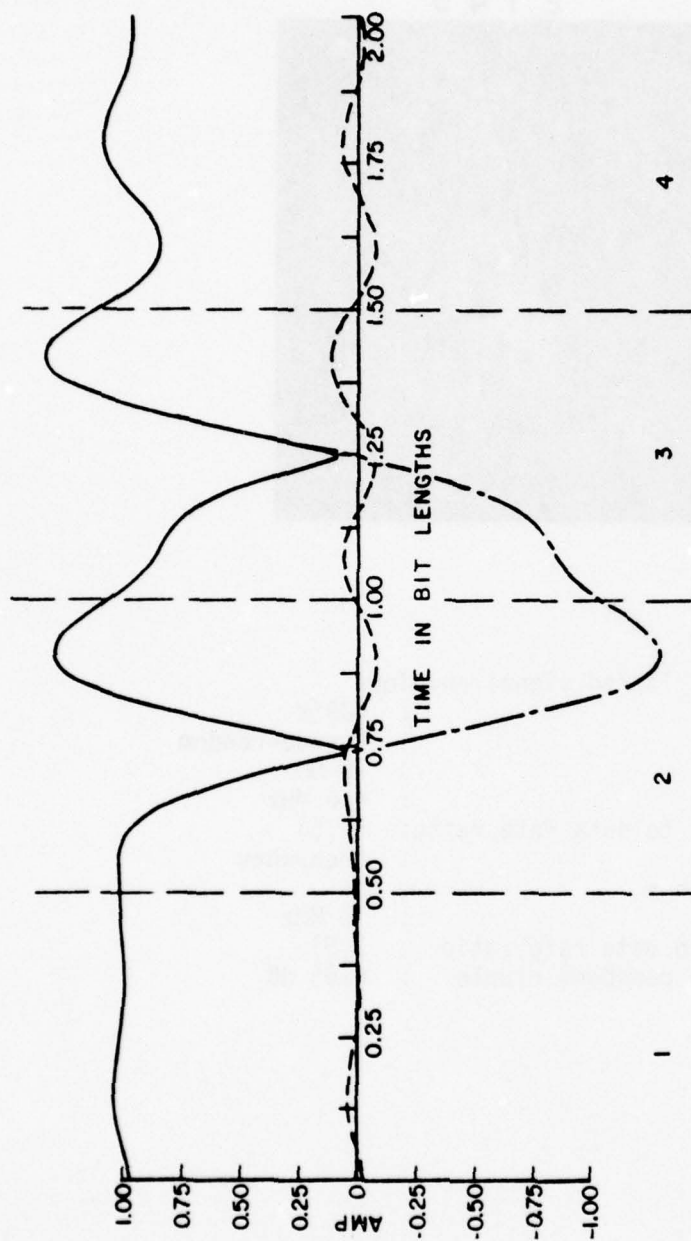   (Bandwidth to data rate ratio : 2.5)
              Peak-to-peak passband ripple   : 0.05 dB

56

In Figs. 16 and 18 theoretical results for SDPSK are presented for the case where a minus ninety degree phase transition is followed by a plus ninety degree phase transition. In Figs. 16 and 18 the response of the signal envelope at the output of the filter differs for the two transitions. This is due to the fact that, as stated in Section IV.B.2, a geometrically-symmetric filter has been employed. Thus, the filter characteristics differ for linear frequency differences above and below the center frequency of the filter. Because a +90° phase shift has a frequency spectrum which is the mirror image of a -90° phase shift frequency spectrum about the carrier frequency, each phase shift will not be effected in a similar manner by the filter. Experimental results were obtained from a pseudo-random input data stream, and, thus, the two different responses are superimposed on the photographs in Figs. 17 and 19. Because the effect of a phase transition on the signal envelope of the next transition is negligible, as illustrated in Figs. 17 and 19, only two phase transitions are shown in Figs. 16 and 18. As the data rate is increased (i.e., the bandwidth to data rate ratio is decreased), the effect of previous transitions cannot be neglected, however. In Fig. 20 the responses associated with the four possible pairs of phase transitions are shown. Numbered one to four, these curves match the four separate traces which can be seen in Fig. 21.

For CDPSK, theoretical results are presented in Figs. 22 and 24 for two consecutive 180° phase shifts. The envelope response is, therefore, the same in both bit intervals. For the experimental results, a pseudo-random input data stream again was employed. Hence, in the photographs in Figs. 23 and 25, the filtered signal with a 180° phase shift and 0° (constant envelope) phase shift are superimposed. Again, in Figs. 22 and 24 only two phase transitions are shown because the effect of a phase transition on the next phase transition is negligible. As before, when the data rate is increased, this effect cannot be neglected, and, thus, the responses associated with the four possible pairs of phase transitions are shown in Fig. 26. Numbered one to four, these curves also match the four separate traces in Fig. 27. Thus, good agreement between experimental results and numerical results has been obtained.

In Fig. 28 a comparison has been made between the response of SDPSK and CDPSK in the same filter. The overshoot and ringing is seen to be greater for CDPSK. The time delay (crossing of the in quadrature responses for SDPSK and zero crossing for CDPSK) is approximately the same for both techniques, however (see Table 1).

The response of both SDPSK and CDPSK to Chebyshev and Butterworth filters is illustrated in Figs. 29 and 30. Note that the time delay and overshoot is less with a Butterworth filter with identical (3 dB for Butterworth) bandwidth and number of poles. This, of course, is due to the less steep roll off of filter out of band and the more linear phase shift in band.

57
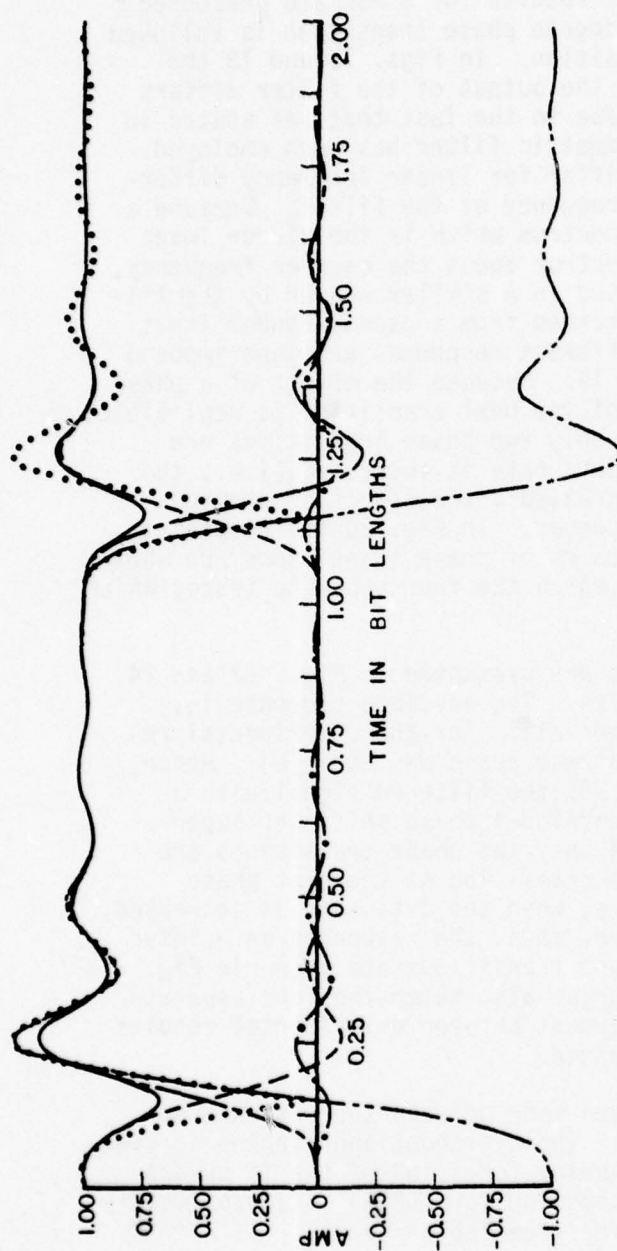
Figure 28. Comparison of theoretical SDPSK and CDPSK filtered baseband signals

Carrier freq. to data rate ratio: 56.0

Filter   : Chebyshev
No. of sections   : 5
Bandwidth to data rate ratio   : 8.0
Peak-to-peak passband ripple   : 0.05 dB

SDPSK
Periodic input data {δ}: -1 1

$-\cdot-$ $\tilde{\mathcal{E}}_x'(t)$

$---$ $\mathcal{E}_y'(t)$

$\underline{\hspace{1cm}}$ $|w(t)| = \sqrt{\mathcal{E}_x'^2(t) + \mathcal{E}_y'^2(t)}$

CDPSK
Periodic input data {δ}: 2 2

$-\cdot\cdot-$ $\mathcal{E}_x'(t)$

$-\cdot-$ $\mathcal{E}_y'(t)$

$\cdots\cdots$ $|w(t)|$

58
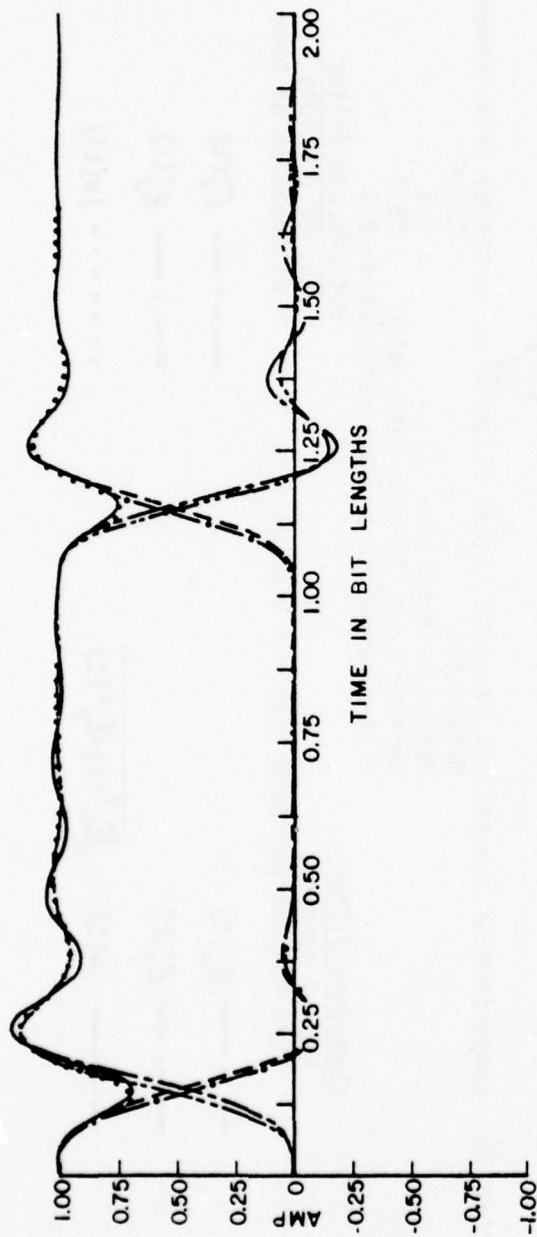
Figure 29. Comparison of theoretical baseband signal filtered by Chebyshev or Butterworth filter

Modulation : SDPSK
Periodic input data {δ} : -11
Carrier freq. to data rate ratio : 56.0
Filter bandwidth to data rate ratio: 8.0

Chebyshev filter
No. of sections : 5
Peak-to-peak passband ripple: 0.05 dB

Butterworth filter
No. of sections : 5
Attenuation at band edge: 3 dB

$\mathcal{E}'_x(t)$

$\mathcal{E}'_y(t)$

$|w(t)|$

$|w(t)| = \sqrt{\mathcal{E}'^2_x(t) + \mathcal{E}'^2_y(t)}$

TIME IN BIT LENGTHS
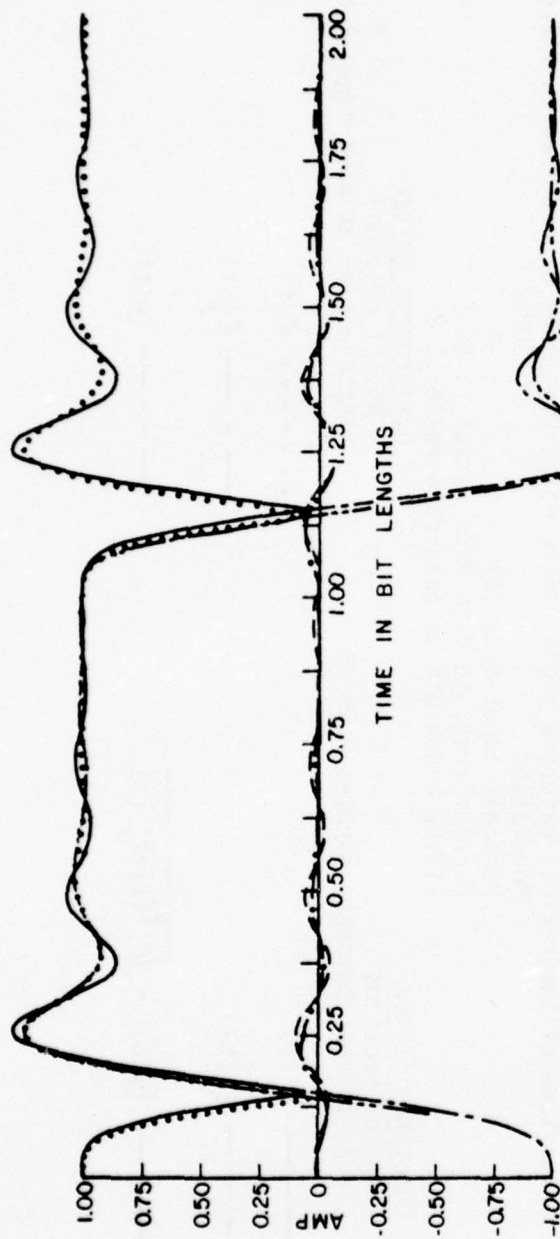
Figure 30. Comparison of theoretical baseband signal filtered by Chebyshev or Butterworth filter

Modulation : CDPSK
Periodic input data {δ}
Carrier freq. to data rate ratio : 56.0
Filter bandwidth to data rate ratio: 8.0

Chebyshev filter
No. of sections : 5
Peak-to-peak passband ripple : 0.05 dB

Butterworth filter
No. of sections : 5
Attenuation at band edge: 3 dB

$- - - \quad \mathcal{E}'_x(t)$

$- \cdot - \quad \mathcal{E}'_y(t)$

$\cdots\cdots\cdots \quad |w(t)|$

$--- \quad \mathcal{E}'_x(t)$

$--- \quad \mathcal{E}'_y(t)$

$——— \quad |w(t)| = \sqrt{\mathcal{E}'^2_x(t) + \mathcal{E}'^2_y(t)}$

60

Tables 1 and 2 provide a listing of the bit signal vectors, $\overline{S}_m$, computed using Eq. (128), from the envelopes shown for the theoretical results. In Table 2, eight combinations of phase transitions are given for each case, because, as stated previously, the mth bit interval is effected significantly by the phase transition occuring due to δ_{m-1}.

As illustrated in Tables 1 and 2 SDPSK has fairly constant amplitude bit signal vectors, whereas the CDPSK bit signal vectors vary in magnitude, although for a given data rate and filter, the average magnitude is about the same. The SDPSK bit signal vectors show a much greater phase error, however. Furthermore, the delay of the filter is approximately the same for both cases. A comparison in BEP performance in the differential detector is, therefore, not easily discernable from this data.

As mentioned in the introduction, analysis of BEP with noise in the case of a filtered input signal is quite complicated and will not be undertaken at this time. A rough estimation of performance can be obtained, however, if it is assumed that the filtered noise is white and Gaussian. This assumption is, of course, not correct, but it will aid in determining the performance of the two techniques to some degree

From Tables 1 and 2 the signal vector magnitudes (L_1 and L_2) and phase error ($\Delta\phi_\epsilon$) for each of the possible pairs of bits can be determined for each case. By employing Eq. (74), the average BEP may then be determined for each case under the assumption of white, Gaussian noise. Table 3 presents the results of such an analysis for the cases studied in Tables 1 and 2. From Table 3 a slight improvement in BEP with a SDPSK modulated carrier can be seen for all cases. However, even more important is the wide variation of BEP for the data bit "1" as compared to "0" for CDPSK. This variation is not present with SDPSK because all phase transitions are of a magnitude of 90°. A slight improvement in performance is also illustrated with the use of a Butterworth filter.

C.   Hardlimiting of the Bandlimited
     DPSK Signal

To be analyzed in this section is the effect of hardlimiting on the bandlimited DPSK signal. Of concern in Section IV.B was the time domain characteristics of the DPSK signal because the BEP is based upon the integration of the signal in the differential detector. With respect to hardlimiting, the power spectral density of the signal is also of interest because, as stated previously, it is desirable to have a minimum regeneration of the filtered sidelobes in this case. Other modulation techniques which attempt to minimize the hardlimiting effect on the signal spectrum are minimum shift keying (MSK) and offset keyed quadrature phase shift keying (OK-QPSK) [5].

61

TABLE 1
BIT SIGNAL VECTORS AFTER FILTERING

Modulation Type	Carrier Freq. to Data Rate	Filter Type*	Modulation Phase Transition at		Signal Vector $\overline{S}_m$	Delay (Portion of Bit)
			Beginning of Bit	End of Bit		
SDPSK	28	1	$+90°$	$+90°$	$.951\underline{/1.27°}$	.296
			$+90°$	$-90°$	$.943\underline{/-2.76°}$	.296
			$-90°$	$+90°$	$.956\underline{/3.45°}$	.296
			$-90°$	$-90°$	$.946\underline{/-.654°}$	.298
	56	1	$+90°$	$+90°$	$.975\underline{/.821°}$	.150
			$+90°$	$-90°$	$.972\underline{/-1.24°}$	.150
			$-90°$	$+90°$	$.979\underline{/1.68°}$	.150
			$-90°$	$-90°$	$.975\underline{/-.371°}$	.150
	56	0	$+90°$	$+90°$	$.976\underline{/.872°}$	.140
			$+90°$	$-90°$	$.973\underline{/-1.20°}$	.140
			$-90°$	$+90°$	$.980\underline{/1.61°}$	.140
			$-90°$	$-90°$	$.976\underline{/-.445°}$	.140
CDPSK	28	1	$0°$	$0°$	$1\underline{/0°}$	--
			$0°$	$180°$	$.931\underline{/.509°}$	.296
			$180°$	$0°$	$.964\underline{/.238°}$	.298
			$180°$	$180°$	$.899\underline{/.881°}$	.298
	56	1	$0°$	$0°$	$1\underline{/0°}$	--
			$0°$	$180°$	$.966\underline{/.234°}$	.148
			$180°$	$0°$	$.984\underline{/.211°}$	.148
			$180°$	$180°$	$.950\underline{/.467°}$	.148
	56	0	$0°$	$0°$	$1\underline{/0°}$	--
			$0°$	$180°$	$.966\underline{/.213°}$	.139
			$180°$	$0°$	$.986\underline{/.210°}$	.139
			$180°$	$180°$	$.952\underline{/.433°}$	.139

*Note: 1   Filter   : Chebyshev
           No. of sections   : 5
           Peak-to peak passband ripple   : 0.05 dB
           Carrier freq. to bandwidth ratio: 7.0

        0   Filter   : Butterworth
           No. of sections   : 5
           Carrier freq. to bandwidth ratio: 7.0

62

TABLE 2
BIT SIGNAL VECTORS AFTER FILTERING

Modulation Type	Carrier Freq. to Date Rate Ratio	Filter Type (see note on Table 1)	Modulation Phase Transition at			Signal Vector $\underline{S}_m$	Time Delay (Portion of Bit)
			Beginning of Previous Bit	Beginning of Bit	End of Bit		
SDPSK	17.5	1	+90°	+90°	+90°	$.927\underline{/2.15°}$	.472
			−90°	+90°	+90°	$.917\underline{/2.59°}$	.486
			+90°	+90°	−90°	$.920\underline{/-4.50°}$	.470
			−90°	+90°	−90°	$.910\underline{/-5.10°}$	.484
			+90°	−90°	+90°	$.925\underline{/5.81°}$	.484
			−90°	−90°	+90°	$.935\underline{/6.26°}$	.484
			+90°	−90°	−90°	$.911\underline{/-1.69°}$	.486
			−90°	−90°	−90°	$.921\underline{/-1.16°}$	.486
CDPSK	17.5	1	180°	0°	0°	$1.0\underline{/0°}$	--
			0°	0°	0°	$1.01\underline{/.491°}$	.476
			180°	0°	180°	$.888\underline{/.611°}$	.476
			0°	0°	180°	$.896\underline{/1.16°}$	.478
			180°	180°	0°	$.950\underline{/.749°}$	.478
			0°	180°	0°	$.949\underline{/.291°}$	.486
			180°	180°	180°	$.837\underline{/1.49°}$	.476
			180°	180°	180°	$.827\underline{/.992°}$	.484

63

OK-QPSK shall be studied in this section (due to its similarity to SDPSK), as a basis of comparison of the effects of hardlimiting.

To analytically determine the power spectral density of a waveform the Fourier Transform of the baseband signal's autocorrelation function must be determined. For SDPSK, this autocorrelation function can be calculated by the method described in [5], to obtain:

$$R_y(\tau) = \begin{cases} 1 - |\tau|/T_b , & |\tau| \leq T_b \\ 0 & , \text{ elsewhere} \end{cases} \tag{129}$$

where $R_y(\tau)$ is the normalized autocorrelation of $y(t)$ from Eq. (127),

$$R_y(\tau) = \lim_{T \to \infty} \frac{1}{E_b} \int_{-T/2}^{T/2} y(t)y^*(t-\tau)dt , \tag{130}$$

where $y^*(\cdot)$ is the complex conjugate of $y(\cdot)$. As this is identical to the autocorrelation function for conventional DPSK, the power spectral density for both cases may be calculated to be

$$G(f) = E_b \left[\frac{\sin\pi\ fT_b}{\pi\ fT_b}\right]^2 \tag{131}$$

(see Fig. 31). Because the power spectral density is the same for both cases, the effect of bandlimiting on the power spectrum, and, thus, the bit energy will also be identical (see Fig. 32). This was illustrated by the equal average bit signal vector magnitudes for both techniques in Tables 1 and 2. As the bit energy is related to the BEP performance in the differential detector, the average BEP with filtering should be approximately identical for both cases. This was illustrated in Table 3.

OK-QPSK involves the employment of two orthogonal binary channels to modulate the carrier. The bit intervals of duration $2T_b$ are offset by T_b seconds (in each channel). The net result of such a modulation scheme is a signal with $0°$, $+90°$, and $-90°$ phase transitions (with probabilities of occurence of 1/2, 1/4, and 1/4, respectively) T_b seconds apart. The power spectral density of OK-QPSK may be espressed as [5]

$$G(f) = E_b \left[\frac{\sin 2\pi fT_b}{2\pi\ fT_b}\right]^2 \tag{132}$$

Note (see Fig. 33) that use of OK-QPSK modulation results in a signal whose bandwidth is half that of DPSK. This fact can also be seen

64

<div align="center">

TABLE 3
BEP IN THE DIFFERENTIAL DETECTOR WITH THE INPUT SIGNAL
FILTERED (WHITE, GAUSSIAN NOISE ASSUMED)

</div>

Modula-tion Type	Carrier Freq. to Data Rate Ratio	Filter Type (see note on on Table 1)	E_b/N_o	Average BEP		
				Bit "0"	Bit "1"	Both Bits
SDPSK	17.5	1	4	.177E-1	.181E-1	.179E-1
			10	.138E-3	.144E-3	.141E-3
			16	.129E-5	.135E-5	.132E-5
	28	1	4	.138E-1	.141E-1	.139E-1
			10	.673E-4	.702E-4	.688E-4
			16	.351E-6	.373E-6	.362E-6
	56	1	4	.112E-1	.112E-1	.112E-1
			10	.381E-4	.380E-4	.381E-4
			16	.132E-6	.132E-6	.132E-6
	56	0	4	.111E-1	.111E-1	.111E-1
			10	.373E-4	.372E-4	.373E-4
			16	.127E-6	.127E-6	.127E-6
CDPSK	17.5	1	4	.129E-1	.242E-1	.185E-1
			10	.648E-4	.292E-3	.178E-3
			16	.391E-6	.394E-5	.217E-5
	28	1	4	.115E-1	.167E-1	.141E-1
			10	.429E-4	.108E-3	.753E-4
			16	.174E-6	.730E-6	.452E-6
	56	1	4	.102E-1	.123E-1	.112E-1
			10	.334E-4	.486E-4	.410E-4
			16	.900E-7	.195E-6	.142E-6
	56	0	4	.101E-1	.122E-1	.111E-1
			10	.296E-4	.472E-4	.384E-4
			16	.886E-7	.186E-6	.137E-6

10dB/DIV.

2.5 MHz/SIDELOBE
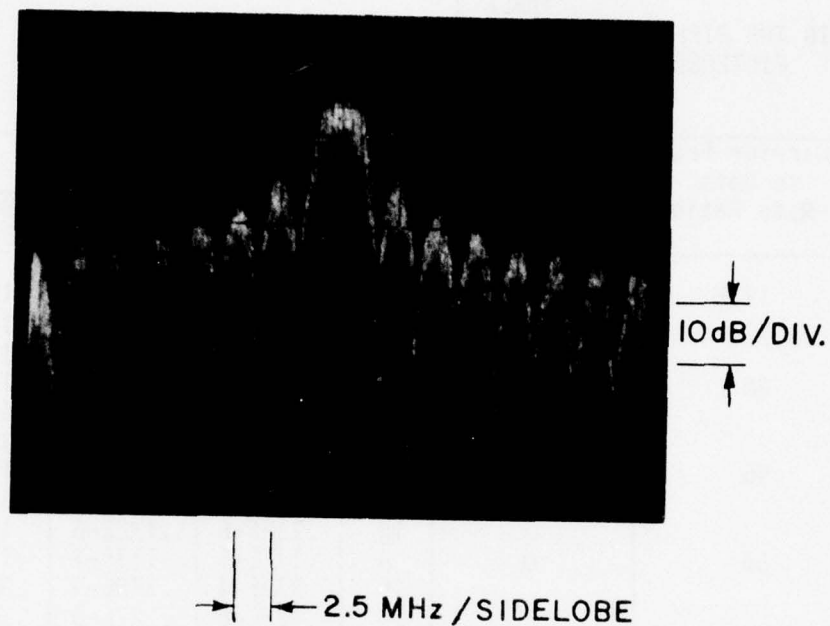
Figure 31. The experimental SDPSK and CDPSK
signal power density spectrum
Carrier freq.: 70 MHz
Data rate   : 2.5 MHz
Input data   : Pseudo-random

10dB/DIV

2.5 MHz /SIDELOBE

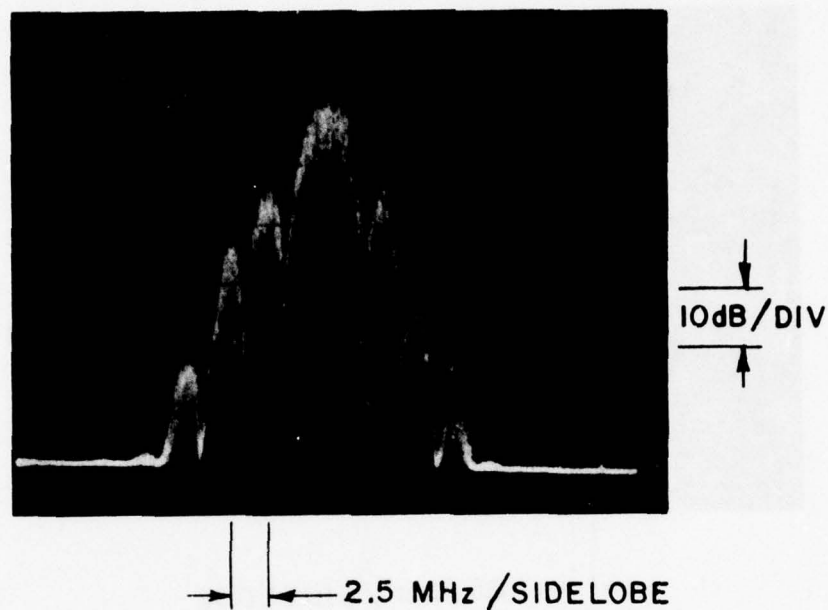Figure 32.   The experimental bandlimited SDPSK and CDPSK signal
             power density spectrum
             Carrier freq.   : 70 MHz
             Data rate   : 2.5 MHz
             Input data   : Pseudo-random
             Filter   : Chebyshev
                No. of sections   : 5
                Bandwidth   : 10 MHz
                Peak-to-peak passband ripple: 0.05 dB

10dB/DIV

←| |←1.25 MHz /SIDELOBE
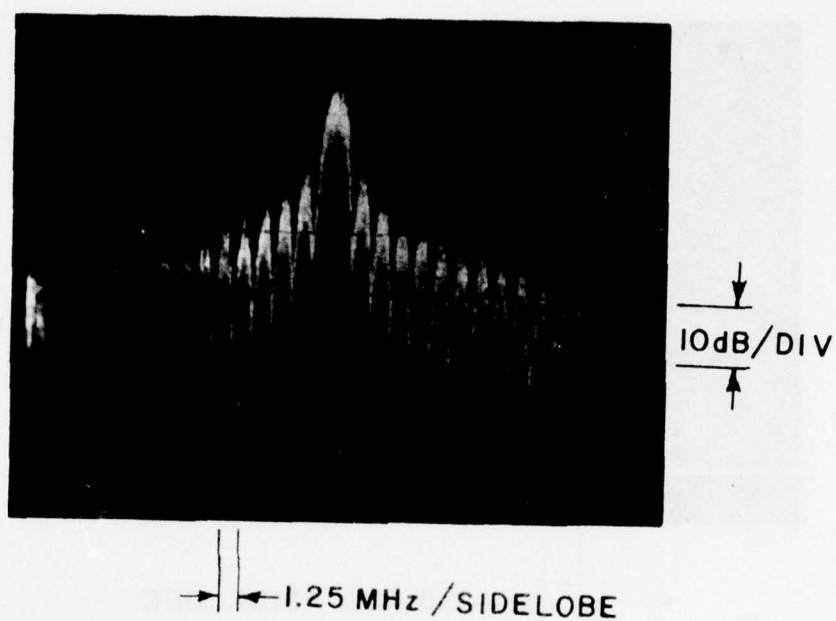
Figure 33. The experimental OK-QPSK signal power
spectral density
Carrier freq.: 70 MHz
Data rate   : 2.5 MHz
Input data   : Pseudo-random

from the time domain analysis of the signal because this signal is a SDPSK signal with only half as many $\pm 90°$ phase transitions. Thus only half the bits are affected by filtering, resulting in only half the energy loss with filtering for OK-QPSK (see Fig. 34). It should also be mentioned that because only half as many transitions occur, the available energy for bit synchronization is half that for SDPSK (see Chapter V).

With hardlimiting of the bandlimited signal, only half the bits in both CDPSK and OK-QPSK are effected as compared to all the bits in SDPSK. With SDPSK the filtered signal envelope has a more constant magnitude than with CDPSK, however. Thus hardlimiting will distort conventional DPSK to a greater extent. This is illustrated in Figs. 35 and 36. For these results the theoretical DPSK signal in Figs. 18 and 24 was hardlimited by simulating the process by the equation

$$Z_0(t) = Z_i(t)/|Z_i(t)| \tag{133}$$

where $Z_0(t)$ is the hardlimited signal and $Z_i(t)$ is the input signal.

Because the CDPSK is more distorted in the time domain, the regeneration of sidelobes will be greater. In Figs. 37 through 39 this effect is demonstrated from the measured signal power density spectrum. Thus, SDPSK will have a regeneration of sidelobes with hardlimiting significantly less than CDPSK and to the same degree as OK-QPSK.

10dB/DIV

|←—1.25 MHz/SIDELOBE

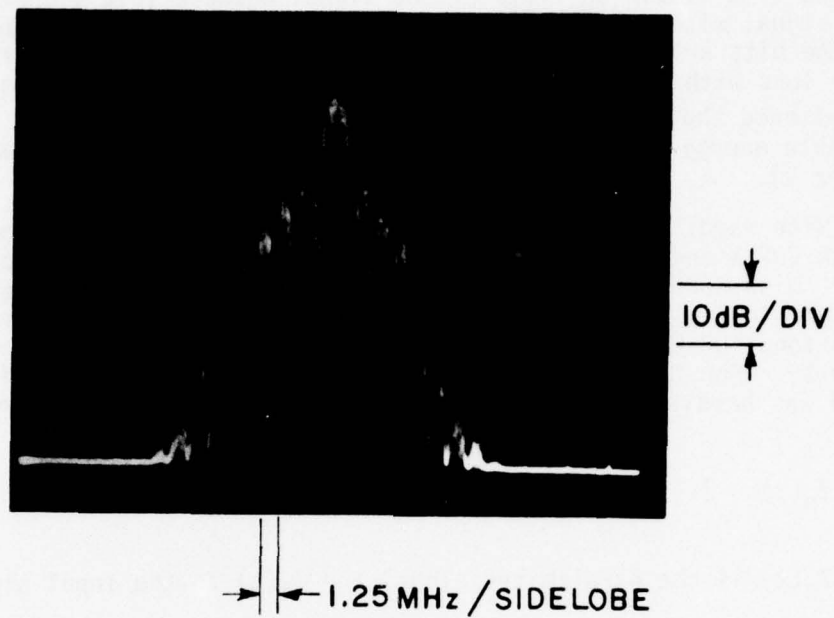Figure 34. The experimental bandlimited OK-QPSK signal
            power density spectrum
            Carrier freq.   : 70 MHz
            Data rate   : 2.5 MHz
            Input data   : Pseudo-random
            Filter   : Chebyshev
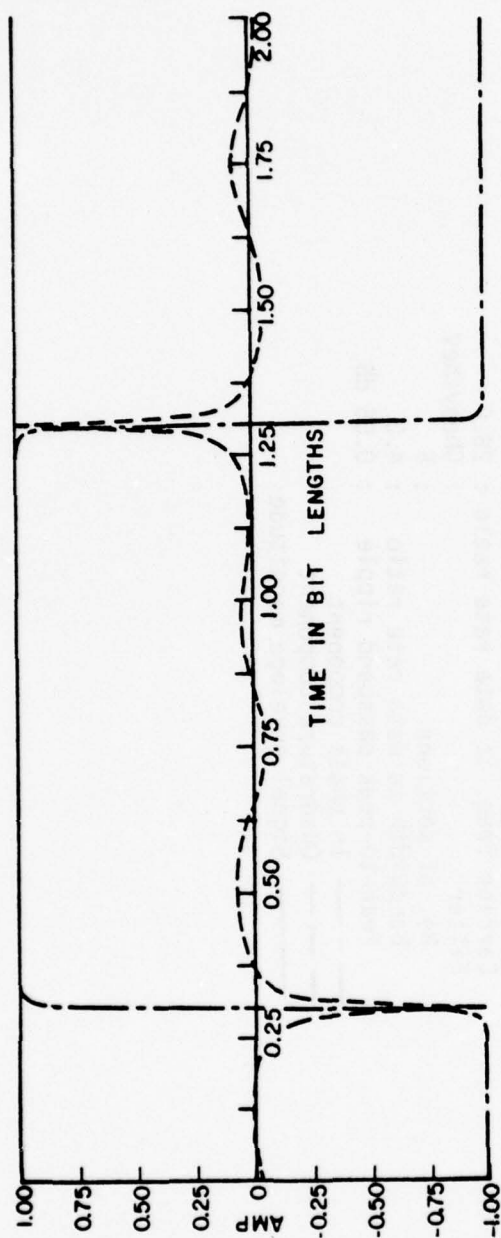   No. of sections   : 5
              Bandwidth   : 10 MHz
              Peak-to-peak passband ripple: 0.05 dB

70

Figure 35. The theoretical bandlimited CDPSK signal after hardlimiting
Periodic input data {δ}   : 2 2
Carrier freq. to data rate ratio: 28.0
Filter   : Chebyshev
  No. of sections   : 5
  Bandwidth to data rate ratio   : 4.0
  Peak-to-peak passband ripple   : 0.05 dB
  ——— In phase component
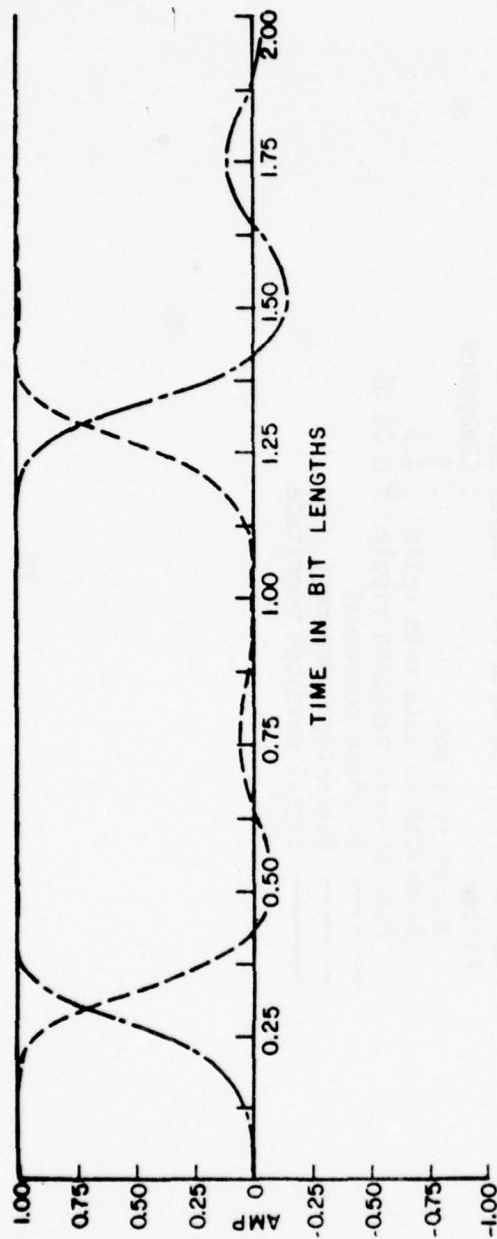 ——— Quadrature component
  ——— Signal envelope magnitude

71

TIME IN BIT LENGTHS

Figure 36. The theoretical bandlimited SDPSK signal after hardlimiting

Periodic input data {δ}   : -1 1
Carrier freq. to data rate ratio : 28.0
Filter   : Chebyshev
  No. of sections   : 5
  Bandwidth to data rate ratio : 4.0
  Peak-to-peak passband ripple : 0.05 dB

— · — In phase component
— — — Quadrature component
——— Signal envelope magnitude

10dB/DIV

←2.5 MHz /SIDELOBE
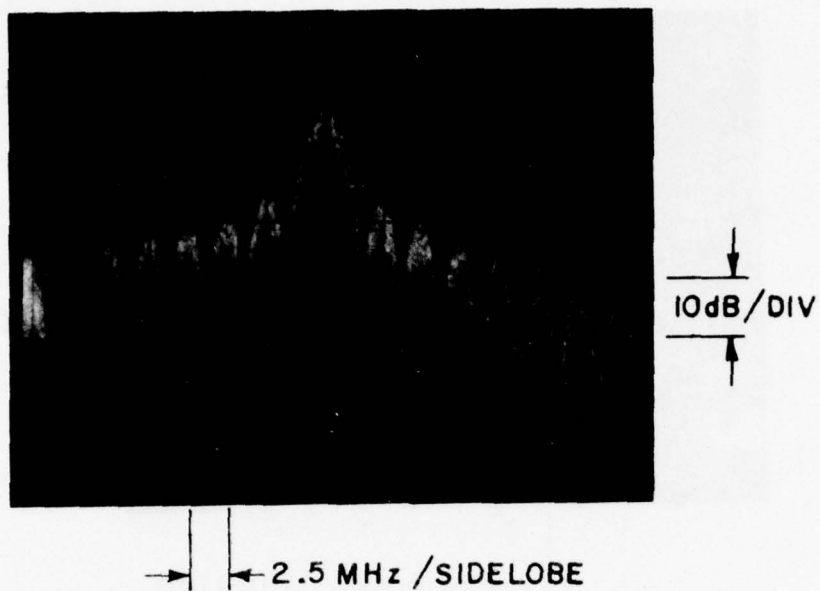
Figure 37. The experimental bandlimited CDPSK signal power
density spectrum after hardlimiting
Carrier freq.   : 70 MHz
Data rate   : 2.5 MHz
Input data   : Pseudo-random
Filter   : Chebyshev
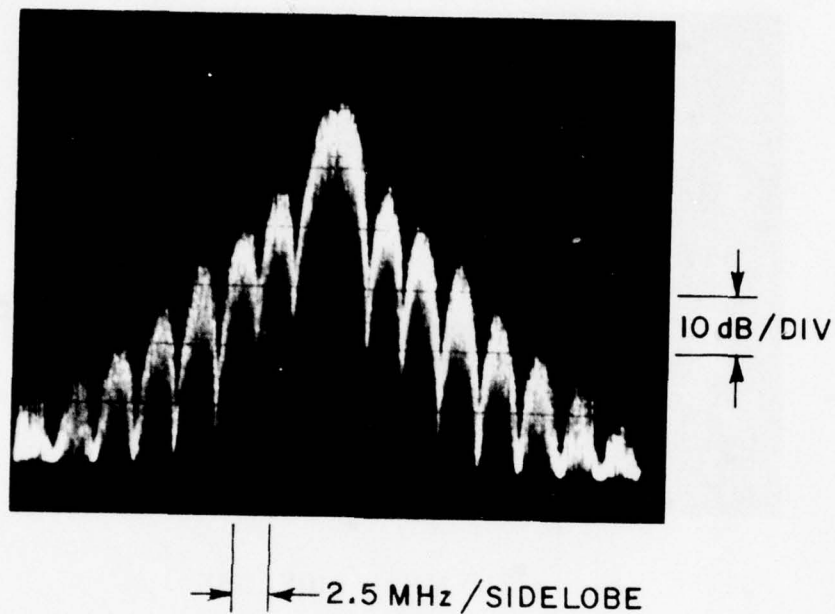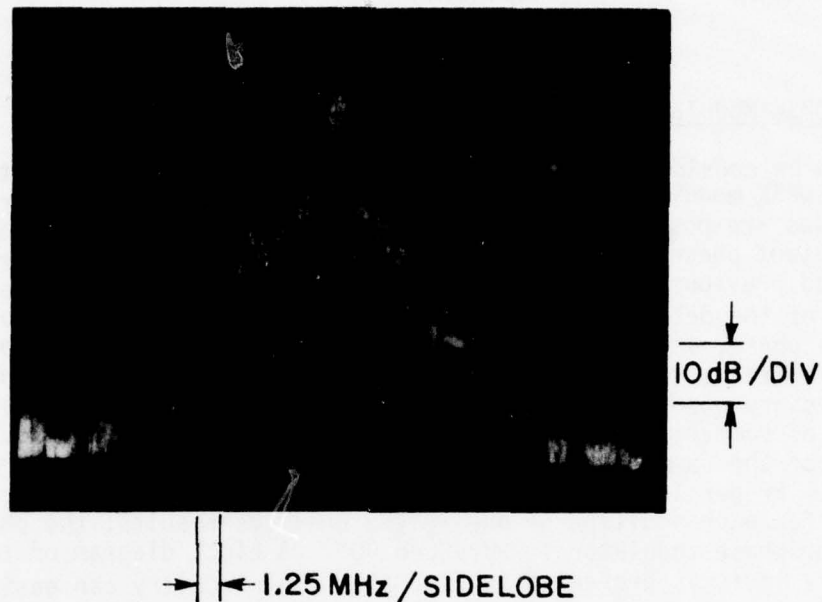 No. of sections   : 5
  Bandwidth   : 10 MHz
  Peak-to-peak passband ripple : 0.05 dB

73

10 dB/DIV

2.5 MHz/SIDELOBE

Figure 38. The experimental bandlimited SDPSK signal power
density spectrum after hardlimiting
Carrier freq.   : 70 MHz
Data rate   : 2.5 MHz
Input data   : Pseudo-random
Filter   : Chebyshev
  No. of sections   : 5
  Bandwidth   : 10 MHz
  Peak-to-peak passband ripple : 0.05 dB

10 dB/DIV

1.25 MHz/SIDELOBE

Figure 39.   The experimental bandlimited OK-QPSK signal
power density spectrum after hardlimiting
Carrier freq.   : 70 MHz
Data rate   : 2.5 MHz
Input data   : Pseudo-random
Filter   : Chebyshev
  No. of sections   : 5
  Bandwidth   : 10 MHz
 Peak-to-peak passband ripple : 0.05 dB

ADDITIONAL ASPECTS OF SDPSK

A. SDPSK Modulation

To be considered in this section is the hardware implementation
of the SDPSK modulator. When generating the signal, any of four out-
put phases are possible and, hence, the use of a quadriphase modulator
whose output phase is dependent on an input bit stream is required.
As stated previously the modulation scheme employed is the trans-
mission of the data bit "1" by a 90° phase shift with respect to the
previous phase, and transmission of the data bit "0" by a -90° phase
shift with respect to the previous phase. One simple way to generate
the necessary quadriphase modulator input bit stream from the data is
the use of summer, whereby the data bit "1" adds one to the previous
results of the summer, and the data bit "0" adds three to the previous
results. Proper logic changes the summer's output to the correct bits
so that for each addition of one to the previous results, the phase of
the quadriphase modulator is advanced 90°. A block diagram of the
necessary logic is presented in Fig. 40. The circuitry can easily be
modified to generate conventional DPSK by grounding the least signi-
ficant bit (LSB) summer input. In this configuration the data bit "1"
causes a 0° phase shift and the data bit "0" a 180° phase shift.
(This is the inverse of the conventional specified in Chapter II, and,
thus, the input data would be inverted to generate the signal for this
convention).

In an actual hardware implementation latches are required on the
input to the modulator for proper operation, due to gate delays. Fur-
thermore the number of IC packages needed can be reduced. The result-
ing circuit schematic is shown in Fig. 41.

B. Bit Synchronization

1. Introduction

Of interest in this part is the generation of the bit timing
information employed in the differential detector. Bit timing infor-
mation is derived from the signal waveform, and, due to the presence
of noise at the input of the receiver, a timing error will result
which has a Gaussian probability density function as shown in [1].
The variance of the timing error will depend on the bit synchroni-
zation circuitry, the signal waveform, and the bit energy to noise
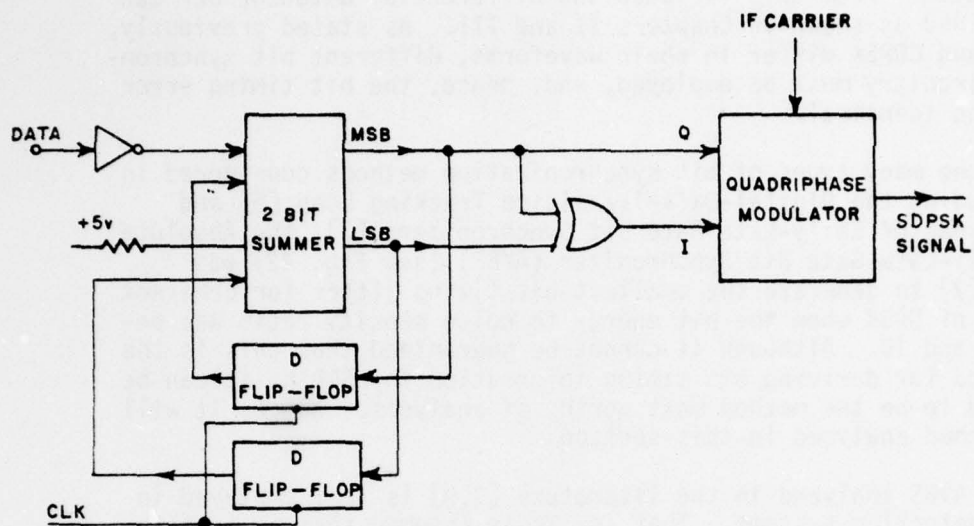
QUADRIPHASE MODULATOR LOGIC

MSB	LSB	I	Q	OUTPUT PHASE
0	0	0	0	270°
0	1	1	0	0°
1	0	1	1	90°
1	1	0	1	180°

Figure 40. SDPSK bit generator and
modulation circuitry.

density ratio. From this variance the differential detector BEP can be determined as shown in Chapters II and III. As stated previously, as SDPSK and CDPSK differ in their waveforms, different bit synchronization circuitry must be employed, and, hence, the bit timing error will not be identical.

Of the many types of bit synchronization methods considered in [7], including the Digital-Data-Transition Tracking Loop [6] and several types of Early-Late Gate Bit Synchronizers [7], the Absolute Value Early-Late Gate Bit Synchronizer (AVBS) (see Fig. 42) was shown in [7] to generate the smallest bit timing jitter for coherent detection of DPSK when the bit energy to noise density ratio was between 0.1 and 10. Although it cannot be guaranteed that this is the best method for deriving bit timing information for SDPSK, it can be considered to be the method most worthy of analysis. Hence, it will be the method analyzed in this section.

The AVBS analyzed in the literature [7,8] is that employed in coherent detection systems. That is, it is assumed that an inphase reference signal is available which is generally generated from a phase-locked loop. However, when DPSK is employed in such systems as TDMA with burst type transmissions, it is not possible to have an accurate inphase reference at all times due to oscillator drifts between transmissions and the initial acquisition time lag of the loop. Thus, the AVBS must be modified to generate bit timing information without an inphase reference signal. This can be performed in a manner similar to differential detection, by the employment of two channels, whereby in quadrature local oscillator signals are used to convert the signal to baseband, as shown in Fig. 43. The response of the system (the error voltage derived from the bit timing error) is calculated in Section V.B.2. The local oscillator frequency was assumed to be at the same frequency as the carrier and the effect of bandlimiting was not considered. Analysis was performed for the case of a modification of the in quadrature local oscillator signals also. From the error voltage versus timing error calculations the bit timing jitter for a given bit energy to noise density ratio can be determined. This has been performed for CDPSK in [7] and from an analysis of the error voltage versus timing error calculations a similar result for SDPSK can be obtained.

2. The AVBS employing the SDPSK signal

The performance of the AVBS will now be considered. Because nonlinear analysis of the AVBS in the presence of noise involves considerable calculation, as demonstrated in [7], analysis will only be performed to determine the behavior of the circuit in the absence of noise. An estimate of the performance of the AVBS with SDPSK in the presence of noise can then be deduced from a comparison of this AVBS
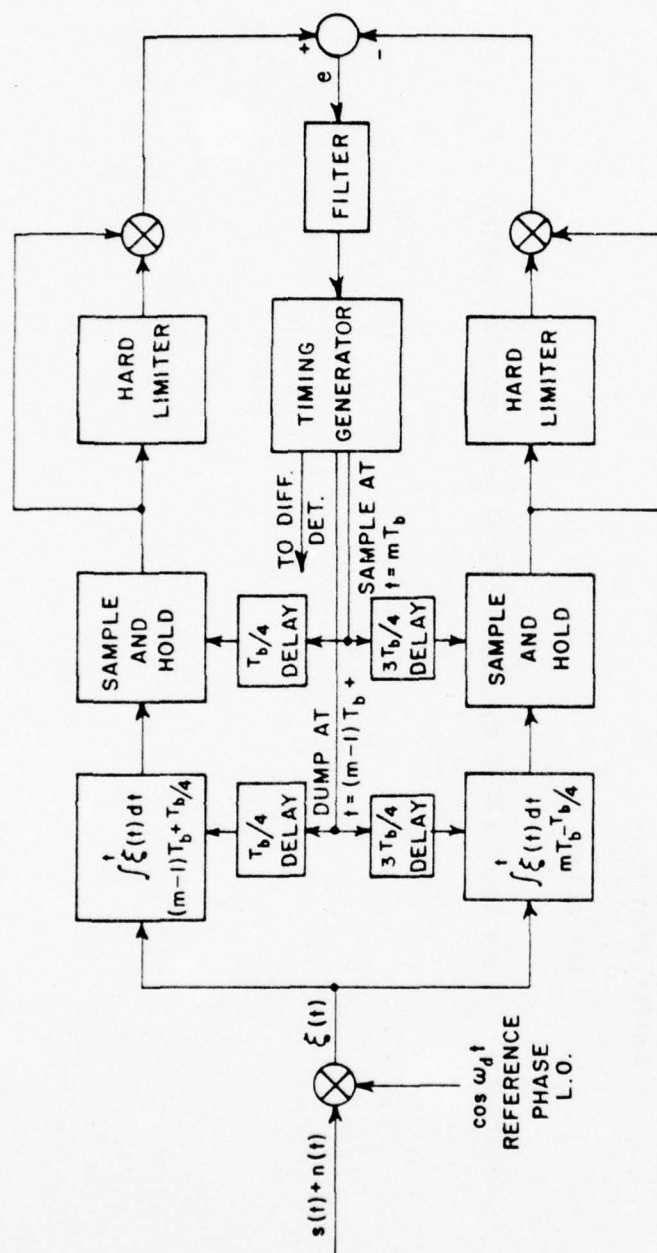
78

Figure 41. Schematic of CDPSK and SDPSK signal generation circuitry.

79

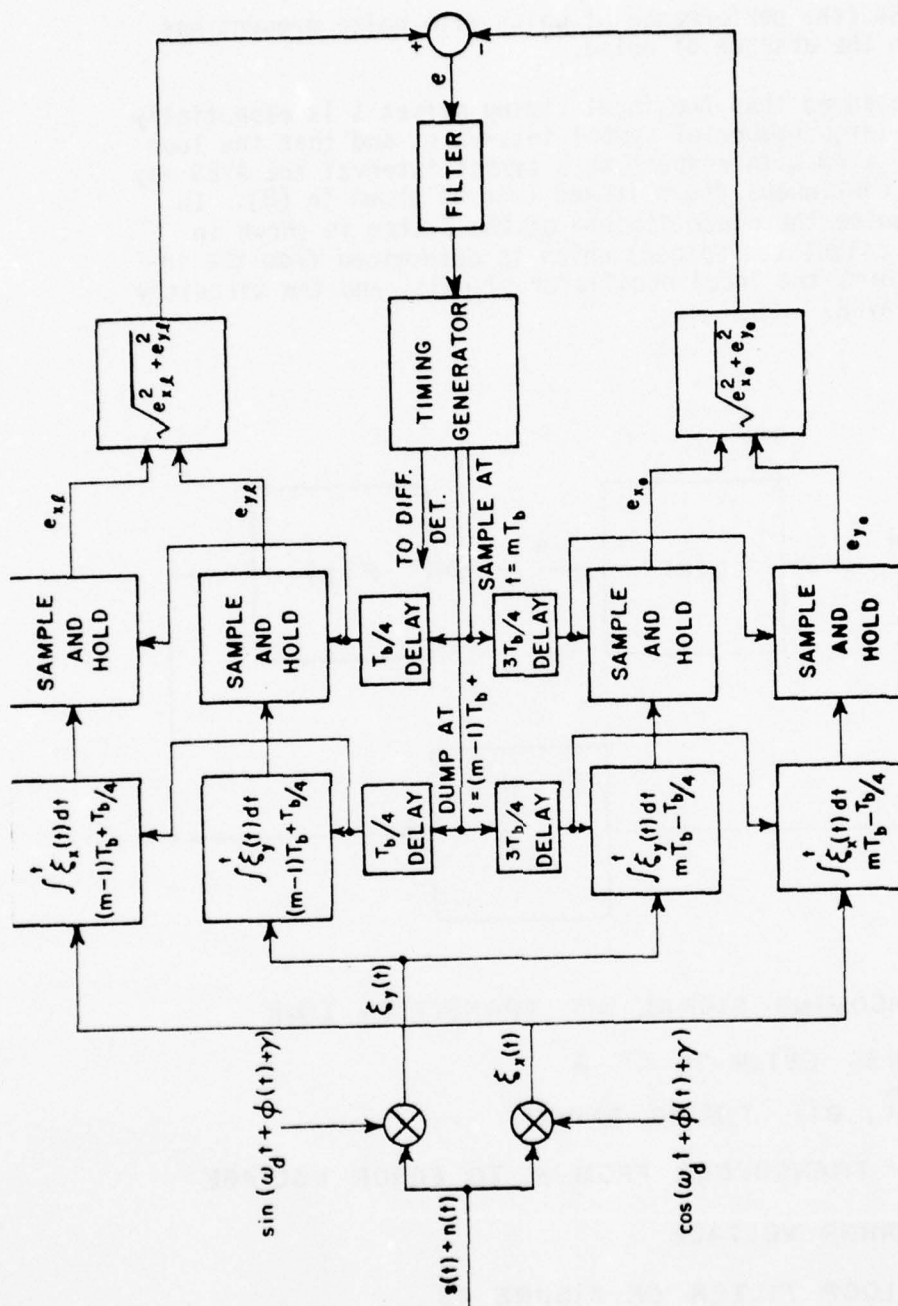Figure 42. Absolute value early-late gate bit synchronizer.

Figure 43. Absolute value early-late gate bit synchronizer; modified for use with CDSPK and SDPSK signals.

81

to that for CDPSK (the performance of which with noise present has been studied) in the absence of noise.

If it is assumed that the input timing offset λ is essentially constant over a large number of symbol intervals, and that the loop response is very slow with respect to a symbol interval the AVBS may be modeled as a continuous phase locked loop as shown in [8]. In the absence of noise the block diagram of the system is shown in Fig. 44. To be calculated is $g(\epsilon)$ which is determined from the input signal waveform, the local oscillator signals, and the circuitry employed in the AVBS.
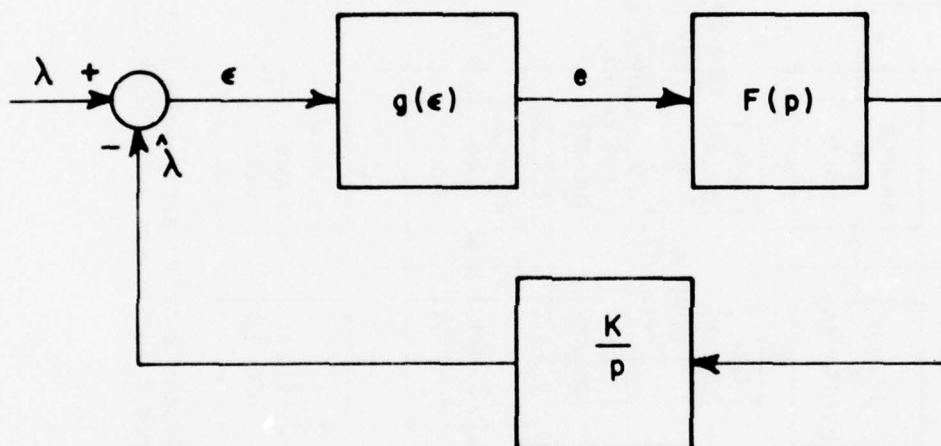
λ ~ INCOMING SIGNAL BIT TRANSITION TIME

$\hat{\lambda}$ ~ AVBS ESTIMATE OF λ

$\epsilon = \lambda - \hat{\lambda}$, BIT TIMING ERROR

$g(\epsilon)$ ~ TRANSDUCER FROM ϵ TO ERROR VOLTAGE

e ~ ERROR VOLTAGE

$F(p)$ ~ LOOP FILTER OF FIGURE 43

K ~ GAIN CONSTANT OF TIMING GENERATOR

Figure 44.   Block diagram of continuous phase locked loop model of AVBS with noise absent.

To compute $g(\varepsilon)$ for the AVBS with conventional DPSK, referring to Fig. 43, let

$$n(t) = 0 \quad , \tag{134}$$

and

$$s(t) = \begin{cases} \cos(\omega_d t + \alpha_r) \quad , \quad (m-1)T_b + \varepsilon < t < mT_b + \varepsilon \\[2mm] -\cos(\omega_d t + \alpha_r) \quad , \quad mT_b + \varepsilon < t < (m+1)T_b + \varepsilon \end{cases} \quad , \tag{135}$$

which corresponds to the transmission of a "1", where α_r is the unknown phase of the received input signal. Assuming $\phi(t)$ is zero and $|\varepsilon|$ is less than $1/4\, T_b$, for the late integrators,

$$e_{x_\ell} = \int_{(m-1)T_b + T_b/4}^{mT_b + T_b/4} s(t)\, \sin(\omega_d t + \gamma)\, dt \quad . \tag{136}$$

Assuming $\omega_d \gg 1/T_b$,

$$e_{x_\ell} = \left(\frac{3T_b}{4} + \varepsilon\right) \cdot \frac{1}{2}\, (- \sin(\alpha_r - \gamma))$$

$$+ \left(\frac{T_b}{4} + \varepsilon\right) \cdot \frac{1}{2}\, (\sin(\alpha_r - \gamma)) \quad . \tag{137}$$

Therefore,

$$e_{x_\ell} = - \left(\frac{T_b}{4} + \varepsilon\right) \sin(\alpha_r - \gamma) \quad . \tag{138}$$

Similarly, for the in quadrature circuit

$$e_{y_\ell} = \left(\frac{T_b}{4} + \varepsilon\right) \cos(\alpha_r - \gamma) \quad . \tag{139}$$

Thus, the magnitude of the voltage produced by the late integrators is given by

$$\left(e_{x_\ell}^2 + e_{y_\ell}^2\right)^{1/2} = \left(\frac{T_b}{4} + \varepsilon\right) \quad . \tag{140}$$

For the early integrators, following the same procedure as above, the magnitude of the voltage output is given by

$$\left(e_{x_e}^2 + e_{y_e}^2\right)^{1/2} = \left(\frac{T_b}{4} - \varepsilon\right) \tag{141}$$

Therefore, the error voltage may be calculated as

$$e = 2\varepsilon \quad . \tag{142}$$

Thus, $g(\varepsilon)$ is 2ε when a "1" is transmitted. When a "0" is transmitted, no phase transition occurs and $g(\varepsilon)$ is zero for all $|\varepsilon|$ less than $1/4\ T_b$. Thus with an input signal with equally probable "1"'s and "0"'s, $g(\varepsilon)$ is given by

$$g(\varepsilon) = \varepsilon \quad , \tag{143}$$

as shown in [8].

To compute $g(\varepsilon)$ for the AVBS with SDPSK, referring to Fig. 43, let

$$n(t) = 0, \tag{144}$$

and

$$s(t) = \begin{cases} \cos(\omega_d t + \alpha_r) & , \quad (m-1)T_b + \varepsilon < t < m T_b + \varepsilon \\ \sin(\omega_d t + \alpha_r) & , \quad m T_b + \varepsilon < t < (m+1)T_b + \varepsilon \end{cases} \tag{145}$$

which corresponds to the transmission of a "1". Assuming $\phi(t)$ is zero and $|\varepsilon| < T_b/4$, and following the same procedure as in the case of conventional DPSK, it is calculated that

$$\sqrt{e_{x_\ell}^2 + e_{y_\ell}^2} = \frac{\sqrt{\left(\frac{3T_b}{4} + \varepsilon\right)^2 + \left(\frac{T_b}{4} - \varepsilon\right)^2}}{2} \quad , \tag{146}$$

and

$$\sqrt{e_{x_e}^2 + e_{y_e}^2} = \frac{\sqrt{\left(\frac{T_b}{4} + \varepsilon\right)^2 + \left(\frac{3T_b}{4} - \varepsilon\right)^2}}{2} \tag{147}$$

Therefore, the error voltage is given by

$$e = \frac{1}{2}\left(\sqrt{\left(\frac{3T_b}{4} + \varepsilon\right)^2 + \left(\frac{T_b}{4} - \varepsilon\right)^2} - \sqrt{\left(\frac{T_b}{4} + \varepsilon\right)^2 + \left(\frac{3T_b}{4} - \varepsilon\right)^2}\right) \quad . \tag{148}$$

84

For the transmission of a "0", the error voltage calculated is identical to that for a "1". Therefore, for SDPSK in the AVBS, $g(\varepsilon)$ is given by

$$g(\varepsilon) = \frac{1}{2}\left(\sqrt{\left(\frac{3T_b}{4} + \varepsilon\right)^2 + \left(\frac{T_b}{4} - \varepsilon\right)^2} - \sqrt{\left(\frac{T_b}{4} + \varepsilon\right)^2 + \left(\frac{3T_b}{4} - \varepsilon\right)^2}\right) .$$

(149)

This function is plotted along with $g(\varepsilon)$ for CDPSK in Fig. 45. Note that the error characteristic for Eq. (149) is not only nonlinear but is less in magnitude than that for CDPSK for all ε. Thus, employing this method of bit synchronization will result in a timing jitter with noise present at the input significantly greater for SDPSK.

One method to improve performance (i.e., increase $g(\varepsilon)$) of the SDPSK bit synchronizer is to modulate the L.O. signal.

Before analyzing L.O. modulation schemes, the actual theoretical limit in the error performance of the AVBS for SDPSK will be examined. With CDPSK, timing error generates voltage errors which are in phase when a "1" has been transmitted. Thus proper combination of the early-late gate outputs results in an error voltage based on twice the timing error for this case or just the timing error on the average. For SDPSK, timing error generates voltage errors which are orthogonal. Thus, the maximum error voltage which can be generated is

$$(\varepsilon^2 + \varepsilon^2)^{1/2} = \sqrt{2}\,\varepsilon .$$

(150)

Analysis has shown that if the phase of the L.O., $\phi(t)$, is advanced by 180° every $T_b/2$ seconds, synchronized with the bit timing (phase transition) estimate, the resulting error voltage is given by Eq. (150), i.e., $g(\varepsilon)$ is given by

$$g(\varepsilon) = \sqrt{2}\,\varepsilon ,$$

(151)

which is plotted in Fig. 45. Note that this system produces a larger error voltage for a given timing error than the CDPSK AVBS. As the error voltage without noise is increased by a factor of $\sqrt{2}$, the effect is similar to an increase in the input signal E_b/N_0 of 3 dB. From [7], the variance of the normalized ($\varepsilon/T_b = \varepsilon_n$) bit timing error of the AVBS with E_b/N_0 greater than 4 (numeric) (for CDPSK) is given by
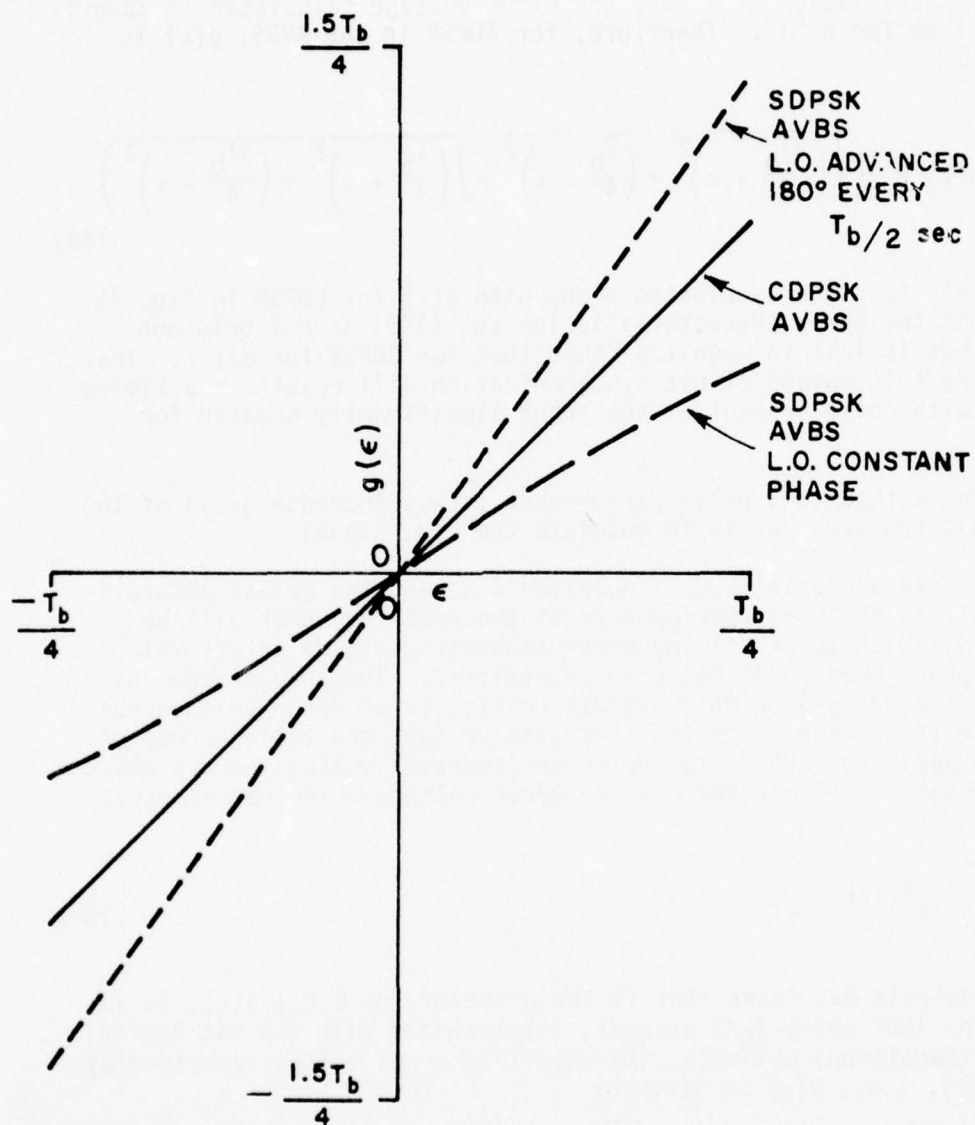
Figure 45. Error voltage versus timing error for the AVBS
with different L.O. signals and input waveforms.

$$\sigma^2_{\varepsilon_n} = \frac{W_L \, T_b}{8 \left(\frac{E_b}{N_o} \right) \mathrm{erf} \left(\frac{\sqrt{E_b/N_o}}{2} \right)} \tag{152}$$

where W_L is the AVBS filter bandwidth. Thus the variance of the timing jitter for both cases can be calculated and the results have been plotted in Fig. 46. The timing jitter is demonstrated in this figure to be less for SDPSK than for CDPSK for E_b/N_o greater than 4, when the filter bandwidth and data rate is held fixed.

The results of this section can be combined with the BEP calculations of Chapters II and III to obtain the actual theoretical BEP of CDPSK and SDPSK in the differential detector with bit timing information generated by the AVBS. As an example of the results possible from such an analysis, Fig. 47 illustrates the BEP versus E_b/N_o when the AVBS has a loop bandwidth equal to one-fourth the data rate ($1/W_L T_b = 4$), and frequency offset is neglected.
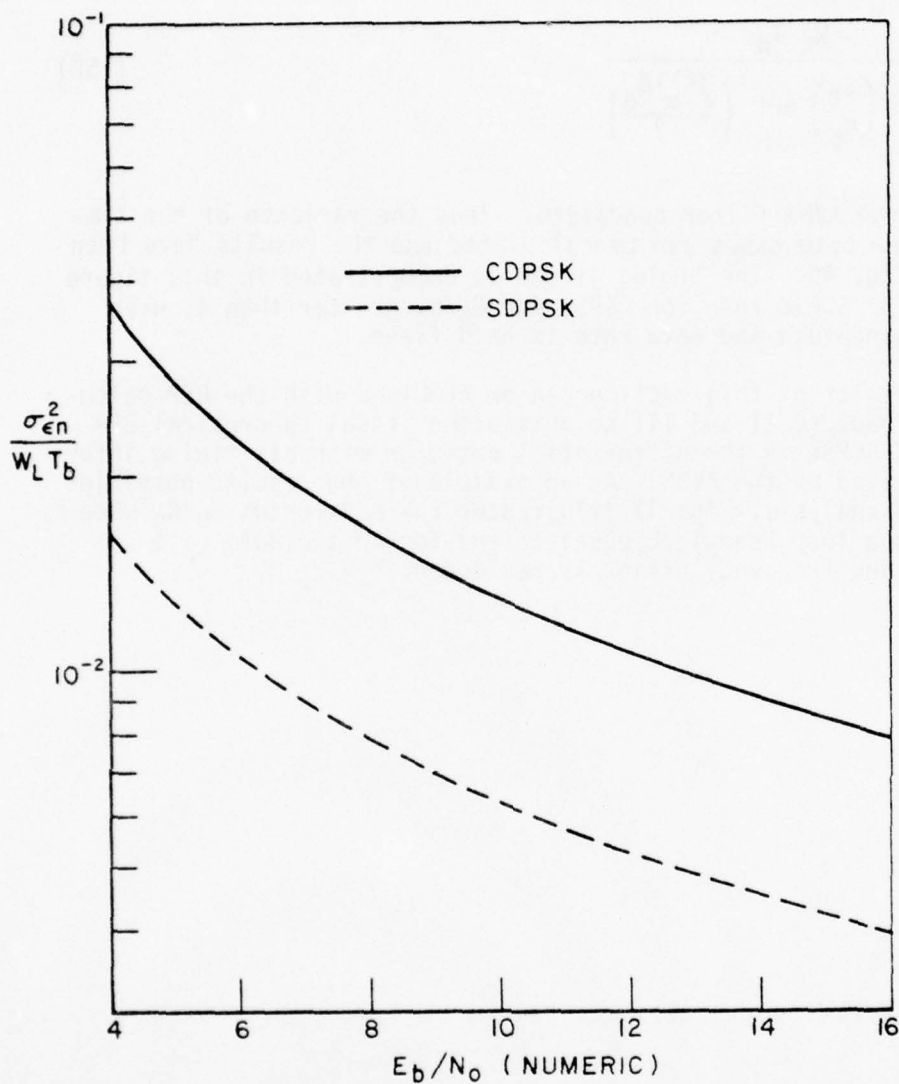
Figure 46. The theoretical normalized timing error variance (for a given number of error samples, $1/W_L T_b$) versus the bit energy to single sided noise density ratio for CDPSK and SDPSK employed in the AVBS.
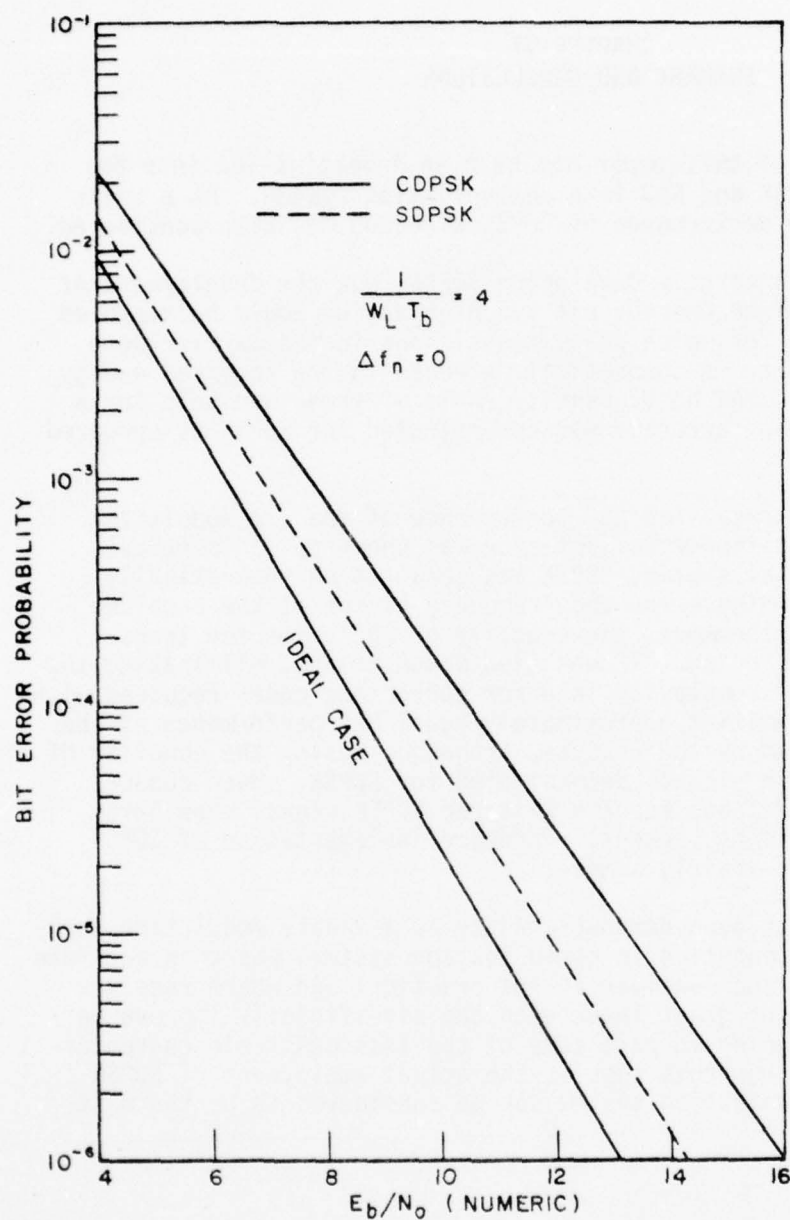
Figure 47. The average bit error probability versus bit energy to single sided noise density ratio in the differential detector with bit synchronization generated by the AVBS with a loop bandwidth one-fourth the data rate.

CHAPTER VI
SUMMARY AND CONCLUSIONS

The purpose of this paper has been an investigation into the performance of SDPSK and SDD in a communication system. As a basis of comparison, the performance of CDPSK with CDD was also considered.

Of initial concern in developing SDPSK, was the development of a modulation technique whereby bit synchronization could be improved by use of a scheme for which phase transitions in the carrier were present at every bit. A theoretical decrease in the required energy per bit to single sided noise density ratio of three decibels for a given synchronization accuracy was demonstrated for SDPSK as compared to CDPSK.

In the ideal case, the BEP performance of the two modulation techniques in the differential detector was shown to be identical. However, in an actual system, SDPSK was shown to be theoretically better for given timing error and frequency offset at the receiver in most cases. Furthermore, the equality of BEP's for the transmission of the bit "0" and "1" was also demonstrated, eliminating the need for additional complexity in error correcting codes required with CDPSK. With bandlimiting, approximately equal BEP performance at the receiver was implied by the results, although, again, the equality of BEP for an "0" and a "1" was demonstrated for SDPSK. Much reduced regeneration of sidelobes for the filtered SDPSK signal when hard-limited was shown to be present. Hardware implementation of SDPSK has been shown to be fairly simple.

Thus SDPSK has been demonstrated to be a viable modulation technique, whose implementation in communication systems where an accurate phase reference at the receiver is not practical and where receiver synchronization is of great importance can significantly improve performance while reducing in part some of the less desirable characteristics of CDPSK. From this thesis, the actual employment of SDPSK with SDD in a communication system can be considered to be the next logical step.

BIBLIOGRAPHY

1. Huff, R.J., "An Investigation of Time Division Multiple Access Space Communication Systems," Dissertation, Ohio State University, 1969.

2. Miller, T.W., "Imperfect Differential Detection of a Biphase Modulated Signal - An Experimental and Analytical Study," Report 2738-5, 23 August 1971, The Ohio State University ElectroScience Laboratory, Department of Electrical Engineering; prepared under Contract F30602-69-C-0112 for Rome Air Development Center, Griffiss Air Force Base, New York.

3. Ziemer, R.E., and W.H. Tranter, Systems, Modulation, and Noise, Boston, Mass., Houghton Mifflin Company, 1976, pp. 64-65.

4. Stanley, W.D., Digital Signal Processing, Reston, Virginia, Reston Publishing Company, Inc., 1975, pp. 129-130, pp. 139-144.

5. Gronemeyer, S.A. and A.L. McBride, "MSK and Offset QPSK Modulation," IEEE Transactions on Communication, August 1976.

6. Simon, Marvin K., "Optimization of the Performance of a Digital-Data-Transition Tracking Loop," IEEE Transactions on Communications, October 1970.

7. Simon, Marvin K., "Nonlinear Analysis of an Absolute Value Type of an Early-Late Gate Bit Synchronizer," IEEE Transactions on Communications, October 1970.

8. Lindsey, W.C. and M.K. Simon, Telecommunication Systems Engineering, Englewood Cliffs, N.J., Prentice Hall, Inc., 1973, pp. 433-434, pp. 458-465.

MISSION
of
Rome Air Development Center

RADC plans and conducts research, exploratory and advanced development programs in command, control, and communications (C^3) activities, and in the C^3 areas of information sciences and intelligence. The principal technical mission areas are communications, electromagnetic guidance and control, surveillance of ground and aerospace objects, intelligence data collection and handling, information system technology, ionospheric propagation, solid state sciences, microwave physics and electronic reliability, maintainability and compatibility.